IDM UID
679HW9

VERSION CREATED ON / VERSION / STATUS
08 Oct 2012 / 1.6/ Approved

EXTERNAL REFERENCE

Report

System Design Description Document (DDD) Diagnostic – Electron Cyclotron Emission

DDD-PBS 55.F1 ECE

Approval Process			
	Name	*Action*	*Affiliation*
Author	**Udintsev V.**	**08-Oct-2012:signed**	**IO/DG/DIP/CHD/DIAG/DIAGE**
CoAuthor			
Reviewers	**Walsh M.**	**09-Oct-2012:recommended**	**IO/DG/DIP/CHD/DIAG**
Previous Versions Reviews	**Vayakis G.**	**01-Oct-2012:recommended v1.1**	**IO/DG/DIP/CHD/DIAG/IVDS**
Approver	**Bora D.**	**10-Oct-2012:approved**	**IO/DG/DIP/CHD**
Document Security: level 1 (IO unclassified) *RO: Udintsev Victor*			
Read Access	**RO, project administrator, LG: EXT_DIAG_COLL, AD: ITER, AD: External Collaborators, AD: Division - Diagnostics - EXT, AD: Division - Diagnostics**		

Change Log				
Title (Uid)	***Version***	***Latest Status***	***Issue Date***	***Description of Change***
System Design Description Document (DDD) Diagnostic – Electron Cyclotron Emission (679HW9_v1_6)	v1.6	Approved	08 Oct 2012	Table 7.1 - corrections to make it consistent with Annex B.
System Design Description Document (DDD) Diagnostic – Electron Cyclotron Emission (679HW9_v1_5)	v1.5	Signed	08 Oct 2012	Table 7.1 updated with the feedback from edge physicists (POP) Links to the Cat 1 closure and the closure statement added Link to teh Flow-Down Memo for Te added.
System Design Description Document (DDD) Diagnostic – Electron Cyclotron Emission (679HW9_v1_4)	v1.4	Signed	05 Oct 2012	Table 7.1 corrected to be consistent with Annex B and IAEA paper/ poster.
System Design Description Document (DDD) Diagnostic – Electron Cyclotron Emission (679HW9_v1_3)	v1.3	Approved	04 Oct 2012	Some changes to make this DDD and Annexes B coherent, following late reviewer's comment.
System Design Description Document (DDD) Diagnostic – Electron Cyclotron Emission (679HW9_v1_2)	v1.2	Approved	02 Oct 2012	Some consistency between this DDD and Annex B added.
System Design Description Document (DDD) Diagnostic – Electron Cyclotron Emission (679HW9_v1_1)	v1.1	Approved	01 Oct 2012	Updated, following CDR findings and panel review for Cat 1. Chits.
System Design Description Document (DDD) Diagnostic – Electron Cyclotron Emission (679HW9_v1_0)	v1.0	Approved	26 Nov 2011	PDF version v1.0; MS Word version is attached on the bottom of this IDM page
System Design Description Document (DDD) Diagnostic – Electron Cyclotron Emission	v0.0	In Work	04 Sep 2011	

(679HW9_v0_0)				

System Design Description Document (DDD)

Diagnostic – Electron Cyclotron Emission

DDD-PBS 55F1

Records of Revisions:

Rev. No.	Date	Descriptions
1.0	26 Nov 2011	Initial publication of the document.
1.1	01 Oct 2012	Second release.
1.2	02 Oct 2012	Third release.
1.3	04 Oct 2012	Fourth release.
1.4	05 Oct 2012	Fifth release.
1.5	07 Oct 2012	Sixth release.
1.6	07 Oct 2012	Seventh release.

	External Number: ITER_D_679HW9	*Date:*
	Name	*Affiliation*
Author	V.S. Udintsev	CHD/Diagnostics
Reviewers	M. Walsh G. Vayakis	CHD/Diagnostics CHD/Diagnostics
Approver	D. Bora	CHD

Table of Contents

1 Acronyms and definitions

3D	Three Dimensional
CAD	Computer Aided Design
CDR	Conceptual Design Review
CL	Correlation Length
CWG	Corrugated Waveguide
CIS	Central Interlock System
DDD	Design Description Document
DA	Domestic Agency
DCM	Design Compliance Matrix
DFW	Diagnostic First Wall
DJF	Design Justification File
DSM	Diagnostic Shield Module
ECE	Electron Cyclotron Emission
ECRH	Electron Cyclotron Resonance Heating
EDH	Electrical Design Handbook
FDR	Final Design Review
HFS	High Field Side
LFS	Low Field Side
ICD	Interface Control Document
IF	Intermediate Frequency
IO	ITER Organisation
I&C	Instrumentation and Control
ICD	Interface Control Document
IS	Interface Sheet
ISS	Interspace Support Structure
MC	Mode Conversion
MMW	Millimeter Wave
MQP	Management and Quality Program
MPD	Multi-Purpose Deployer
PA	Procurement Arrangement
PCDH	Plant Control Design Handbook
PCS	Plant Control System
PCSS	Port Cell Support Structure
PDR	Preliminary Design Review
PR	Project Requirements
QC	Quality Class
QO	Quasi-Optical
RF	Radio Frequency
RH	Remote Handling
RHC	Remote Handling Class
SC	Safety Class
SRD	System Requirement Document
SIC	Safety Important Component
UP	Upper Port
VH	Vacuum Handbook
VQC	Vacuum Quality Class
VUV	Vacuum Ultraviolet

2 Introduction

This DDD is an evolving document which describes the design of a single diagnostic system:

55F1 Electron Cyclotron Emission Diagnostic, or ECE

The main plasma ECE diagnostic is planned to be used for the measurements of plasma electron temperature profile with good spatial and temporal resolutions. Secondary objectives are to obtain information on non-thermal electron populations and the power loss due to ECE. From the recent ITER Measurement Requirements, the electron temperature profile should be resolved with the resolution of a/30 (~70 mm) and accuracy of 10% in the plasma core, for the temperature range 0.5 – 40 keV, and with a spatial resolution of 5 mm for r/a > 0.85. In addition, one important requirement is to detect the Neoclassical Tearing Mode (NTM) when the island size is small enough to cause a deleterious effect on the confinement, i.e. before it reaches its saturated width and causes the mode locking, thus triggering the major disruption. The instruments of ECE on ITER are Michelson interferometry (O- and X-modes) and heterodyne radiometers (Ordinary, or O-mode, 122 – 230 GHz; eXtraordinary, or X-mode, 244 – 355 GHz for B_t = 2 – 5.3 T). The principal limitations of the system are restricted radial region of observation due to harmonic overlap and degraded spatial resolution due to the relativistic broadening.
The system divided into three main parts: the front-end, which collects the radiation from the plasma and transmits it through to the pit; the transmission system which transports the ECE emission from the front-end and distributes it to the instrumentation and the instrumentation which is housed at a distance from the tokamak in an ITER-provided building (Fig. 2.1).
The section headings have been established using the procedure for the preparation review and approval of the DDDs: **ITER_D_2M24AM**.
For a procurement based on functional specifications, the DDD has to be filled up in a first issue prior to the CDR to demonstrate readiness for this review, which precedes the PA issuance.
The PA Annexes B will refer to a specific version of the DDD, named DDD-CDR level. This DDD shall be updated as the design matures, particularly at the PDR and FDR.
The link to the Category 1 CDR chits and their resolution is given here (folder): https://user.iter.org/?uid=4FDYWE. The CDR closure statement is located at: https://user.iter.org/?uid=A6GZ66.

Initial System Classification

ECE on ITER is being designed to measure the plasma electron temperature profile with good spatial and temporal resolutions. It must also contribute to the measurements of βp and runaway electron parameters (current and energy), the power loss contribution of ECE and the detection of MHD modes.
The system is SIC-1 for the vacuum boundary.
The ECE diagnostic has no measurement for SIC purpose and the loss of the measurements will not cause the stop of machine or plasma operation. QC1 can be assigned to the components that form the vacuum boundary. The ex-vessel waveguides beyond the vacuum boundary are QC3.

The seismic class is SC1(S) for SIC components only (Seismic load SL – 2 Category IV (Extremely Unlikely) – see Annex 18 for details).

The vacuum class is VQC 1A for the primary window assembly and VQC 3A for the second window.

The Remote Handling Class is RHC2 for refurbishment as a part of the Equatorial Port 9 drawer, RHC3 for refurbishment within its drawer and RHC1 for in-vessel calibration and alignment.

The justification of classifications is given in Section 21, as well as in the Annex 2.1.

2.1 Applicable documents list

[A1] Design review procedure v.1.12: **2832CF**
[A2] Procedure for the preparation review and approval of the DDDs: **2M24AM**
[A3] ITER project requirements: **27ZRW8**
[A4] System requirement document SRD-55 (diagnostics) from DOORS: **28B39L**
[A5] Guidelines for System load specifications: **33TTPJ**
[A6] ITER RH compatibility procedure: **34DKDK**
[A7] Plant Control Design Handbook: **27LH2V**

2.2 Reference document list

[R1] DDD55N Diagnostic system engineering **29M88L**
[R2] Plant Description_Ch-08_Diagnostics **2WBD7N**
[R3] ITER Vacuum handbook **2EZ9UM**
[R4] ITER material property handbook **32SAC7**
[R5] Compliance Matrix SRD -55 **3356ZK**
[R6] Key risks for diagnostics **2V4PB8**

3 Brief description

3.1 Primary role of this diagnostic system in the ITER program

TABLE 3.1. Role of the 55F1 ECE diagnostic in the ITER program.

Title	Parameter	Contribution	Operation Role
04. Plasma energy	006: βp	Supplementary	1a.1 MP
05. Radiated power	008: Main plasma Prad	Supplementary	1a.2 BC
14. H-mode, ELMs and L-H mode transition indicator	032: ELM temperature transient	Backup	2. PHY
15. Runaway electrons	034: Emax	Supplementary	2. PHY
15. Runaway electrons	035: I runaway	Supplementary	2. PHY
23. Electron temperature profile	**052: Core Te**	**Primary**	**1b. AC**
23. Electron temperature profile	053: Edge Te	Supplementary	2. PHY
27. High frequency instabilities (MHD, NTMs, AEs, turbulence)	**061: NTM δT / Te. (complex; 100ms integration time)**	**Primary**	**1b. AC**
27. High frequency instabilities (MHD, NTMs, AEs, turbulence)	063: TAE δN / n, δT/T	Supplementary	2. PHY

The Electron Cyclotron Emission diagnostic (PBS 55F1) provides essential information for plasma operation and for establishing performance characteristics. It measures the electron temperature profile (edge/core), electron temperature fluctuations and radiated power in cyclotron frequency range from the plasma providing information on the following parameters as reported in the PR (Project Requirements (PR) (27ZRW8)): Edge Electron Temperature Profile, Core Electron Temperature Profile, ELM temperature transient, NTM and TAE δT/Te, as well as contributes to the measurement of βp and runaway electrons study. The role of the diagnostic is summarized in Table 3.1.

The solutions of category 1 & 2 chits are available here https://user.iter.org/?uid=4FDYWE & https://user.iter.org/?uid=73MTBM

3.2 Justification and Outline for the 55F1-F10 diagnostic

A primary measurement prioritization is given below:

1. Core electron temperature profile measurement and contribution to the plasma energy measurement
2. NTM temperature perturbation (δT/Te) measurement
2. ELM temperature transient measurement
3. Radiated power measurement in cyclotron frequency range
4. Edge electron temperature profile and TAE temperature perturbation (δT/Te) measurements
5. Contribution to the runaway electron parameters study (E_max, I_runaway)

As can be seen, the overall highest priority in a variety of ITER operating phases was identified as the **Core electron temperature profile measurement** and **NTM temperature perturbation (δT/Te) measurement.** The front-end has been optimized within the existing geometrical/integration constraints to fulfil the measurement requirements.

The front-end of the diagnostic is located in the central DSM (drawer) of the Equatorial Port 9. Two lines-of-sight are included into the current design. Besides the principal, perpendicular, line-of-sight, a second one exists for additional measurements and redundancy. For this line, a toroidal angle of about 10 degrees is proposed. The second line enables other measurements such as the detection of the presence of non-thermal electron population and radial correlation length measurements for MHD and the plasma turbulence, while providing redundancy for the high priority measurements, should the radial view not be available.

The front-end optics configuration of each line-of-sight consists of a focusing element (an elliptical mirror) and a flat mirror thus forming a Gaussian beam, which can be thought of as projecting the radiation pattern at the mouth of the exit waveguide (in HE11 mode for the heterodyne radiometer) to the resonance plane in the plasma. Depending on the design of the front end, the focusing mirror is subject to surface heat of several of kW/m^2 and volumetric neutron loads of several of kW/m^3. Presently, a hot reference (hot source) is considered as options in the design to provide the absolute calibration of the system. The proposed assembly has been designed to accommodate all other diagnostics in the port plug. The radiation from each antenna is transmitted to the port interspace quasioptically to match the polarising beam splitters, before transmission to the diagnostic hall by waveguide system. Two confinement systems for each principal inventory of radioactive or hazardous material are provided by windows and the waveguide structures. In the diagnostic hall, the signal is distributed between ECE instruments by a set of switches and gratings. Te system will be used also to acquire data, pre-process the data and then pass it to the CODAC system.

The system may also be calibrated and aligned in-situ after installation and during shutdowns after maintenance, although this capability is not currently assessed.

Figure 3.1 shows the general layout of a typical transmission line for the ECE diagnostic.

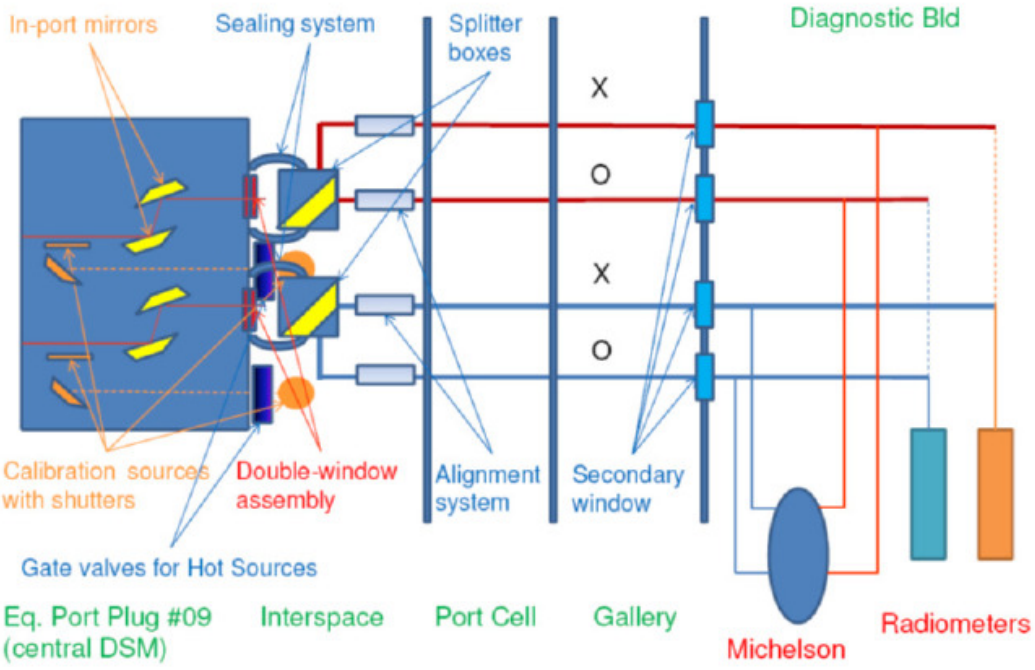

Figure 3.1. Schematic of the baseline transmission lines of the ECE system. The oblique line-of-sight is indicated in red; the perpendicular line-of-sight is indicated in blue. FTS system consists of two Michelsons, for X- and O-mode measurements.

3.3 Present state-of-the-art for similar existing diagnostics

In 1973, it was proposed that electron cyclotron emission measurement could be used as a plasma diagnostics tool and by the middle of 1980s; the electron cyclotron emission diagnostic was well established due to progress in the measurement technology and tools to calibrate the instrument absolutely. Here, we briefly describe about advance features in ECE diagnostic systems relevant to ITER ECE system.

Measurement of electron temperature profile (references herein are local to this sub-section)

The ECE system is used to measure electron temperature profile with good spatial and temporal resolution and study non-thermal electrons parameter. The temperature profile needs to measure optically thick ECE harmonic radiation at equatorial plane in radial direction, while non-thermal electron study requires ECE radiation in multiple harmonic in radial as well as oblique direction. For this JET ECE system is good example for both types of measurements. The hardware implementation of the JET system is most recent and stable. The calibration of the system is stable; therefore, the electron temperature profile can be measured with a good accuracy and stability [1]. The radiometer has 96 channels that give frequency separation corresponding to < 1 cm for JET magnetic field gradient and with frequency response of 1 MHz [2]. For Michelson ECE measurement there three line of sight with two orthogonal linear polarizations (X and O-mode). In this, one is for radial measurement done by a rectangular waveguide and two oblique (at about 9.5^{o} and 20.5^{o} respect to the radial direction) measurements done by a combination of fixed mirrors, feeding the nearly radially oriented smooth circular waveguides. All three antennas are located approximately equatorial plane on the low filed side and connected to a multi-channel Michelson interferometer through 60 meter long transmission line. Each oblique antenna signal is split into O-mode and X-mode and fed to Michelson with quasi-optical arrangement. The optical layout is same for all channels. This is a so-called Martin-Puplett interferometer with four

helicodal sectors on circular rotating wheel mirror [3] of radius 150 mm. The combined output beam is measured by He cooled InSb detector. The interferometer gives interferogram with ~ 5 ms time resolution and output spectrum covered from 1st harmonic to 4th harmonic (~ 75 – 350 GHz for magnetic field of B_H of 3 T).

For ITER high toroidal field (~ 5.3 T) operation, 2nd harmonic ECE frequency is up to 355 GHz. Therefore, one has to design radiometer for that frequency. There is good example of high frequency radiometer installed on Alcator-C. This radiometer operates in frequency range 234 to 306 GHz with 32 channels and a frequency response of 1 MHz [4].

Calibration

Absolute calibration of the ECE measuring system is important and necessary to receive absolute measurements of the radiation temperature. A hot/cold black body source with known physical temperature is used into calibration. A hot body source of glass ceramic or silicon carbide or liquid nitrogen cooled Eccosorb absorbers are used as source. If the radiometer or Michelson interferometer operated maximum signal to noise ratio, coherent averaging within a few minutes is sufficient to determine the temperature difference with the necessary accuracy. In this method, the calibration accuracy is about 10%. An end to end calibration can be done by placing the calibration source inside vessel when the vacuum vessel is open or make arrangement to keep the source inside vacuum. It is also possible to simulate the condition by duplicating the antenna and the vacuum window section of the transmission line. A detail survey and assessment on ECE calibration technique is presented in 21st ITPA on diagnostics [5], and review of this is described in reference [6].

Transmission line

In ITER, the ECE measurement frequency range of interest is 70 to 1000 GHz. A very low power signal of the thermal black body calibration source with wide band frequency rang need to be transmitted over a long distance (~ 30 - 40 m) from tokamak to the diagnostics hall. Therefore a very low loss transmission line is needed. A literature survey on transmission line and ECE spectra measurement on various fusion research machines (see Table 3.1) deduced that the measurements are generally available up to 450 GHz; the higher frequencies are accessed at Alcator-C (measurement from 160 – 800 GHz) [6] and FTU (from 100 – 900 GHz) [7]. Quasi-optical arrangement of 10 m length is used for Alcator-C ECE system and a smooth wall square over size waveguide (light pipe) of 16 meter is used for FTU ECE. Among these two examples of wideband ECE measurement; the smooth wall square waveguide may be prospective for the ITER ECE transmission line. Other prospective option for the transmission line waveguide is a circular corrugated waveguide. This type of waveguide transmission line has being used on DIII-D [8], JT-60 [9] and LHD [10].

Table 3.1. Transmission line and ECE spectra measurement ranges on different tokamaks.

	TFTR	**JET**	**JT-60**	**DIII-D**	**Alcator C-mod**	**FTU**	**Tore Supra**	**ITER**
Spectral region (GHz)	75 - 540	75 - 800	100 - 1000	60 - 900	100 - 800	70 - 900	50 - 1000 (currently 78 – 126 GHz)	70 - 1000 GHz
Transm. Line	Quasi-optical Lenses	Over - sized WG	Corr. WG	Corr. WG	Quasi-optical Mirrors	Light pipe	Quasi-optical Lenses	Corr. and smooth-wall WG
Spectral Resolution (GHz)	3.7	7.5	3.5	4	5	4.5	2-16	10 GHz
Scanning time (time resolution) (ms)	14	10.7	>15	6	15	5	16 - 250	2 – 20

References

[1] P. Blanchard, E. de la Luna, C. Gowers and JET-EFDA contributors, EFDA–JET–CP (04)01/02

[2] E. de la Luna, G. Conway, J. Fessey, R. Prentice, D.V. Bartlett, J. M. Chareau, C. Gowers, J. Sánchez, W. Suttrop, V, Tribaldos and JET-EFDA contributors,EFDA–JET–CP(04)01/18

[3] A. Simonetto, C. Sozzi, S. Garavaglia, J.A. Fessey, S. Nowak and JET-EFDA contributors, EFDA–JET–PR(11) 09

[4] R. Chatterjee , P.E. Phillips , J. Heard , C. Watts , R. Gandy , A. Hubbard, Fusion Engineering and Design 53 (2001) 113–121

[5] G.D. Conway, et al., *ECE and reflectometer calibration: ITER_D_3622CE*

[6] Marco Zerbini, C.SOZZI, A. SIMONETTO, in Proc. Of 15th Joint Workshop on ECE and ECRH, Edited by John Lohar,

[7] A. E. Hubbard, T. C. Hsu, P. J. O'Shea and the Alcator C-Mode Group, PFC/JA-95-11

[8] P. Buratti, O. Tudisco & M. Zerbini Infrared Physics, Vol. 34, 533-541, (1993)

[9] M. E. Austin et al. Review of Sci. Inst. **68(1)** 480 (1997)

[10] Nagayama Yoshio et al. Journal of Plasma Fusion Res. **79**, 601 (2003)

[11] Y. Nagayama, K. Kawahata et al. Review of Sci. Inst. **70** 1021 (1999)

MHD/fluctuation measurements (references herein are local to this sub-section)

Measurements of ECE are nowadays used extensively in the diagnosis of fusion plasmas. Most tokamaks and stellarators have extensive ECE measurement systems and these routinely provide measurements of the spatial profile of the electron temperature; the location, type, and size of MagnetoHydroDynamic (MHD) modes; and information on suprathermal populations. More sophisticated dedicated applications can provide the amplitude and location of broadband temperature fluctuations, the length of the spatial correlations of the underlying fluctuations, and two dimensional images of MHD modes [1].

MHD modes are routinely detected and studied by means of ECE, as these modes perturb the electron temperature profile. In Tore Supra and TEXTOR, detailed studies of the precursor for sawteeth were recently performed by means of conventional ECE [2] and ECE-Imaging [3]. It has been concluded that, before a crash, the hot core gets displaced with respect to the magnetic axis, then drifts outwards by as much a few cm and may be reshaped. Observation of the fast magnetic reconnection process has been achieved by utilizing the good temporal resolution of the ECE diagnostic. The heat pulse is seen far outside the inversion radius. The colder plasma develops a magnetic island on the former magnetic axis, after the hot core expulsion.

On TCV tokamak in Lausanne, Switzerland, ECE radiometers with some channels which are frequency-tunable are been used to track the evolution of Neoclassical Tearing Modes (NTMs) [4 – 5] and to use this information for their real-time control. In the Tokamak à Configuration Variable (TCV), global plasma oscillations have been discovered in fully non-inductively driven plasmas featuring electron internal transport barriers with strong ECRH/ECCD. These oscillations are linked to the destabilisation and stabilisation of MHD modes near the foot of the ITB and can lead to large oscillations of the total plasma current and line-averaged density, among others. They are intrinsically related to the fact that ITBs have large pressure gradients in a region of low magnetic shear. Therefore, the ideal MHD limit is relatively low and infernal modes can be unstable. Depending on the proximity to the ideal limit, small crashes or resistive modes can appear which affect the time evolution of the discharge. Being near marginal stability, the modes can self-stabilise due to the modification of the pressure gradient and local q profile. The plasma recovers good confinement, reverses shear and the internal transport barrier builds up, until a new MHD mode is destabilized. TCV results show that this cycling behaviour can be controlled by modifying the current density or the pressure profiles, either with Ohmic current density perturbation or by modifying the ECH/ECCD power. It is demonstrated that many observations like $q \geq 2$ sawteeth, beta collapses, minor disruptions and oscillation regimes in ITBs can be assigned to the same physics origin: the proximity to the infernal mode stability limit.

The real-time NTM suppression system has been implemented on AUG. The approach relies in part on locating the NTM via ECE measurements, and, since (3,2) NTMs in AUG commonly occur with rotation frequencies greater than 20 kHz, the upgraded fast ECE DAQ is required for this task [6]. The ECRH steerable mirrors are pointed such that ECRH power is deposited at the flux surface corresponding to the center of the island. The real-time equilibria are also used to calculate the location of the rational q-surface where the NTM will form. Prior to NTM formation, the ECRH mirrors may be steered to point at this surface. A combination of the ECE-

based NTM location and equilibrium-based *q*-surface location is processed by a Bayesian filter to optimize the targeting of the ECRH.

The transport of particles and energy across magnetic field lines in tokamaks is observed to be larger than predicted by neoclassical theory, leading to a degradation of the core confinement properties. This can cause a problem for future fusion devices, such as ITER or DEMO. Generally, turbulence driven by microinstabilities is believed to be the cause of this 'so-called' anomalous transport [7]. These turbulent fluctuations can be electrostatic and electromagnetic in nature. Unlike magnetic fluctuations, which break the nested flux surfaces, electrostatic fluctuations do not destroy the nested magnetic topology; but, enhanced transport occurs because of ExB drifts resulting from the fluctuating electric fields. Therefore, if one wants to establish a relation between the micro-fluctuations and the large-scale transport, measurements of various fluctuating components (electron density and temperature, $E_{\theta,}$ B_r), together with their phase relationships, are needed.

Correlation ECE radiometry has been proved to be a reliable tool to obtain information on microturbulence properties and on properties of small-scale modes of various origins on many fusion machines [8 - 9]. The first W7-AS measurements have given evidence of a broadband high-frequency component [10] in the spectra. On TEXT, the poloidal characteristics of the fluctuations were measured by an ECE imaging system [11 - 12] and the poloidal wavenumber spectrum was estimated to have an averaged k_θ of 2 cm^{-1}. Two-dimensional profiles of the temperature fluctuations have been measured on TEXT and RTP [12]; results have suggested different origins of fluctuations (ITG-driven on RTP, electron drift wave driven on TEXT). Tore Supra [13 - 14] has reported small-amplitude narrow-band modes identified as TAEs [13]. On DIII-D, electron temperature fluctuation spectra measured in NBI-heated L-mode plasmas are found to be similar in frequency and normalised amplitude to density fluctuations, with the latter increasing with a radius. Nonlinear gyrokinetic simulations compare well with experimental results for density fluctuations and heat diffusivity, but overestimate electron temperature fluctuation amplitudes at midradius [15].

On TCV, the temperature fluctuation measurement by ECE is achieved by cross-correlation between two radially-separated ECE channels for which temperature fluctuations are correlated, but thermal noise is uncorrelated [16]. Broadband electron temperature fluctuations (20 – 150 kHz, central frequency ranging from 20 to 90 kHz) are found in Ohmically heated (OH) discharges – extending radially between $0.3 < r/a < 0.8$, as seen from the equatorial midplane from low field side (LFS) of the machine. Their amplitude decreases with increased electron density, which is in qualitative agreement with predictions from quasi-linear gyrokinetic calculations performed with the gyrokinetic code GS2 at $r/a = 0.35$ [17]. The mixing length of the heat diffusivity calculated from GS2 decreases with increased collisionality, as does the measured heat diffusivity from power balance analysis.

To measure the average amplitude of temperature fluctuations in tokamak plasmas of smaller than 1 - 2%, one needs to get rid of the thermal noise [18]. This can be achieved by cross-correlation of two ECE signals whose temperature fluctuations are correlated while the noise fluctuations are uncorrelated. This can be done by observing the same plasma volume from two different directions or by using two sample volumes that only partly overlap. Mathematically, correlation between the two signals is the measure of degree to which the two signals are similar [19]. For two real signal sequences *x(n)* and *y(n)* with finite length, the cross-correlation sequence $r_{xy}\ (l)$ can be defined as:

$$r_{xy}(l) = \sum_{n=i}^{N-|k|-1} x(n)\, y(n-l) \ , \qquad (3.1)$$

where l is the time shift (or *lag*) parameter, $i = 1$, $k = 0$ for $l \geq 0$, and $i = 0$, $k = l$ for $l < 0$.
To identify the common normalized temperature fluctuation for two ECE signals $S_1(t)$ and $S_2(t)$, the cross-correlation sequence at zero time lag can be written as:

$$r_{12} \propto \overline{(S_1 - \overline{S}_1)(S_2 - \overline{S}_2)} = \overline{\tilde{T}_{e1}\tilde{T}_{e2}} + \overline{O}(\tilde{N}_1, \tilde{N}_2) \ , \qquad (3.2)$$

where the second term is small, compared to the first one, if care is taken that S_1 and S_2 are not exactly the same signals. If $T_{e1} = T_{e2} = T_e$, it is possible to get the normalized temperature fluctuation amplitude, after normalizing Eq. (3.2) to the mean signal level:

$$\frac{\tilde{T}_{e,RMS}}{\overline{T}_e} = \sqrt{\frac{r_{12}}{\overline{S}_1 \overline{S}_2}} \ . \qquad (3.3)$$

The statistical noise level can be defined as follows:

$$\Delta\left(\frac{\tilde{T}_{e,RMS}}{\overline{T}_e}\right) = \sqrt{\frac{\Delta r_{12}}{\overline{S}_1 \overline{S}_2}} = \frac{1}{\sqrt[4]{M}} \sqrt{\frac{\sigma_1}{\overline{S}_1}\frac{\sigma_2}{\overline{S}_2}} \ , \qquad (3.4)$$

where σ_1 and σ_2 are the standard deviations of $\tilde{S}_1$ and $\tilde{S}_2$, and M is the total number of samples. It is clear that a long sampling time is required to reduce the statistical error below the coherent temperature fluctuation amplitude. For example, to resolve fluctuations with an amplitude of 2% with a resolution of 0.3%, and taking ratio $\sigma_i / \overline{S}_i \sim 5\%$, one gets $M \sim 8 \cdot 10^5$ samples. For the sampling rate of 400 kHz (for fluctuations with typical frequencies below 200 kHz), the sampling time is estimated to be about 0.2 s.

References

[1] A.E. Costley, "50 Years of ECE Research", Fusion Sci. Technol. **55**, 1 (2009)

[2] V.S. Udintsev *et al.*, Plasma Phys. Control. Fusion **47**, 1111 (2005)

[3] H.R. Park *et al.*, Phys. Rev. Lett. **96**, 195004 (2006)

[4] V.S Udintsev *et al.*, Plasma Phys. Control. Fusion **50**, 124052 (2008)

[5] G. Turri *et al.*, Plasma Phys. Control. Fusion **50**, 065010 (2008)

[6] N.K. Hicks *et al.*, in Proc. of 35th EPS Conference on Plasma Phys. Hersonissos, 9 - 13 June 2008 ECA Vol.**32D**, P-4.082 (2008)
[7] W. Horton, Rev. Mod. Phys. **71**, 735 (1999)
[8] G. Cima *et al.*, Rev. Sci. Instrum. **66**, 798 (1995)
[9] H.J. Hartfuss *et al.*, Plasma Phys. Control. Fusion **38**, A227 (1996)
[10] C. Watts, Fusion Sci. Technol. **52**, 176 (2007)
[11] B.H. Deng *et al.*, Phys. Plasmas **5**, 4117 (1998)
[12] B.H. Deng *et al.*, IEEE Trans. Plasma Sci. **30**, 72 (2002)
[13] V.S. Udintsev *et al.*, Plasma Phys. Control. Fusion **48**, 33 (2006)
[14] M. Goniche *et al.*, Fusion Sci. Technol. **53**, 88 (2008)

[15] A.E. White *et al*., Phys. Plasmas **15**, 056116 (2008)

[16] V.S. Udintsev *et al*., Fusion Sci. Technol. **52**, 161 (2007)

[17] M. Kotschenreuther *et al*., Comput. Phys. Commun. **88**, 128 (1995)

[18] G. Cima *et al*., Phys. Plasmas **2**, 720 (1995)

[19] J.G. Proakis, D.G. Manolakis, Digital Signal Processing, Prentice Hall, New Jersey (1996)

Non-thermal electron population and wall reflection measurements (references herein are local to this sub-section)

In scenarios with strong additional heating (radio frequency, neutral beam and possibly alpha heating), deformations of the electron distribution function can occur [1 - 2]. In such cases, there is no single value of the 'temperature' and temperature ceases to be a useful parameter—a description of the velocity distribution is needed. ECE is affected by such distortions. Simultaneous observation of several ECE harmonics and oblique ECE observation may provide information on the velocity distribution.

It is not possible to uniquely determine the electron distribution function from a measurement of the ECE, but an approach where the calculated spectrum is fitted to the measured spectrum is possible in principle and requires the development of codes that can handle non-Maxwellian distributions. In general, reflections of the radiation cannot be eliminated in the experiments and so models of the combination of the plasma inside a reflecting chamber are needed. Codes that take all these effects into account are obviously substantial undertakings requiring significant computing power to run. Fortunately, the challenge of handling these effects was taken on by many talented theorists who worked steadily to improve the theoretical basis. A comprehensive review of the early theoretical developments has been published by Bornatici et al [3]. For later developments the reader is referred to the other papers cited in the following reviews [4 - 5]. A nice overview of physics and methods to evaluate the non-thermal electron population parameters is given in the paper by C. Sozzi and D. Farina [6], as well as in the paper on TCV results from oblique ECE measurements and modelling by T.P. Goodman [7].

Attempts were also made to measure the electron density by measuring the emission in optical gray/thin harmonics [8]. These measurements are complicated by reflections of the radiation in the plasma containing chambers. It has never been possible to achieve a completely effective radiation dump. Nevertheless, by modeling the wall reflections, estimates of the electron density have been obtained and these have compared well with those made by other means. There were also direct measurements of the wall reflection coefficient by probing the plasma simultaneously at optically thick second and optically thin (or gray) third harmonics [9 - 10].

One of the ECE requirements is to measure the total emitted power. Since the emission is of the same order in the two polarizations, this means simultaneous broadband measurements are needed in at least one of the views.

For the non-thermal electron distribution functions, the oblique view is able to provide an indication and estimation of any non-Maxwellian distribution. As described in Taylor and Harvey, Fusion Science and Technology 55 (2009) 67, the radial and oblique views (with different toroidal angles of 10 and 20 degree) will give different emission in the non-Maxwellian case, particularly in the third harmonic (Figs. from the paper shown below). Figure on the right shows ECE spectra simulated by GENRAY. The ECE radiation temperature, T_{rad}, is plotted

versus the emission frequency normalized to the fundamental cyclotron frequency on axis, $f/f_{ce}(0)$, where $f_{ce}(0)$ = 149 GHz.

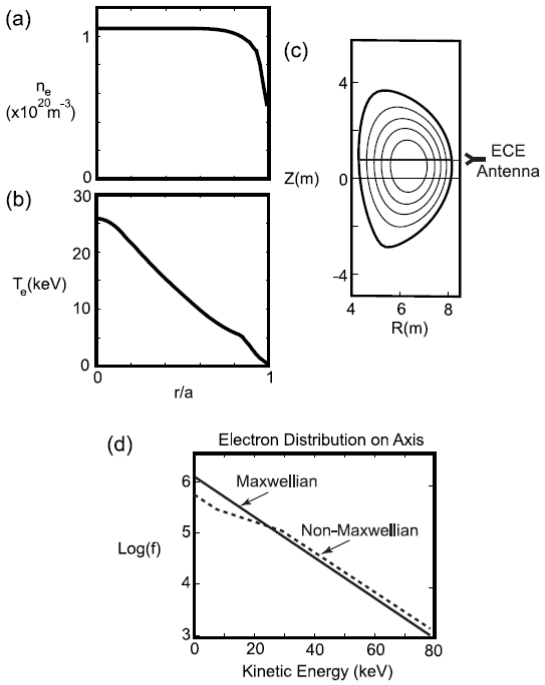

Fig. 2. ITER H-mode plasma parameters used to model ECE. (a) The electron density profile, (b) the electron temperature profile, (c) the poloidal cross section of the plasma magnetic equilibrium, and (d) the electron energy distribution on-axis for the Maxwellian (solid line) and non-Maxwellian (dashed line) cases. The non-Maxwellian distribution has the electron temperature increased by a factor of 2 between 0.75 and 1.5 times the electron thermal velocity.

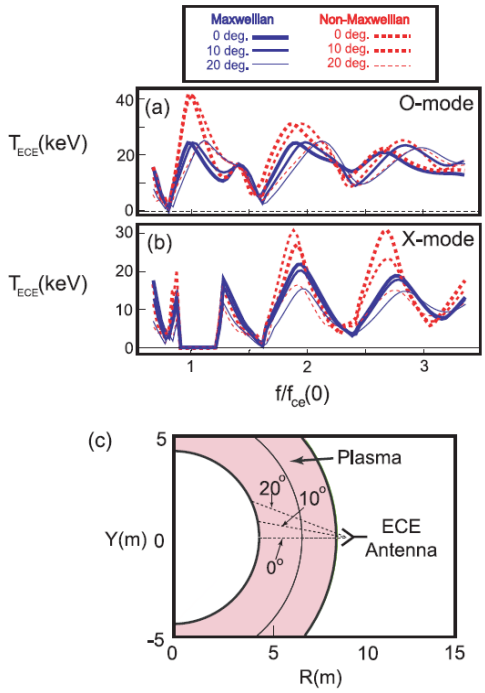

Fig. 3. Simulated ECE spectra for the H-mode plasma shown in Fig. 2. (a) O-mode and (b) X-mode ECE spectra plotted versus emission frequency normalized to the fundamental cyclotron frequency on-axis [$f_{ce}(0)$ = 149 GHz]. Emission spectra are shown for an ECE antenna pointing with its axis 0, 10, and 20 deg to perpendicular to the outer plasma magnetic flux surface (as illustrated in Fig. 3c). ECE spectra are plotted for a Maxwellian electron distribution (solid blue lines) and the non-Maxwellian distribution shown in Fig. 2d (red dashed lines).

For the measured O-mode ECE from the H-mode plasma and 10-degree ECE antenna orientation, the energies contributing to the measured ECE are similar for the Maxwellian and non-Maxwellian electron distribution. For the perpendicular view the electrons contributing to the measured ECE have energies in the range 0-10 keV at fundamental increasing to 40-70 keV at third harmonic. For the 10-degree oblique view, the electrons contributing to the measured ECE have energies in the range 10-25 keV at fundamental increasing to 30-60 keV at third harmonic. For the 20-degree oblique view the electrons contributing to the measured ECE have energies in the range 30-80 keV at fundamental increasing to 30-140 keV at third harmonic.

For the measured X-mode ECE from the H-mode plasma, the trends of viewing higher electron energies at higher harmonics and more oblique angles are similar to the O-mode polarization results. However, the electron energies to which the ECE is sensitive are about half as high as for the O-mode polarization. Also, the range of energies contributing to emission at a given angle and harmonic are much narrower than for O-mode polarization.

The emission flux spectra for fundamental O-mode and second harmonic X-mode emission measured at the edge of the plasma, for the H-mode plasma with a Maxwellian and Non-Maxwellian bulk, respectively, the electrons contributing to the measured ECE are defined as follows: the perpendicular view is sensitive to electrons with kinetic energies below 10 keV, and the 10-degree oblique view is sensitive to electrons with kinetic energies in the range 5-20 keV. The 20-degree view is sensitive to electrons with kinetic energies in the range 30-80 keV.

In summary, the perpendicular viewing antenna will be sensitive to electron kinetic energies of less than 10 keV, and the 10-degree oblique view will be sensitive to energies in the range 5-20 keV. The 20-degree oblique view will be sensitive to energies in the range 20-70 keV.

The first question is: can the moderately oblique view be used for T_e measurements if the plasma electron distribution remains Maxwellian at high T_e? The answer from the paper mentioned above is: if the bulk of the electron velocity distribution remains Maxwellian, modelling results predict that the moderately oblique views could be used to measure $T_e(R)$, even if an energetic electron tail is present. In addition no viewing dump would be required to measure $T_e(R)$ with the moderately oblique views, refraction effects should be minimal and the radial resolution of the moderately oblique views should be similar to a perpendicular view.

The second question is: if the electron energy distribution has a bulk distortion, can a two-temperature distribution be reconstructed with only two views, one perpendicular and one moderately oblique? There is a clear benefit to having oblique views at two different angles. For example in the H-mode case, with a non-Maxwellian, two-temperature bulk, the O-mode fundamental ECE spectra from the perpendicular and 10-degree views were very similar reaching T_{rad} ~ 40 keV, close to the 50 keV temperature component in the bulk. In contrast, the 20-degree view measured a maximum T_{rad} ~ 25 keV, the temperature of the rest of the energy distribution. However, by using O-mode and X-mode spectral measurements over several harmonics, it should be possible to reconstruct a two-temperature bulk distribution from only one oblique and one perpendicular view. For example, the ratio of the T_{rad} from the 10-degree and the perpendicular views at the O-mode fundamental is very different to the ratio between the same views at the X-mode third harmonic.

To take full advantage of this, **simultaneous, broadband measurements** must be made with the radial and oblique views. This must at a minimum be in one (the same) polarization in each view. However, greater information is obtained if measurements are made in **both** views since, as described in the paper, the electron energies to which the ECE is sensitive are about half as high for the O-mode as the X-mode polarization. In any case, it will be a difficult task to determine the full distribution function from a single oblique view; measuring both polarizations doubles the number of constraints, almost equivalent to a second viewing angle.

Taken together, this means that at a minimum, three simultaneous measurements are required. Four would be much more valuable; therefore, the transmission line properties shall be as close as possible. Note that having four instrumental channels allows some redundancy for the primary Te measurement. The additional constraints in this case are the budget allocated for the instruments and the space reservation required for the integration of the diagnostic in the tokamak complex and to the diagnostic building.

Presently, in the PR/SRD, determination of non-thermal electron populations by ECE is assigned to evaluation and physics studies. In scenarios with strong additional heating (radio frequency, neutral beam and possibly alpha heating), deformations of the electron distribution function can occur. In such cases, there is no single value of the ‘temperature’ and temperature ceases to be a useful parameter—a description of the velocity distribution is needed. ECE is affected by such distortions. Simultaneous observation of several ECE harmonics and oblique ECE observation may provide information on the velocity distribution. For the reasons mentioned above, a capability of the diagnostic to assess non-thermal parameters is limited and, thus, the measurement role is supplementary. The runaway electrons measurement, as stated in the

PR/SRD, shall cover the energy range from 1 to 100 MeV, and I-runaway from 0 to 1 MA, which clearly cannot be fulfilled by the ECE diagnostic alone. It is not possible to uniquely determine the electron distribution function from a measurement of the ECE, but an approach where the calculated spectrum is fitted to the measured spectrum is possible in principle and requires the development of codes that can handle non-Maxwellian distributions. In general, reflections of the radiation cannot be eliminated in the experiments and so models of the combination of the plasma inside a reflecting chamber are needed. In short, the diagnostic contribution to the full measurement of the runaway electrons energy range is limited but still can provide some useful information about the EDF distortion. Therefore, a supplementary role for this measurement is justified.
The updated baseline design will include four circular smooth-wall waveguides for the transmission lines (both perpendicular and oblique). The rectangular smooth-wall waveguides and circular corrugated waveguides are analysed as alternative design options. The experimental characterization of all types of possible transmission lines will be executed during the preliminary design phase. Based on experimental results, the choice that enables most of the measurements given by PR/SRD will be made for the transmission lines, ensuring that the diagnostic performance is met to the specifications given for the primary measurement roles (temperature profile measurements, NTM amplitude).

During the Preliminary Design Phase, simulations with GENRAY and ECESIM will be ran for different plasma scenarios (for worst cases; including half-Bt) to identify limitations of the diagnostic in ITER. Some preliminary assessment for the oblique line resolution is also reported in the following presentation: SPECE simulations for ITER by D. Farina (9FFLLP).

[1] A.J.H. Donné *et al.,* Nucl. Fusion **47**, S337 (2007)
[2] de la Luna E. *et al* 2003 *Rev. Sci. Instrum.* **74** 1414
[3] M. BORNATICI, et al, 'Electron Cyclotron Emission and Absorption in Fusion Plasmas', Nucl. Fusion, 23 1153 (1983)
[4] G. TAYLOR, 'Recent Developments in Electron Cyclotron Emission Research on Magnetically Confined Plasmas', Fusion Science and Technology, 52, 119 (2007)
[5] N. C. LUHMANN et al, 'Chapter 3: Microwave Diagnostics' Special Edition of Fusion Science and Technology on MFE Diagnostics, 53 No 2, 335 (2008)
[6] C. Sozzi, D. Farina *et al*., in Proc. of EC-15 Workshop, Yosemite Park, USA (2008)
[7] T.P. Goodman *et al*., Fusion Sci. Technol. **53**, 196 (2008)
[8] W. H. M. CLARK, 'Precision of Electron Cyclotron Emission Measurements from DITE Tokamak', Plasma Physics and Controlled Fusion, 25, No 12, 1501 (1983)
[9] M. Austin *et al*., 'Electron Temperature Measurements from Optically Grey Third Harmonic Electron Cyclotron Emission in DIII-D Tokamak', Phys. of Plasmas, 3, No 10, 3725 (1996)
[10] V.S. Udintsev *et al*., Rev. Sci. Instrum. **72**, 359 (2001)

Discrepancy between Thomson scattering and ECE (references herein are local to this sub-section)

TFTR and JET have reported a "TS - ECE discrepancy" at higher (Te > 5 keV) temperatures in auxiliary heated (ICRF + NBI) plasmas. Because Thomson scattering measurements are subject to statistical noise which leads to scatter in the measurement points, it was not at first clear that this was indeed a real effect and since it was contrary to expectations, and potentially very important, very careful experimental work was needed [1]. Systematic errors can occur in both ECE and Thomson scattering measurements and could lead to such an effect. No such errors were found. The observation of a similar effect on JET, where

the instrumentation was not only different but in the case of Thomson scattering a different approach was adopted (LIDAR rather that conventional), confirmed the existence of the effect [2]. The initial thoughts were that a population of relatively high energy electrons existed in the plasma and they had the effect of raising the average electron energy. ECE and Thomson scattering measurements sample the velocity distribution in different ways and so this could perhaps lead to the discrepancy. However, it was soon realized that because ECE measurements probe the plasma from the low field side, and therefore only sample the low energy electrons in the velocity distribution, they should be relatively immune to such populations. A more likely explanation was advanced by Taylor et al [3] and that is that the discrepancy may result from the strong coupling from the energetic ion beams used to heat the plasma with the plasma electrons in the low energy range. As a consequence the electron velocity distribution is distorted in this region and the ECE is enhanced. This could also explain the difference between the radiation temperatures of the second and third harmonics observed on JET. The optical depth is not so high in the third harmonic and so more of the velocity distribution is sampled in the measurement. On the other hand, given that electron-electron collisions are very effective at restoring a Maxwellian velocity distribution it is not at all clear how such a distortion can exist quasi-statically.
Recently, studies were perfomed at Alcator C-Mod to see whether or not discrepancy has been present. Experimental data at C-Mod show that TS - ECE agrees up to 8 keV: data do not show TS-ECE Discrepancy [4]. Future experiments at higher Te are planned to reach higher temperatures.

[1] A.E. Costley, “50 Years of ECE Research”, Fusion Sci. Technol. **55**, 1 (2009)
[2] E. DE LA LUNA et al, ‘Impact of Bulk Non-Maxwellian Electrons on Electron Temperature Measurements’, Rev. Sci. Instrum. 74, 1414 (2003))
[3] G. TAYLOR et al, ‘Electron Cyclotron Emission Measurements on High β TFTR Plasmas’, Proc. Ninth Joint Workshop on Electron Cyclotron Emission and Electron Cyclotron Resonance Heating (EC-9), 485, Borrego Springs, California, January, 1995.
[4] A.E. White et al., in Proc. of EC-17 Workshop, The Netherlands (2012).

3.4 Particular challenges for implementation on ITER

The main challenges for the implementation on ITER are as follows:

- Front-end optics designs should be optimised for required spatial resolution and to accommodate plasma height variation to fulfil measurement requirements;
- Design of the vacuum- and radiation-compatible hot body source and shutter mechanism;
- Integration of the front-end optics, the hot body calibration sources and shutter mechanism into the Equatorial port plug;
- Design and integration of the of the primary confinement barrier and alignment system with front waveguide holder;
- Design of the ex-vessel supports for waveguides which would be able to withstands the stresses induced by electromagnetic forces, thermal expansion and mechanical loads;
- Protection of transmission line, quasioptics and microwave solid state components from ECH and other stray radiation;
- Design of instrumentation able to perform fluctuation and profile measurements with sufficient resolution simultaneously to meet measurement requirements;
- Provide a capability to perform real-time analysis for feedback control;
- Design and integration of optics arrangement for Michelson interferometer four channels.

4 Special safety considerations

- The primary confinement barrier should be monitored by SVS for possible leaks.
- Protection from ECH stray radiation and ECH power during start-up.

On ITER, two confinement systems shall be provided for each principal inventory of radioactive or hazardous material unless formal project approval for a single confinement system is given. Each confinement system shall include one or more static barriers or dynamic components to confine the inventory at risk. The transmission lines of all microwave systems on ITER should provide confinement function in all situations. Other requirements, such as boundary monitoring, are also important. The first confinement barrier must withstand 2 bar peak pressure, and must be tested up to 3 bar peak pressure.

The design and choice of material for windows should not only provide the required confinement function, but also not degrade the performance of the diagnostic by introducing reflections, mode conversion, or signal losses. There are several options which can fulfil the requirements, for example, a "standard" double-window assembly with the window interspace monitored by the SVS (see *ITER_D_2MPLC2* - **Technical Bases for the Technical Specifications of the Window Assembly** (in work) and **ITER Practice for Replaceable Non-Metallic Windows,** *ITER_D_2NDP8C* - Executive Summary: ITER Practice for Windows), as has been proposed for the ECE (55F1F10). The general strategy for window assemblies on ITER is given below:

- 1st: the primary sub-assembly, which includes parts that are exposed to the primary vacuum of the vacuum vessel. During accidental conditions, such as a loss of coolant inside the vacuum vessel, a failure of the primary sub-assembly could lead to a contamination of the inter-space volume and the secondary vacuum system piping. The safety classification of the primary window sub-assembly is consequently SIC-1.
- 2nd: the secondary sub-assemblies, which mitigate the consequences of a primary sub-assembly failure and are not required for ITER to reach a safe state, are SIC-2 classified.
- 3rd: the interspace pressure monitor used to detect a failure in the primary sub-assembly or in the secondary sub-assembly, are SIC-2 or Safety Relevant classified, depending on the maximum inventory of air entering the Vacuum Vessel.
- 4th: the temperature monitoring devices and the cooling devices, which may be used for the high power pulsed laser windows are SIC-1 classified.
- 5th: the valves installed on high power pulsed laser viewing lines are SIC-2 classified.
- 6th: the monitoring of the optical and wave signal transmission and light scattering enabling to detect the ageing of the window assemblies are Safety Relevant.
- 7th: other devices such as gas heating devices, window heater, … which might be contemplated in the future so as to improve the robustness of the primary window sub-assemblies would be not SIC classified.

Although the secondary window assemblies are SIC-2 components, the requirements for their design, validation, manufacture, factory acceptance and installation will be the same as primary window sub-assemblies, which are SIC-1 classified.

ECE diagnostic will interface torus vacuum through double-walled diagnostic window assembly. Space in between these two walls will be monitored by service vacuum system (SVS). The schematic representation of the primary confinement barrier for the ECE is given in Fig. 4.1.

For the VV inventory second confinement barrier for ECE, a single window is considered at the Gallery – Diagnostic area boundary. The material for this window is not finalized yet, but it could be similar to this for the secondary window in the primary confinement barrier.

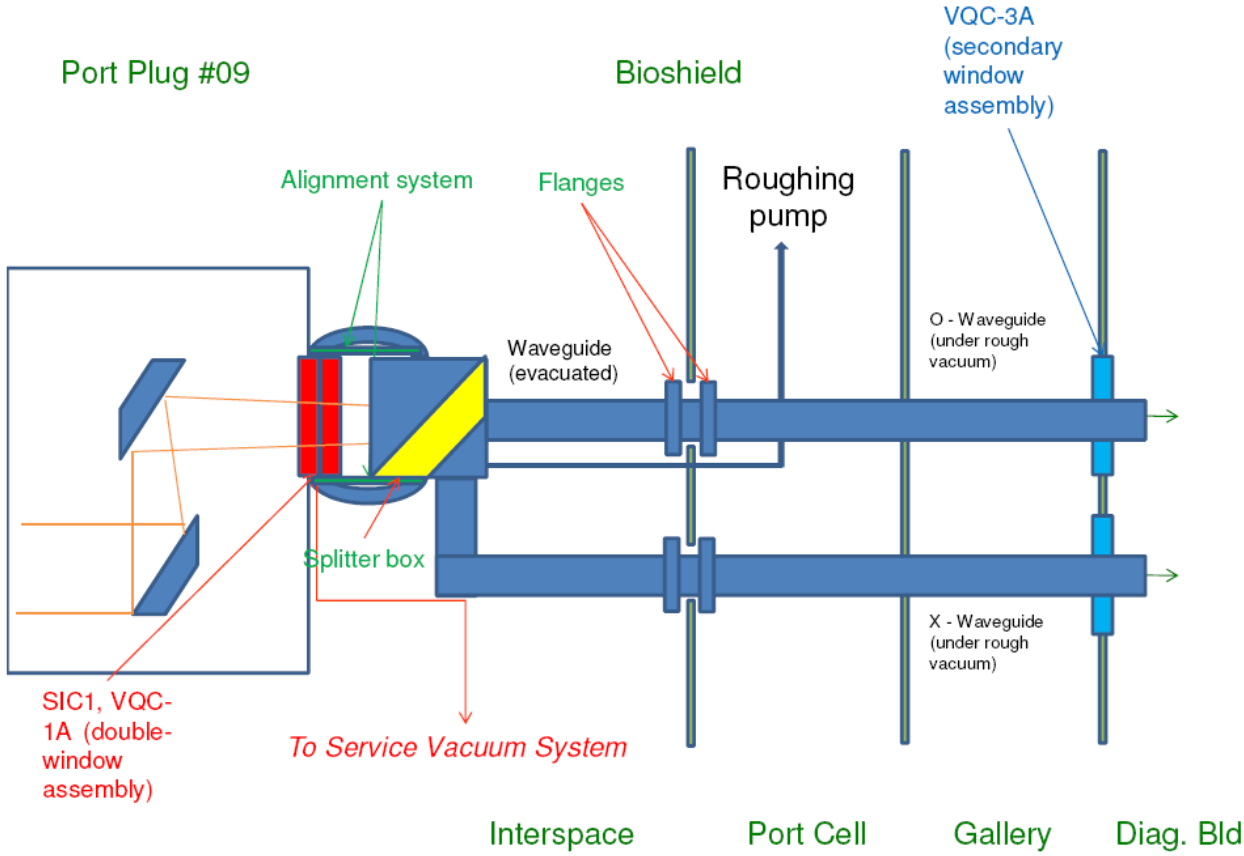

Figure 4.1. Primary confinement barrier for 55F1F10 ECE diagnostic. The secondary windows, and the waveguide leading to it, are classified as SIC-2.

5 Assumptions

5.1 Location

The system is located in the Equatorial Port 9, in the central drawer (DSM). The waveguides are routed through the interspace, Bioshield and the Port Cell to the Gallery and further to the Diagnostic Area. The waveguides are supported by the Interspace Support Structure and the Port Cell Structures.

The CAD models are presented in details in Section 9 of this DDD.

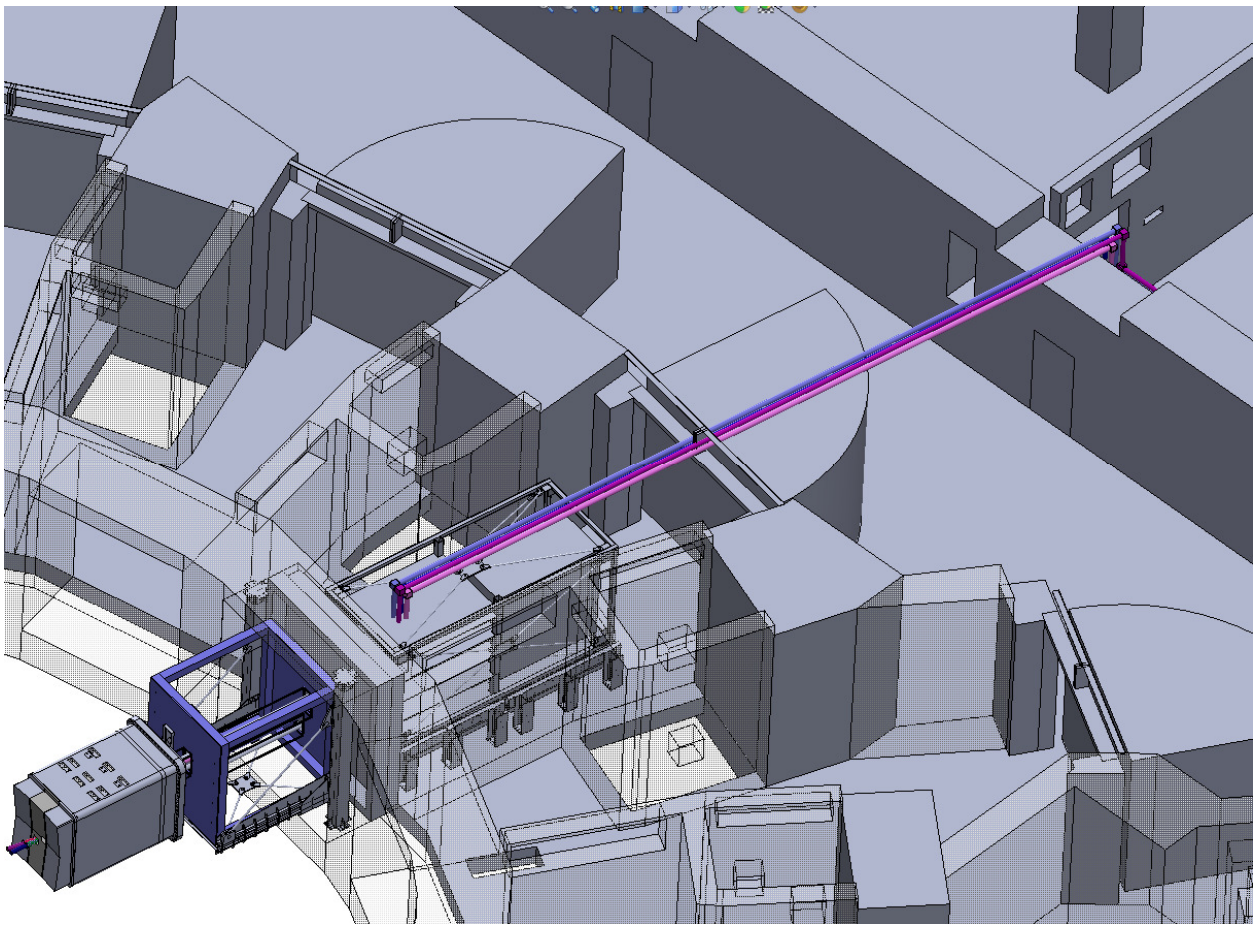

Figure 5.1. Overview of the 55F1 ECE system components in the Equatorial Port 9.

5.2 Space allocation

- Space in the middle drawer (DSM), as viewed from the plasma, in the Equatorial Port Plug 9 is reserved for the ECE front-end optics and hot sources.
- Space on the flange of the Equatorial Port Plug 9 to accommodate double-window assembly and guiding system.
- Space in the Interspace structure to support waveguides.
- Penetrations in the bioshield to route waveguides.
- Space in the Port Cell structure to support waveguides, vacuum pump and splitter boxes.

- Space in gallery with penetrations to route the waveguides.
- Space for mm-wave and electronics equipments in the dedicated diagnostic areas (Building 74).

5.3 Availability of particular capabilities not included in the proposed design

In-vessel remote handling tools (Multi-Purpose Deployers (MPD) – articulated arms) will be required to perform the front-end maintenance, alignment and calibration during D-T operational phase. The MPD is not in the scope of the PA associated with 55F1; however, the end-effector design for the in-vessel hot source to interface with the end-effector on the MPD is the responsibility of the diagnostic developer.
Interspace Support Structure and Port Cell Support Structures should be available to host and support waveguides of the 55F1 diagnostic in the interspace and in the port cell (see Annex 5.1).
Due to the possible high activation of the interspace and/or port cell components, a solution for the ECE equipment handling compatible with RH requirements may be developed.
The RH tooling required for refurbishment of the ECE components within the drawer in the Hot Cell Facility is subject for development by the design developer, unless these refurbishment operations can be performed by standard (baseline) RH tools in the Hot Cell Facility.

6 Detailed Design Description

6.1 Functional specifications for this system

6.1.1 Requirements from PR and SRD

The overview of system requirements for 55F1 ECE diagnostic from PR/SRD is given in the Table 6.1.

The system has a primary role in the measurement of the core electron temperature profile (measurement parameter 052) and high frequency instabilities (measurement parameter 061) that includes MHD, NTMs (δT/Te complex; 100 ms integration time), and Alfven Eigenmodes (AEs). The system has a backup role in the measurement of H-mode, ELMs and L-H mode transition indicator (i.e. measurement parameter 032). The ECE diagnostic has a supplementary role in the measurement plasma energy (measurement parameter 006), radiated power (measurement parameter 008), runaway electrons (measurement parameter 034 & 035), edge electron temperature profile (measurement parameter 053) and high frequency instabilities (i.e. TAEs δN/N & δT/T, measurement parameter 063). The range of measurements and the required accuracy are given in the corresponding column in Table 6.1.

ITER is unable to operate without a working diagnostic providing every 1a-group parameter. For advanced operation, ITER is unable to operate without a working diagnostics providing every 1b-group parameter.

Table 6.1. Overview of the system requirements for 55F1 ECE Diagnostic from PR/SRD.

Title	Parameter	Role	Highest Operation Role	Range Value Coverage	Condition	Time Resolution	Spatial Resolution	Accuracy
04. Plasma energy	*006: βp*	*Supplementary*	*1a.1 MP*	*.01 - 5*	*Ip > 3 MA*	*100 us*	*Integral*	*5% @ βp=1*
05. Radiated power	*008: Main plasma Prad*	*Supplementary*	*1a.2 BC*	*0.1 MW - 1 GW*	*Default*	*1 ms*	*Integral*	*10%*
14. H-mode, ELMs and L-H mode transition indicator	032: ELM temperature transient	Backup	2. PHY	0.05 - 10kev	r/a > 0.85	0.1 ms	5 mm	5%
15. Runaway electrons	*034: Emax*	*Supplementary*	*2. PHY*	*1 - 100 MeV*	*(blank)*	*10 ms*	*-*	*20%*
15. Runaway electrons	*035: I runaway*	*Supplementary*	*2. PHY*	*(0.05 - 0.7) x Ip*	*After thermal quench*	*10 ms*	*-*	*30 % rel.*
15. Runaway electrons	*035: I runaway*	*Supplementary*	*2. PHY*	*0 - 1 MA*	*Failed breakdown*	*10 ms*	*-*	*50 kA*
23. Electron temperature profile	**052: Core Te**	**Primary**	**1b. AC**	**0.5 - 40 keV**	**r/a < 0.85**	**10 ms**	**a/30**	**0.1**
23. Electron temperature profile	*053: Edge Te*	*Supplementary*	*2. PHY*	*0.05 - 10 keV*	*r/a > 0.85*	*10 ms*	*5 mm*	*0.1*
27. High frequency instabilities (MHD, NTMs, AEs, turbulence)	**061: NTM δT / Te. (complex; 100ms integration time)**	**Primary**	**1b. AC**	**(0.1 - 5) x 1E-2**	**Te > 1 keV,**	**100Hz - 10kHz**	**(m,n) < (2,1),(3,2). dr=50mm**	**1 x 10-3**
27. High frequency instabilities (MHD, NTMs, AEs, turbulence)	*063: TAE δN / n, δT/T*	*Supplementary*	*2. PHY*	*5E-6 - 5E-4*	*(blank)*	*30 kHz - 2 MHz*	*n = 10 - 50*	*0.3*

6.1.2 Other ITER diagnostics interaction

Measurement parameter 52: Core electron temperature profile

This parameter is for advanced control (Group 1b). 55F1 ECE system and 55C1 Core Thomson scattering are primary diagnostic systems for core electron temperature measurement. Thomson scattering provides the measurement of temperature versus position which is then converted into temperature profiles for a given equilibrium. The Thomson scattering system based on LIDAR principle (the same optical elements are used for both the laser beam and for the collected scattered light inside the same port) can utilize two different lasers, so a trade off can be made between time and spatial resolution [*A.J.H. Donné et al, Nucl. Fusion **47**, S337 (2007)*]. One laser (t = 300 ps) could provide about 7 cm resolution (a/30) at moderate time rate (10 Hz), while the second laser (t = 1 ns) would allow for a faster measurement rate (100 Hz) with a more coarse spatial resolution (20 cm). For a spatial resolution of 6–7 cm detectors would be required with response time better than 300 ps and large spectral bandwidth (Te in ITER could reach values above 30 – 40 keV, leading to a very broad scattering spectrum).

ECE would provide a measurement which would be less sensitive to first-mirror degradation because of the long wavelength (about 1000 times longer than that of Thomson scattering). Therefore, stainless steel mirrors with modest optical quality requirements can be used. The diagnostic will provide Te with a large bandwidth (>10 kHz). The high temperatures foreseen in ITER (30–40 keV) will affect the spatial resolution, due to the larger relativistic and Doppler broadening, which will lead to a widening of the radial extension from which a given frequency in the ECE spectrum is emitted. The target of a/30 would be possible only in regions with a low enough value of Te (typically r/a > 0.5 for Te(0) = 30 keV on ITER). The relativistic downshift at the high temperatures in ITER is substantial and will strongly limit the access to the plasma. It is important to remark that the high temperature scenarios considered for ITER (Te(0) up to 40 keV) would degrade the spatial resolution of Te due to a further widening of the emission layer. In the case of LIDAR the very wide spectrum will reduce the accuracy of Te at the highest temperatures but not affect the spatial resolution.

In scenarios with strong additional heating (radio frequency, neutral beam and possibly alpha heating), deformations of the electron distribution function can occur. In such cases, there is no single value of the ‘temperature’ and temperature ceases to be a useful parameter—a description of the velocity distribution is needed. Both ECE and Thomson scattering will be affected by such distortions but differently. Having two independent diagnostics that sample the velocity distribution in different ways is a great advantage in this situation since it makes it obvious that such distortions are present. Simultaneous observation of several ECE harmonics and (if access restrictions allow for) oblique ECE observation may provide information on the velocity distribution.

55E5 X-Ray Crystal Spectrometer (core high resolution) is a backup system, and 55E7 Radial X-Ray camera is a supplementary diagnostic for this measurement.

The measurement of the core Te is required for Advance Control (AC). The ECE diagnostic could generate an estimate of the core temperature profile (or a fraction of the core profile) as fast as 10 ms for control purposes. To do this optimally, the system would require equilibrium data and absolute calibration.

Measurement parameter 053: Edge electron temperature profile

Edge electron temperature profile is for evaluation and physics studies (Group 2). 55F1 ECE diagnostic has a supplimentary role. The study of the edge resolution made in late 90-s by D. Bartlett confirms that it does not meet the 5 mm ITER target requirement. The edge resolution is between 4 and 7 cm in X-mode. To meet the ITER requirements of having a spatial resolution of 5mm in the edge region, an Edge Thomson scattering system (55C2) is foreseen (primary role for this measurement).

The backup systems are 55ED X-Ray Cristal Spectrometer (Edge High resolution) and 55EI X-Ray Cristal Spectroscopy Edge Imaging. Another supplementary role is assigned to 55E7 Radial X-Ray camera.

Measurement parameter 061: NTM δT / Te (complex; 100ms integration time)

This parameter is for advanced control (Group 1b). 55F1 ECE system is the only system to deliver this measurement; therefore, it has a primary role. For the purpose of NTM detection, ECE is an essential measurement because it gives the localization of the island. NTMs on ITER (m/n = 2/1, 3/2) will be localized at r/a = 0.5 – 0.85. The critical island width is expected to be between 20 – 40 mm, defined as $\Delta r = \Delta T_e/(dT_e/dr)$. The ECH deposition widths for the NTM stabilization are in the range of 30 – 70 mm. The island with the width of $w > 20$ mm is detectable by ITER ECE. Thus, assumption for ECE channel separation of 20 mm or smaller at NTM radii is adequate for the mode detection. The response time of the feedback system once the mode is tracked is in the order of 30-50 ms. An integration time of 100 ms for mode signature detection in the T_e profile is comparable to the growth time of the NTM.

Response to the NTM in ECE measurements is limited by the intrinsic resolution of the instrument which includes the relativistic broadening and the antenna pattern. Also, the signal-to-noise ratio limits the minimum island size to about 2 cm for a $\Delta T_e/T_e$ ~1%. To make the NTM detection and ECH feedback more efficient, correlation technique with another ECE line-of-sight or with magnetic diagnostics can be used to increase the sensitivity of the measurements. Similar approach is being successfully used on AUG.

Measurement parameter 063: TAE dn/n, dT/T

This parameter is for evaluation and physics studies (Group 2) and expected to be processed off-line for pulse periods where TAE physics are interesting based on fast data from many diagnostics. 55F1 ECE system has a supplementary role for this measurement. Moving MHD modes, fishbones and Toroidicity-Induced Alfven Eigenmodes (TAEs) can be detected as a temperature fluctuation. By measuring at 2 or more points, the wavenumber characteristics of these modes can be deduced. For relatively long-lived, quasi-coherent modes, the sensitivity of ECE is very high, and quantitative measurements of the temperature perturbation level and mode profile can be made. This is not necessarily the case if growth on a short timescale needs to be observed, as would be the case for a control system.
55F9 HFS Reflectometry, 55F2 LFS Reflectometry and 55C5 Toroidal Interferometer/Polarimeter are primary diagnostic systems for the measurement of dn/n. For reflectometers, this assumes that the raw data can be stored during density sweeps and correlated with magnetics.

55C5 TIP should be sensitive to the full range of modes listed, but cannot discriminate in n number; nevertheless it is considered to have a primary role.
The 55C5 interferometry/polarimetry system gives line-integrated values along its lines-of-sight. 55C6 Polarimeter and 55E15 Beam Emission Spectroscopy are backup systems for TAE dn/n. 55B1 Radial Neutron Camera, together with 55E7 Radial X-ray Camera, are supplementary systems for dn_e/n_e and dTe/Te. Note that 55F1 ECE system is only for dTe/Te measurement, whereas 55E7 Radial X-ray Camera gives a cross-product for dn_e/n_e and dTe/Te.

Measurement parameter 006: poloidal beta (βp)

A ratio of the magnetic energy to the pressure of the plasma is a useful figure of merit of the plasma confinement and energy. This parameter is for basic control (Group 1a2). The primary diagnostics for this measurement are 55AF Diamagnetic Main Loop and 55AG Diamagnetic Compensation Coils. 55F1 ECE system has a supplementary role because it only contributes to the Te(r) in the estimation of βp. Other diagnostics with supplementary role for this measurement are 55C1 Thomson Scattering LIDAR (Core), 55E1 CXRS Based on DNB (Core) and various magnetics such as 55A2, A9, AC (inner), AH, AO (Divertor).

Measurement parameter 032: ELM temperature transient

For the very small bandwidth (~ 1 GHz) necessary for optimum edge measurements on ITER, for temperature perturbations exceeding a few % the time resolution of ECE is very good (< 1 μs). Thus the diagnosis of significant ELM-associated temperature perturbations by ECE will only be limited by the spatial resolution, similar as for the measurement parameter 053 – edge temperature profile. That is why 55F1 ECE system has a backup role for this measurement.

55E7 Radial X-ray Camera has the primary role for this measurement, whereas 55C2 Edge Thomson scattering and 55EC CXRS Based on DNB (Edge) have supplementary roles.

Measurement parameter 008: main plasma Prad

This parameter is for machine protection (Group 1a1). The power loss from ECE is a part of the total power loss from the plasma which roughly equals to 10% of the latter. Therefore, surveying the ECE up to the high frequencies (of about 1 THz) to reach optically thin plasmas is the contribution to this measurement from 55F1 ECE. From the comparison between optically thick and thin harmonics spectra, a direct measurement of the wall reflection coefficient is also possible. This measurement will probably be performed during each experimental campaign on ITER, to account for possible changes in the inner wall reflectivity.

The primary role to measure the power loss from the plasma is assigned to bolometers (55D1). The ITER measurement requirement is a time resolution of 10 ms (3 ms during disruptions) and a spatial resolution of 20 cm for bulk-plasma profiles and 5 cm in the divertor. The required time resolution for bolometers is similar to what is achieved on present-day machines, whereas the required spatial resolution is significantly higher than that achieved on present-day machines with around 100 lines of sight. Consequently, several hundreds of lines of sight are required on ITER given the two-dimensional nature of the profile reconstruction problem. At present 300–350 bolometer channels are foreseen, most of which are nearly in the same poloidal cross-section. 55E7 Radial X-ray Camera has the backup role for this measurement, whereas 55E3 VUV (Main Plasma) and 55E5 X-Ray Crystal Spectrometer (core high-resolution) have supplementary roles.

Measurement parameters 034 and 035: runaway electrons – Emax and runaway current

These parameters are for evaluation and physics studies (Group 2). ECE emission spectrum is sensitive to the presence of non-thermal electon population. In scenarios with strong additional heating (radio frequency, neutral beam and possibly alpha heating), deformations of the electron distribution function can occur. In such cases, there is no single value of the 'temperature' and temperature ceases to be a useful parameter—a description of the velocity distribution is needed. ECE is affected by such distortions. Simultaneous observation of several ECE harmonics and oblique ECE observation may provide information on the velocity distribution. However, there is only only one oblique line-of-sight in the ITER ECE design; therefore, a capability of the diagnostic to assess non-thermal parameters is limited and, thus, the measurement role is supplementary. It is not possible to uniquely determine the electron distribution function from a measurement of the ECE, but an approach where the calculated spectrum is fitted to the measured spectrum is possible in principle and requires the development of codes that can handle non-Maxwellian distributions. In general, reflections of the radiation cannot be eliminated in the experiments and so models of the combination of the plasma inside a reflecting chamber are needed.

The primary diagnostics for Emax are 55B7 Radial Gamma Ray Spectrometers, 55BD Vertical Gamma Ray Spectrometers, 55G1 IR Cameras, Vis/IR TV (Midplane) and 55E7 Radial X-ray Camera. For the runaway current measurement, the primary systems are 55B7 Radial Gamma Ray Spectrometers, 55BD Vertical Gamma Ray Spectrometers, 55E7 Radial X-ray Camera, 55EE Hard X-ray Monitor (H-phase) and 55G1 IR Cameras, Vis/IR TV (Midplane).

6.1.3 Functional Analysis

Hereafter the functional breakdown is reported for two levels (Level A: general, Level B: more details)

Level A

1 Receive mm-wave
2 Route signals
3 Analyse signals
4 Provide real-time measurements for PCS
5 Provide quasi-real-time measurements for operator's feedback
6 Determine off-line output parameters

Level B

1 Receive mm-wave

10 View plasma through the apertures in the Diagnostics First Wall (DFW)
11 Withstand thermal, EM, nuclear, seismic and gravity loads
12 Receive mm-waves to/from plasma
13 Provide in-situ alignment & calibration (By RH tools)

2 Route Signals

20 Route quasioptically mm-waves through the Equatorial Port Plug 9

21 Transmit signals through the windows assembly to ensure vacuum integrity and safety

22 Split polarizations in the splitter boxes

23 Route mm-waves in the waveguides through the Port Interspace, Bioshield, Port Cell and Gallery to the Diagnostic Area

24 Distribute mm-waves; RF-IF transformations for different bands (radiometers), full-band survey (Michelson)

3 Analyse signals

30 Downconvert signals from RF to IF range of frequencies for different bands

31 Detect and digitize IF signals

32 Distinguish useful signal from noise; generate signals vs frequency (channel nrs)

33 Store raw signals, noise and calibration data to local controller storage

34 Store Transmit all data to CODAC PSH

4 Provide real-time measurements for PCS

40 Adapt calculation model to conditions

41 Evaluate errors, validity and quality

42 Calculate Edge/Core electron temperature profiles vs time; estimate the total plasma ECE radiation; calculate NTM amplitude

43 Provide PCS with real-time data

5 Provide quasi-real-time measurements for operator feedback

50 Adapt calculation model to conditions

51 Evaluate errors, validity and quality

52 Calculate electron temperature profiles vs time, the total plasma ECE radiation, NTM amplitude

53 Calculate spectral characteristics of TAEs and turbulence

54 Store processed data (CODAC)

6 Determine off-line output parameters

60 Contribute to crosscheck with other Temperature, MHD and turbulence diagnostics

61 Contribute to determination of the final temperature profiles and spectral characteristics for MHD and turbulence

A block level diagram is sketched in Fig. 6.1. For RAMI analysis, some parts of the present functional block level diagram were used to evaluate the potential risks for the machine operation (see Section 19 for details).

6.1.4 Measured parameters

Table 6.1 lists and describes the parameters measured by the 55F1-F10 ECE diagnostic (see Section 6.1.1).

Note that, on ITER, a scenario with $3x10^{20}$ m^{-3} flat density profiles in the core are very unlikely to be realised; a density profile peaking of 2 with maximum value of $2.5x10^{20}$ m^{-3} is feasible when operating near n_{GW} ($2.7x10^{20}$ m^{-3} for 17 MA), though *[A. Loarte, Private Communication]*. This needs to be taken into account for the correct Te-profile reconstruction for which the information on the electron density profile is required.

6.1.5 Complementar y parameters

To provide the necessary measurements, ECE diagnostic relies upon the equilibrium and electron density profiles provided by PCS and CODAC.

Diagnostic can be used in the NTM protection loop.

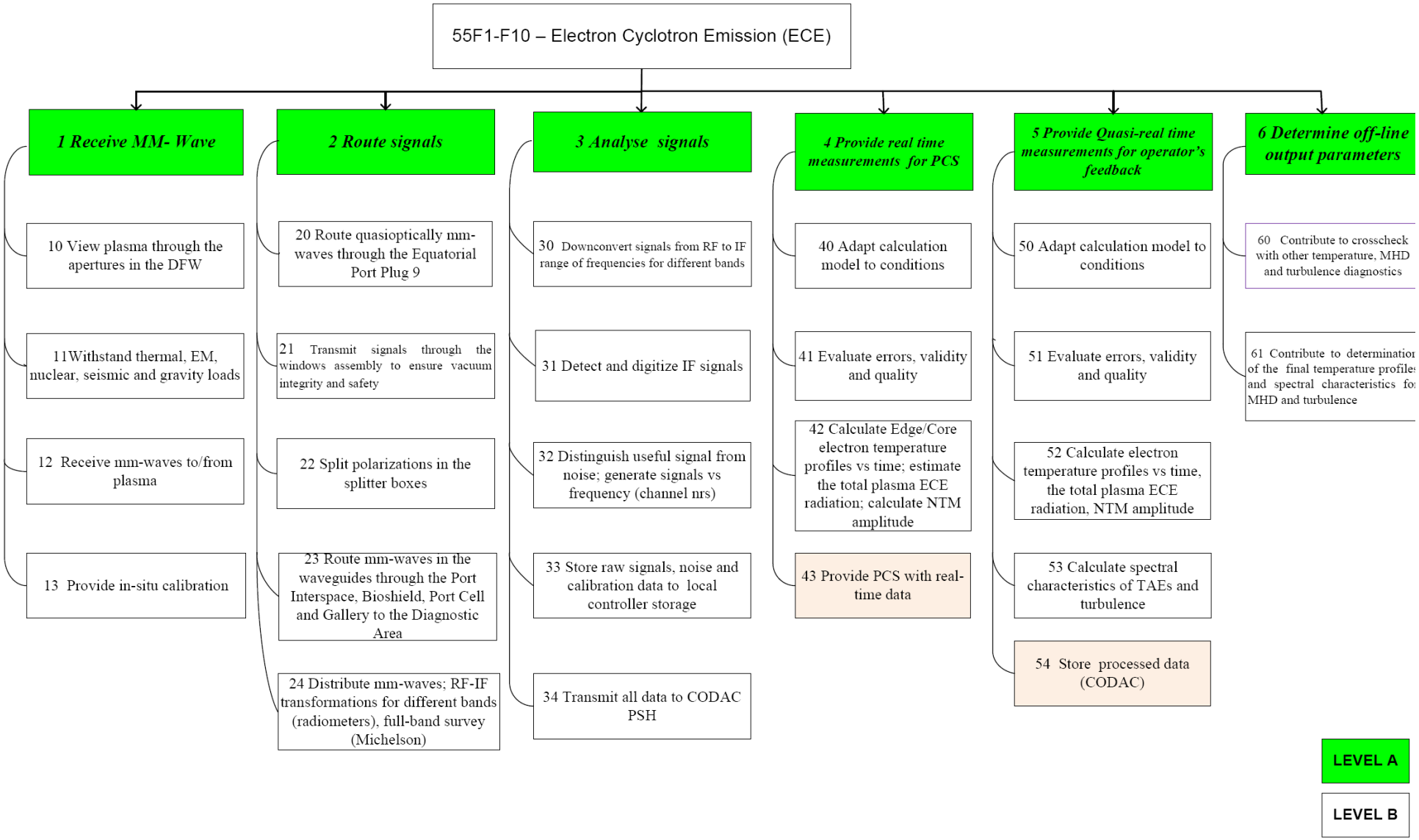

Figure 6.1. Functional breakdown for 55F1 ECE system.

6.1.6 Other assumptions and analysis

The system can be used in a feedback loop for NTM stabilization.

6.1.7 Set of specifications for the 55F1 ECE system

The assessment of the diagnostic performance and its specifications are given in Section 7.

6.2 Description of design development and optimization

6.2.1 Basic principles

The ECE diagnostic is based on the measurement of electron cyclotron emission power from the plasma. Due to the inverse dependence of the B-field strength with respect to major radius R, the emission frequency for a cyclotron harmonic has a one-to-one correspondence with a location along the radius. Under conditions typical in a tokamak, the emission at certain harmonics is "optically thick", i.e. emits as a blackbody, so the measurement of the power at these frequencies is directly related to the electron temperature of the plasma:

$$P = kT_e\Delta f \qquad (6.2.1)$$

where k is Boltzmann's constant and Δf is the frequency bandwidth of the measurement. There are two propagation modes of ECE in a magnetic field, one with the electric field parallel the magnetic field, the ordinary or O-mode, and the other with the electric field perpendicular, the extraordinary or X-mode. For modern day tokamaks and ITER, the first harmonic O-mode and second harmonic X-mode emission is blackbody across most of the plasma radius so measurement of the emission over these frequencies gives the temperature profile as a function of time: $T_e(R,t)$.

Charged particles in a plasma can be subject to natural oscillations. The frequency of these electrostatic oscillations is called the plasma frequency ω_p. For the electrons, one gets:

$$\omega_{pe} = \sqrt{n_e e^2 / \varepsilon_0 m_e} \quad , \qquad (6.2.2)$$

where e and m_e are the electron charge and the rest mass respectively, n_e is the local electron density, and ε_0 is the dielectric permittivity in vacuum. During the period of the plasma oscillation, the local perturbation of the electron density, with respect to the undisturbed ion density, will be constrained within the distance called *Debije radius* r_{De}:

$$r_{De} = \mathrm{v}_{Te}/\omega_{pe} = \sqrt{\varepsilon_0 T_e / e^2 n_e} \quad , \qquad (6.2.3)$$

where T_e is the electron temperature in *keV*, and v_{Te} is the electron thermal velocity, adopting a Maxwellian electron velocity distribution.

Another kind of motion appears when one adds a magnetic field to the plasma. Then, charged particles also gyrate around the magnetic field lines due to the Lorentz force. This force is always

perpendicular to the local magnetic field direction and to the particle velocity vector (see Fig. 6.2). If the particle is an electron, its rotation frequency ω_{ce} is called the *electron cyclotron frequency*:

$$\omega_{ce} = 2\pi f_{ce} = \frac{eB}{\gamma m_e}. \qquad (6.2.4)$$

Here, f_{ce} is a frequency in Hz, e and m_e are the electron charge (in *Coulomb*) and the rest mass (in *kg*) respectively, B is the absolute value of the local magnetic field in T, and $\gamma = 1/\sqrt{1 - \mathrm{v}^2/c^2}$ is the relativistic Lorentz factor. For non-relativistic plasmas (v << c), one can assume γ to be equal to 1. If $\gamma >> 1$, the term $(1 - \mathrm{v}^2/c^2)$ describes the *relativistic line broadening*.
The radius of the circular rotation is called the *Larmor radius*:

$$\rho_{Le} = \frac{\gamma m_e \mathrm{v}_\perp}{eB}, \qquad (6.2.5)$$

where $\mathrm{v}_\perp$ is the velocity component perpendicular to $\vec{B}$. Since the electron gyration is

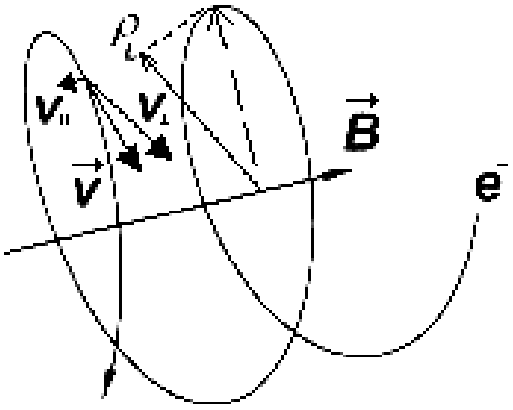

FIG. 6.2. Gyration of an electron around the magnetic field line. The rotation direction is a clockwise, as it is seen in the direction of $\vec{B}$. The Larmor radius is indicated as ρ_L.

periodic, it emits the radiation in a series of harmonics:

$$\omega_{cen} = \frac{n\omega_{ce}}{1 - \frac{\mathrm{v}_\parallel}{c}\cos\theta}. \qquad (6.2.6)$$

Here n is a harmonic number, $\mathrm{v}_\parallel$ is the velocity component parallel to $\vec{B}$, θ is the angle between the line of observation and $\vec{B}$. The term $(1 - \frac{\mathrm{v}_\parallel}{c}\cos\theta)$ is called *the Doppler broadening*. For $0 < \theta < 90^0$, one speaks of oblique ECE observation. If $\theta = 90^0$, Eq. (6.2.6) can be rewritten as:

$$\omega_{cen} = n\omega_{ce} = 2\pi n f_{ce}. \qquad (6.2.6a)$$

In reality, one will always encounter the situation where the Doppler and/or relativistic broadening cannot be completely neglected (e.g. because of the width of the antenna pattern). The electron emission lines have a finite width, as follows from the velocity distribution function. The line widths due to the relativistic and Doppler broadening can be approximated by:

$$\Delta f_{cen}^{rel} = n f_{ce} (\frac{\mathrm{v}_{Te}}{c})^2 \ , \tag{6.2.7a}$$

$$\Delta f_{cen}^{Doppler} = n f_{ce} \frac{\mathrm{v}_{Te}}{c} | N_r \cos\theta | , \tag{6.2.7b}$$

where N_r is the refractive index. These line broadenings play a role only if they are larger than the bandwidth of an individual ECE channel. For example, when relativistic (non-thermal) electrons are present in the plasma, or when the angle θ between the magnetic field vector and the observation line is different from 90^0. For the relativistic broadening, the line is also shifted towards lower frequencies. The Doppler broadening has a symmetrical Gaussian shape. In many cases, however, these lines broadening mechanisms can be neglected.

ECE radiation coming from the plasma is attenuated by waveguide losses. The source temperature T seen by the radiometer can be defined as follows:

$$T = \frac{T_e}{A} + T_{RN} + T_{EM} . \tag{6.2.8}$$

Here, A is the attenuation factor (aas derived from dB's), T_{RN} is the equivalent radiometer temperature noise, and T_{EM} is the parasitic noise due to electromagnetic pick-up (or any other systematic noise in the system – see [*V.S. Udintsev et al., Fusion Sci. Technol. 50, 508 (2006)*]).
Following [*H.J. Hartfuss, "Coherent Versus Incoherent Detection Schemes", in Proc. of the EC-7 Workshop, Hefei, China, p. 267 (1989)*], the noise equivalent power (NEP) for one polarisation direction due to fluctuations of the intensity of the thermal radiation can be written as:

$$NEP = kT(B_{IF} 2B_V)^{\frac{1}{2}}, \tag{6.2.9}$$

where B_{IF}, B_v are the IF and video bandwidths, respectively. The minimum detectable temperature difference $\tilde{T}_{\min}$ is obtained when the black body radiated power is equal to the NEP (i.e. when signal to noise ratio is unity):

$$k\frac{\tilde{T}_{\min}}{A} B_{IF} = k(\frac{T_e}{A} + \mathrm{T_{RN}} + \mathrm{T_{EM}})(B_{IF} 2B_V)^{\frac{1}{2}}, \tag{6.2.10a}$$

which can be rewritten as:

$$\frac{\tilde{T}_{\min}}{\overline{T}_e} = \sqrt{\frac{2B_V}{B_{IF}}}\left[1 + \frac{T_{RN} A}{\overline{T}_e} + \frac{T_{EM} A}{\overline{T}_e}\right]. \tag{6.2.10b}$$

If $T_e / A \ >> \ T_{RN}$, T_{EM}, Eq. (6.2.10b) reduces to:

$$\frac{\tilde{T}_{\min}}{\overline{T}_e} = \sqrt{\frac{2B_V}{B_{IF}}}\,. \qquad (6.2.10c)$$

For example, for B_v = 110 kHz and B_{IF} = 110 MHz (both values are taken at -3 dB), the minimum detectable normalized temperature is of 4.5 % (the thermal noise level). In experiments, however, it is often found that if the mean signal measured by the acquisition is smaller than 300 bits, the normalized RMS $\tilde{T}_{\min}/\overline{T}_e$ is highly influenced by the $(T_{RN} + T_{EM})$ term and, thus, is dominated by parasitic noise. These results are further confirmed by analysis of the correlated noise in the next Section. It is important to mention that, if any modes with a narrow bandwidth are present in the plasma, Eq. (6.2.10c) will be modified to:

$$\frac{\Delta T_{\min}}{\overline{T}_e} = \sqrt{\frac{B_{NBM}}{B_R}}\,, \qquad (6.2.10d)$$

in which B_{NBM} is the bandwidth of the mode ($0 < B_{NBM} < B_V$), and B_R is the bandwidth corresponding to the "effective" radial structure size ($0 < B_R < B_{IF}$). The radial width W_{IF} is determined by the radial resolution of the diagnostic.

6.2.2 Known restrictions

There are two main limitations to ECE measurements in tokamaks:

1. Harmonic overlap

Depending on the aspect ratio (a/R) the ECE harmonics overlap to some extent so over certain frequency ranges there are two or more emission locations for a given frequency (see Fig. 6.3). Since the last resonant zone is often not optically thick, the emission power is a combination from multiple regions and cannot be used for T_e. In practice this winds up limiting profile coverage coverage to the outer two-thirds of the plasma major radius, but this is still enough to cover the full minor radius.

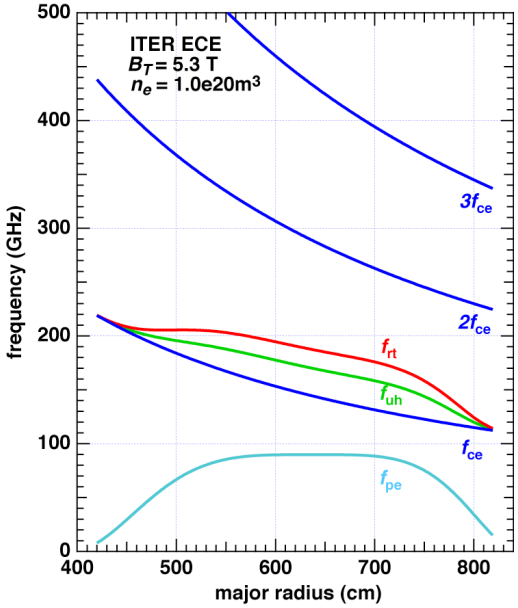

Figure 6.3. Plot of ECE and related frequencies versus major radius in ITER. Shown are the cyclotron frequencies f_{ce}, the plasma frequency f_{pe}, the upper hybrid resonance f_{uh} and the right-hand cutoff f_{rt}.

2. Cutoff

The propagation of electron cyclotron waves in the plasma is subject to various cutoffs and resonances. In particular the 1st harmonic O-mode and the 2nd harmonic X-mode can be affected by the cutoffs at the plasma frequency f_{pe} and right-hand frequency f_{rh}, respectively. Typical values of these are shown in Fig. 6.2.1. Both fpe and frh are functions of electron density and when this gets high enough, the wave is cutoff and cannot propogate to the antenna. This occurs quite often in modern tokamak experiments and is expected to happen in ITER.
For ITER another major limitation for ECE measurements arises because of the high electron temperature. For T_e's in the ranges of 10's of keV, relativistic frequency broadening becomes large so that the emission is no longer well localized. This is discussed in more detail in Section 7 of the present DDD.

6.2.3 Design history

Originally (in 2001 – see "**N 55 DDD 6 01-06-01 W 0.3**" Historical Baseline DDD document), the ECE system's front-end employed a Gaussian beam telescope with first two mirrors (see Fig. 6.4). The telescope could be thought of as projecting the radiation pattern at the mouth of the exit waveguide (in HE11 mode) to the resonance plane in the plasma. The mirror focal lengths were chosen to minimise the spot size in the core of the plasma for the minimum O-mode frequency, subject to the additional constraint of a first mirror size no larger than 200 mm aperture. The mirrors were assumed to be ellipsoidal. The telescope tube was to hold the first two mirrors in factory pre-aligned position.

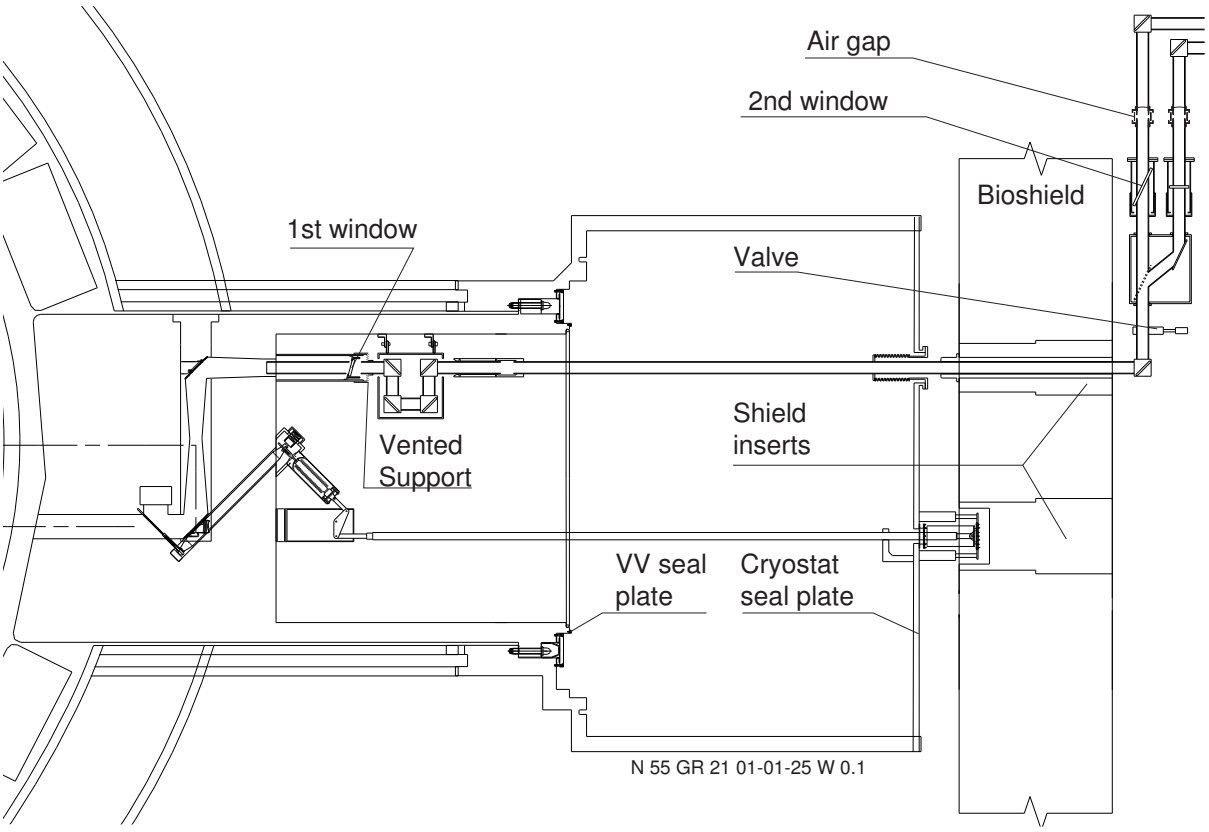

Figure 6.4. Schematic of the ECE front-end emphasising the location of vacuum boundaries and vents (historical baseline).

The 1st vacuum barrier was designed to be a fused silica window of 150 mm nominal diameter, supported on a plane inclined 15° to the direction of beam propagation to mitigate standing wave effects, and designed for over pressures to 5 bar in the primary vacuum side, and 2.5 bar on the secondary vacuum side.

The interspace waveguide was a straight piece of corrugated waveguide, with an oversize bearing and coupling assembly forming the second half of the movement compensation mechanism. In addition, it was designed to provide a gap in the transmission line which helps attenuate spurious waveguide modes.

For each waveguide, outside the cryostat and bioshield there was a design of a QO beam splitter, using a conductive grid printed onto a fused quartz substrate and inclined at the Brewster angle. This beam splitter has to separate the O and X polarisations with low power loss.

The secondary vacuum window was an in-waveguide SiN Brewster angle window (with 71° inclination).

The radiation from each antenna was designed to split in O and X-mode. Thus there were 4 waveguides transporting the radiation to the diagnostic hall, where the instrumentation was located. The waveguide was of the oversize circular corrugated type, with a diameter of 89.5 mm.

The waveguide was designed to be evacuated to reduce calibration uncertainties due to water absorption. Rough vacuum is sufficient for this purpose. The waveguide was interrupted by an air gap to ensure that, should both vacuum windows fail, the system vents into the pit. The pumping station for the waveguides was also in the pit. The total length of waveguide required was ~ 30 m for each line. An automated system of switches and selectable beam-splitters was to be provided to allow for the selection of transmission lines in real-time, with a switch-over delay of 0.25 s or less (see Fig. 6.5).

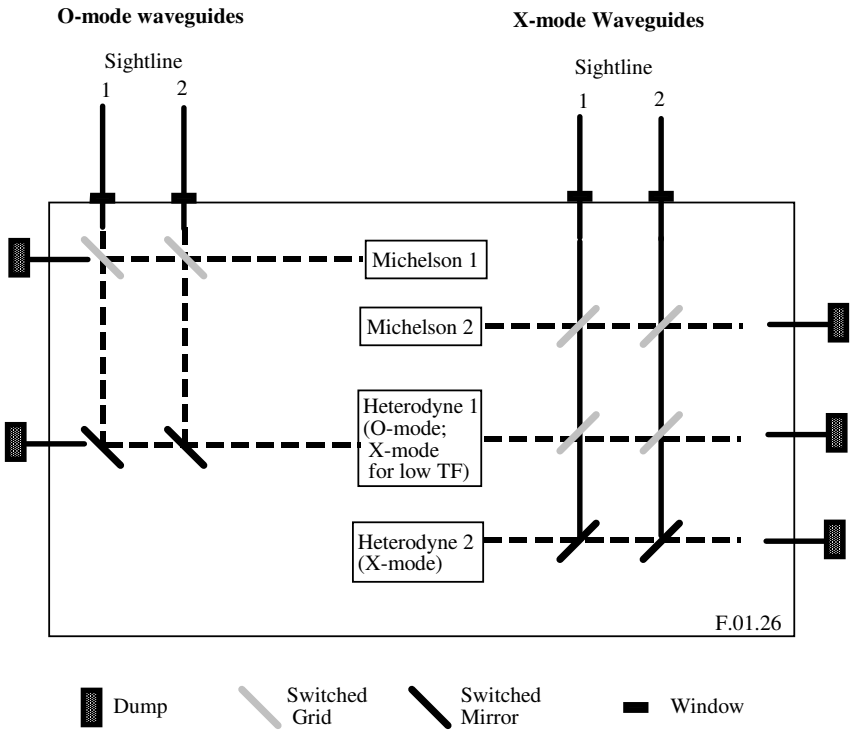

Figure 6.5. Connection diagram for the sightline switch-over unit (historical baseline).

The nominal specifications for the historical baseline design instruments are given in Tables 6.2, 6.3 and 6.4.

Table 6.2. Nominal specification for the O-mode heterodyne radiometer (historical baseline).

Parameter	Value	Comment
Type	Multi-band, Broadband multichannel receiver	
Frequency range	122 GHz – 230 GHz	
Channel separation (122-139 GHz)	1 GHz (18 Chan.)	F-band waveguide (edge); 1 mixer
Channel separation (141-169 GHz)	2 GHz (15 Chan.)	D-Band waveguide; 2 mixers
Channel separation (172-218 GHz)	3 GHz (16 Chan.)	G-Band waveguide; 2 mixers
Channel Separation (222-230 GHz)	4 GHz (3 Chan)	1 mixer
Duty cycle	continuous	
Detector	Mixer / IF Amp/ Detector	
Video BW	1 µs – 100 µs	Further integration to be performed digitally
Dimensions (L x W x H)	3 x 3 x 2 m	Excludes PSUs and electronics

Table 6.3. Nominal specification for the X-mode heterodyne radiometer (historical baseline).

Parameter	Value	Comment
Type	Multi-band, Broadband multi-channel / single channel receiver	
Frequency range	244 GHz – 355 GHz	
Channel separation (244-278 GHz)	2 GHz (18 Chan.)	edge; 2 mixers
Channel separation (282-298 GHz)	4 GHz (5 Chan.)	1 mixer; limit of multi-channel capability
Channel separation 302-338 GHz	4 GHz (10 Chan.)	10 mixers
Channel separation (343-353 GHz)	6 GHz (3 Chan.)	3 mixers
Duty cycle	continuous	
Detector	Mixer / IF Amp/ Detector	
Video BW	1 µs – 100 µs	Further integration to be performed digitally
Dimensions (L x W x H)	3 x 3 x 2 m	Excludes PSUs and electronics

Table 6.4. Nominal specification for the O- and X-mode Michelson spectrometers (historical baseline).

Parameter	Value	Comment
Type	Reciprocating mirror Martin-Puplett type Michelson interferometer.	
Spectral range	70 GHz – 1 THz	
Resolution	10 GHz	
Scan rep. rate	20 ms	
Duty cycle	continuous	
Detector	Indium Antimonide Hot Electron Bolometer	
Noise Equivalent Temperature at input	10 eV	
Dimensions (L x W x H)	3 x 2 x 2 m	Excludes detector, PSUs and Liquid He Supply equipment.

6.2.4 Current design

The baseline system design consists of two lines-of-sight, one looking perpendicular to the plasma and the second one oblique with the toroidal angle of 10 degrees. Each line-of-sight consists of: 1) front-end optics (focusing mirrors, hot source assembly with a shutter), 2) double-windows assembly, 3) quasioptical beam splitter, 4) transmission lines (TLs), and 5) instrumentation in the diagnostic building. Each sub-system is designed to enable the system to meet or exceed the measurement requirements where possible. The system requirements can be summarized as requiring the following measurement capability in the plasma:

- O-mode core temperature profile measurement (O-mode radiometer, full Bt):
  - 122 – 230 GHz
- X-mode core temperature profile measurement (X-mode radiometer, full Bt) :
  - 244 – 355 GHz
- X- and O-mode survey (Michelson interferometers):
  - Full bandwidth up to 1 THz
- X-mode core temperature profile measurement (O-mode radiometer switched to the X-mode line, half-Bt)
  - 122 – 230 GHz

The ITER Research Plan **ITER Research Plan (IRP) (2FB8AC v2.2)** specifies that the half-current/ half-field scenario is a necessary element of the development plan.

The details of each part of the systems are given in the following sub-sections.

6.2.4.1 Front-end assembly

In the port plug there are two quasi-optical front end assemblies based on Gaussian beam optics. The primary reason for having two lines is redundancy, so that if something happens to one line, the second line can be used for the all-important ECE measurements. A secondary reason is so that one line can view the plasma at a slight oblique angle to give additional information about the electron distribution function; explanation of this feature is given in Section 7. Both views will have a heated blackbody source to allow absolute calibration of the ECE instruments including the front end optics and transmission line.

The front-end feature a single focussing ellipsoidal mirror as the first element, with a simple turning mirror as the second element to create the required labyrinthian design that prevents streaming of neutrons directly through the port plug; a snap shot of the proposed design is given in Fig. 6.6. The ellipsoidal mirror focusses an aperture or beam waist at the back of the port plug to a beam waist near the low-field side edge of the plasma. Proper selection of the ellipsoidal mirror focal length yields an optimum spot size in the plasma for both O and X-mode measurements. A Gaussian telescope configuration was considered, but abandoned in favor of the simpler, single focussing mirror design. A Gaussian telescope has the desirable characteristic of beam waists that are independent of wavelength; however, properly executed, this would require a large distance between the mirrors which would have to be taken up by multiple 90-degree bends in the limited port plug space. The motivation in the design is for simplicity to minimize the risk of failure in operation.

For the current design the effective focal length f^* of the ellipsoidal mirror M1 is 152 cm and it is positioned at R = 972 cm, 152 cm from the edge of the ITER plasma (nominally at R = 820 cm). Then at the back end of the port plug, the aperature or field stop FS is located such that the distance from the ellipsoidal mirror is equal f^*. For this design, the flat turning mirror M2 can be located anywhere in between the ellipsoidal mirror and the aperture; the only requirement is that the total distance (M1,M2) + (M2,FS) remains 152 cm. The aperture at the back end of the port plug can be the actual aperture of a waveguide; or a field stop, either a physical one, like a variable iris, or a virtual one, defined by the optics of the beam splitter.

The front end design also includes an in-situ blackbody hot calibration source to calibrate the instruments including the entire transmission line. The planned source operates at a temperature of up to 800 ˚C. There is a shutter plate that is mechanically swung into view implemented in the design. In operation the source would be viewed both at the hot temperature and at ambient temperature to obtain a differential calibration.

The front-end design shall enable all the measurements as they are given by PR/SRD, without degrading the diagnostic performance, and to comply with the engineering design constraints given by the CMM (ITER_D_A6UBTX - The 3D and 2D CAD Model Approval Interfacing System Control Sheet (PC-CMAF ECE-CMM-L1-level) v1.0) for the integration in the Equatorial Port 9, DSM (drawer) 2. The front-end is an integral part of the transmission line; the overall design desire for achieving the good calibration is to have the total TL losses < 15 dB for the Te-profile range of frequencies.

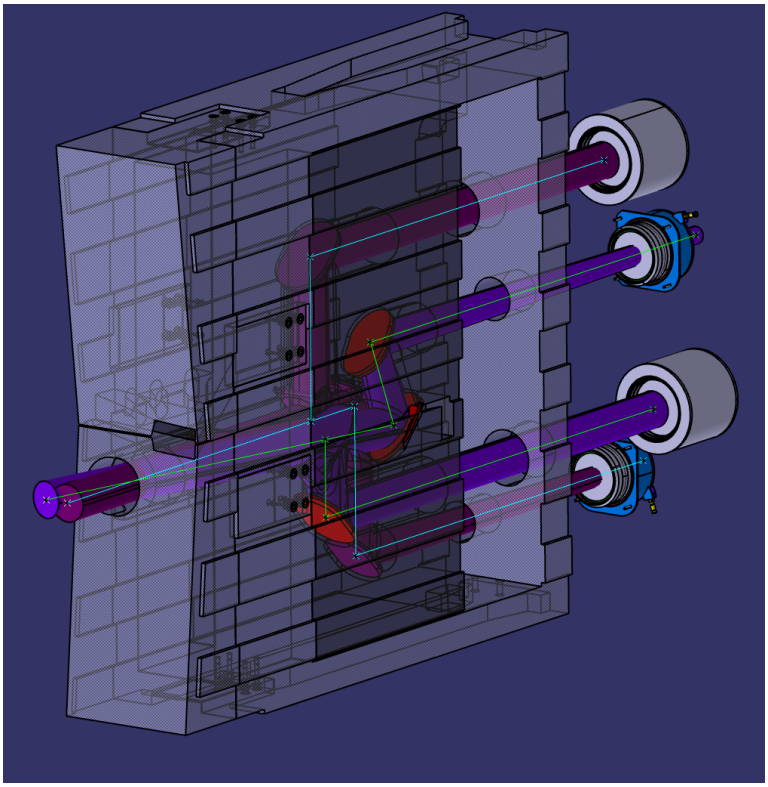

Figure 6.6. CATIA snap shot of ITER-ECE front end optics proposed design employing a single focusing mirror (M1) that images an aperture FS to the edge of the plasma.

It is expected that large number of plasma disruptions will occur during ITER operation, especially during plasma commissioning and exploratory physics studies. Disruptions are very damaging for Plasma Facing Components (PFC) of a large machine such as ITER. It is expected that, for the unmitigated disruption, about 300 MJ of plasma thermal energy shall be radiated in about 3 ms during the Thermal Quench. The surface melting of PFC materials by 3 ms energy flash are: Be - 1.4 MJ/m^2, W - 2.6 MJ/m^2, Stainless Steel 316L - 0.7 MJ/m^2.

ITER Disruption Mitigation System is constrained by capabilities of ITER pumping and gas processing system, EM loads on the plasma facing components, harsh (nuclear) environment within vacuum vessel, available space in the port plugs, interfaces with plasma diagnostics and other systems. DMS will be controlled by Plasma Control System.

It is expected that large energy loads shall be generated during disruption mitigation. Massive Gas Injection (MGI) of Ne or Ar shall be used for mitigation of TQ energy loads. At 800 m^2 plasma surface area the average energy load shall be 0.375 MJ/m^2. The peaking factor for radiation is expected in the range 1-5 which could result in local peak energy loads in the range 0.375 – 1.875 MJ/m^2 (**ITER_D_492H39** and **ITER_D_4EUBT9**, slides 12 - 13). This load shall be taken into account for the sensitive PFCs, such as First Wall apertures and mirrors.

The first (plasma facing) ECE mirror is located inside the Diagnostic Shield module in EqP9 1.52 m away from the First Wall. The First Wall aperture diameter is 0.162 m. The viewing factor of the plasma from the first mirror is calculated to be 0.0028. For the range of loads given above, one gets the range of loads on the first ECE mirror between 1 kJ/m^2 - 5.3 kJ/m^2 (the Thermal Quench duration is still 3 ms).

In the absence of validated models accounting for the extremely complex physics phenomena associated with the propagation of injected gas into the plasma during MGI, the required number of toroidal locations for the ITER system is estimated here simply by adopting the same toroidal radiation profile as measured on JET (**ITER_D_4D66RY**, **ITER_D_4EUBT9**, as

reported at STAC meeting in May 2011). Assuming a poloidal peaking factor 2, four locations are sufficient to reduce the peak heat load below the melting limit for both Beryllium and Stainless Steel. A further increase in the number of toroidal locations does not yield much improvement in the peaking factor.

Experimental results from present tokamaks and estimates for ITER therefore show that mitigation of Thermal Quench thermal loads using MGI of Ne or Ar is feasible in ITER without violating limits on the Current Quench duration. The required gross amount of Ne is in the range 0.5-2 kPa*m^3 and 4 toroidal injection locations are thought to be necessary to provide the required uniformity of the re-radiated energy.

For 100 kPa m^3 of Ne injected, one gets the $2.5x10^{25}$ particles in the vacuum vessel. Taking rougly the volume equal to 1000 m^3, the density is calculated to be $2.5x10^{23}$ m^{-3}, and the total pressure for T = 1000 K gets to about 4 kPa = 0.04 bar.

ECE mirrors are recessed deeply inside the Equatorial Port DSM (central); the radiation that reaches the first mirror shall be calculated from the numbers given above using the solid angle defined by the aperture in the FW. The resulting load is not expected to cause damage to the first mirror, and the further design implementation will be assessed for the PDR. However, one has to study the local effect of the gas injection, which may occur close to the DMS valve at the time scale of 0.1 s.

For the load on ECE window assemblies from the injected gas, the windows at the port flange are designed for 2 bar pressure (tested at 3 bars); they will withstand the pressure shock and to protect the quasioptical splitter box interspace waveguides from damage and contamination.

Maximum allowable burst of gas into ITER Vacuum Vessel to recover operational conditions without significant operation delay is:

Gas for MGI	ITER system limit (kPa*m^3)
D_2	50
He	40
Ne	100
Ar	100 (<10)

The ELM energy deposition on the first wall is very different to the DMS case. DMS deposits mostly photon energy on the walls. ELMs deposit particle energies, convected by filamentary transport. For the ELMs, the energy density is a sensitive function of the ELM energy loss from the plasma. The ELM energy is also extremely localized, and follows field lines, unlike the DMS photon energy deposition. ELM energy deposition will occur on millisecond timescales and according to IO heat load specifications uncontrolled can deposit up to 20 MJ/m2 per ELM at the secondary divertor interaction point with the wall (the maximum expected flux density). Controlled ELMs are expected to deposit no more than about 1 MJ/m2 per ELM at the same location. An ELM can interact randomly at almost any point on the low field side main chamber wall, with more or less intensity depending on the location. However, no ELM energy is expected to land on the DFW front surface provided the recess has been correctly chosen. All will interact with the FW panels to either side of the port.

In summary, the loads from DMS will be included in the Load Specification for the ECE diagnostic (**ITER_D_6XRG6J**), though DMS (as of now) itself is not planned be placed in Equatorial Port 9.

6.2.4.2 Hot source design

The calibration source is needed for in-situ absolute intensity calibration of the front-end components of the diagnostic. The source is a blackbody emitter, and will be needed for a two-temperature calibration of the system sensitivity. It is placed so that emission can be diverted into the optics using a mirror/shutter arrangement. The in-situ calibration allows the diagnostic to provide a fully independent measure of electron temperature despite expected degradation of the front end components between rare opportunities for access. The hot calibration source must operates up to 800° C, must not interfere with nearby diagnostics, and must meet the requirements for the highest quality ITER vacuum albeit during periods when plasma is not being produced.
The calibration will be carried out for two or more signal levels to allow for offset-linear dependence of the signal level and for noise. One signal level corresponds to each discrete temperature of the black body. The interferometer is relatively insensitive so the measurements are built up from discrete spectral scans repeated over many hours. The interferometer will support measurements from 100 GHz to 1 THz. While calibration prescription seems to vary with experimentalist, the total time for a calibration might be 8 hours or more.
The opportunities for calibration are built in to the operation plan for ITER. The need for calibration will probably not exceed a few times each year. It is likely that the calibration will be carried out with the toroidal magnetic field in operation -- note that the magnets are superconducting. The opportunity to replace the source will occur perhaps once every five years.

The candidate heating sources were identified and then critically evaluated to identify the methods that are applicable to the hot calibration source for the ITER ECE diagnostic system. The design requirements for the ITER ECE calibration source are extremely challenging. Long-term stability is one of the big questions and one of the most difficult to quantify. None of the existing calibration sources has had to operate in situ for the length of time specified in the requirement or in as a harsh environment. The requirements are intended to quantify the challenges. The source that we have designed and tested is expected to meet these requirements:

The Hot Source shall meet the following requirements:

- To be suitable for high vacuum and high radiation environment,
- Allow for high emissivity, *>.95* for *100-500 GHz*, *>.75 500-1000 GHz*, useable up to *1500 GHz*
- To operate at *~700° - 800°C* (*>400°-500°C* above ambient temperature),
- To have uniformity *±10°C,*
- To reach equilibrium temperature in less than 1 hour,
- To have short term stability (*24Hrs*) *~±2°C* and long term stability (*>3yrs*) *±10°C* in the ITER environment.

The most promising material for the hot source surface appears to be SiC: it provides the required emissivity for the desired frequencies; has low activation under typical ITER conditions, and is able to cope with high temperatures required for the diagnostic calibration. A report on the continued development of a prototype hot source for the ITER ECE diagnostic is available in Annex 6.2.1.

6.2.4.3 Double-window assembly

The tritium confinement in ITER relies on two confinement boundaries, and differential pressures on both sides of each boundary, so that the pressure in the contaminated areas is always less than the outside pressure, to prevent the outside atmosphere from tritium or contaminated dust release.

- The first confinement boundary includes the Tokamak metallic walls, vacuum extensions and several types of feed-through (optical, micro-wave, electrical, mechanical), incorporating non-conventional element such as glass / ceramic material in contrast with metallic materials. This boundary also forms part of the vacuum confinement boundary.
- The second confinement boundary envelops the first one; it includes the Tokamak building walls.

For 55F1 ECE the waveguides continue through the second confinement boundary up to the sources located in the Diagnostic Building. Thus window assemblies shall be placed on both confinement boundaries.

- For the primary boundary, the basic concept relies on a system of two independent windows made of glass / ceramic materials with monitored conditions (see Fig. 6.7).
- For the secondary boundary, the common concept relies on a single window element.

The window assembly incorporates two wedged window elements likely made of natural or synthetic Crystalline Quartz Z-Cut. Each of them is bonded on a metallic ferrule by Aluminium Diffusion Bonding on a flat surface. Water-free (low OH content) fused silica might also be envisaged for the window material.
Details of the proposed double-window assembly for the primary confinement barrier are given in Annex 6.2.2.

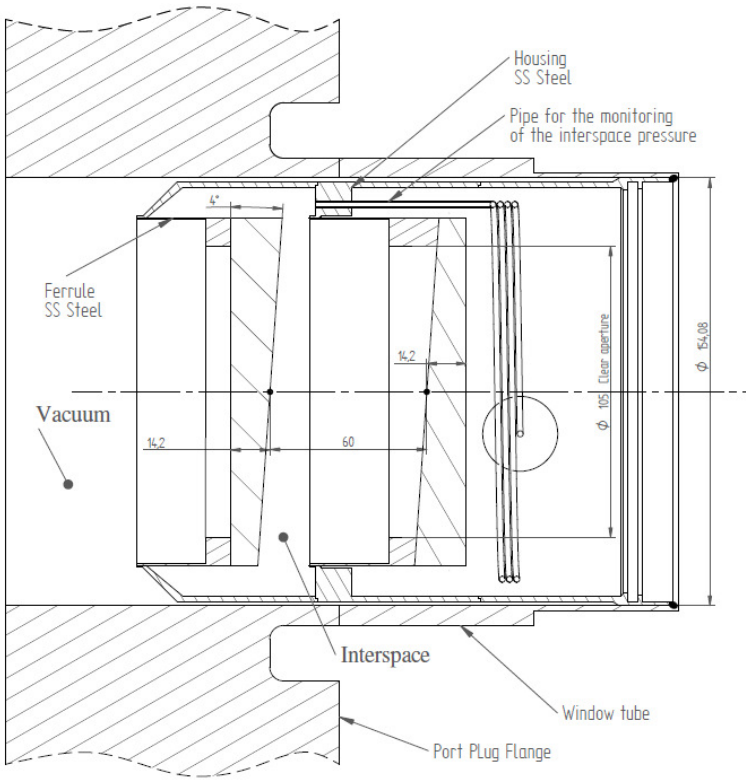

Figure 6.7. Conceptual design for the window assembly on the first confinement boundary.

The estimation of the transmission loss of the primary window was performed at General Atomic, DIII-D Michelson interferometer facility. A millimeter wave Echo absorber at liquid Nitrogen temperature has been used as a black body source and a Michelson interferometer as a wide bend frequency resolved detector. The transmission curve is shown in Fig. 6.8. This transmission curve is obtained by taking ratio of two frequency spectra with and without window in the transmission

path. There are three water vapor absorption lines that eliminated by data interpolation method. The single walled window transmission is 68% for frequency range 100 to 400 GHz and nearly 65 to 60% for frequency range 400 to 900 GHz. The total transmission of all windows (including secondary window at the gallery – diagnostic hall area) is 31 to 21%. The total vacuum window attenuation (power loss) is, therefore, 69 to 79%. That gives power loss of 5 to 6.8 dB for frequency range 100 to 900 GHz.

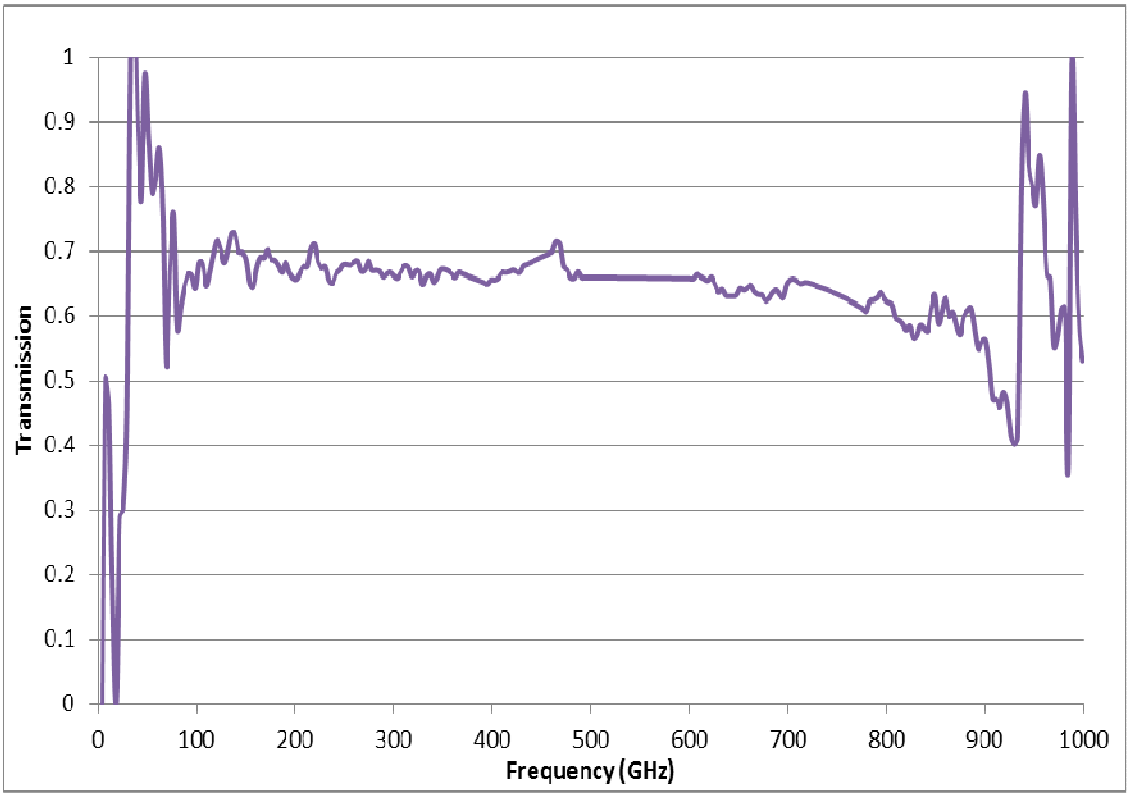

Figure 6.8. Measured transmission of wedge quartz window.

6.2.4.4 Polarizer splitter box

The ECE radiation is collected by front-end optics arrangement in the port plug and a radiation beam is put out from the tokamak vessel through vacuum double walled window. This beam contains both modes (i.e. O-mode and X-mode) of radiation. It is required to split the mode before transmitting through waveguide towards the ECE measurement room. In this section described a design of the polarizer splitter unit. The design is basis on Gaussian beam theory. It consists of two Gaussian beam telescopes made out of three parabolic mirrors and one flat mirror. There is wire grid beam splitter to select mode of the beam (see figure 1). We consider that the radiation beam come out from the smooth walled circular waveguide of 72 mm diameter and further propagate towards plasma.

Mirror focal length and Optical component size (references are local to this sub-section only)

The beam waist size at the circular waveguide mouth should be 0.76*radius of WG for optimize coupling of 87% between the WG and a quasi-optical component of the splitter box [1]. This is 27.36 mm in beam waist (ω_0) and beam diameter is 54.72 mm.

We consider the focal length of the first parabolic mirror is 330 mm that is similar to our Michelson interferometer mirror [2].

The beam size at the mirror PM1 is calculated by using following expression [3],

$$\omega(Z) = \omega_0 \left[1 + \left(\frac{\lambda Z}{\pi \omega_0^2}\right)^2\right]^{1/2}$$

The mirror size is optimized for frequency f = 120 GHz. For Z = 330 mm, the beam size ω(Z) on PM1 is 28.99 mm and diameter of the beam is 57.98 mm. The mirror is at 45° that gives beam size of 40.99 mm. For 99.97 % power coupling to the mirror, the size of the mirror at least 3 times of the beam size at the mirror. The size of mirror PM1 is 120 mm and all optical components within telescope are also 120 mm.

The focal length of second parabolic mirror is 515 mm. This gives beam size of 42.7 mm at outside of the splitter unit telescope. The magnified beam size gives minimum diversion of the beam at the port plug ellipsoidal mirror of focal length 2100 mm for 115 GHz.

Mode conversion due to tilt and axial shift

Misalignment between the quasi optical components and the waveguide axis leads to mode conversion and the transmitting power goes into the higher order modes. The fractional mode converted power due to tilt Δθ (i.e. in Radian) between quasi optical components axis and the waveguide is approximately:

$$P_{tilt} = 3.9\left(a\,\Delta\theta/\lambda\right)^2 - 5.6\left(a\,\Delta\theta/\lambda\right)^4$$

And the fractional power due to axial shift δ is estimated by following expression:

$$P_{axial} = 2.3\left(\delta/a\right)^2 - 2.2\left(\delta/a\right)^4$$

Where a is the radius of the waveguide and λ is the wavelength of the microwave.

For the axial tile of 0.1 degree and shift of 2 mm the fractional mode converted power ≤ 1 % with circular smooth walled waveguide of diameter 72 mm.

References:

[1] Paul F. Goldsmith, *Quasioptical system, Gaussian beam Quasioptical propagation and Applications* IEEE Press, Institute of Electrical and Electronics Engineers Inc. New York

[2] Sidney A. Self, APPLIED OPTICS **22** 658 (1983)

[3] K. Okhubo, S. Kubo et al. *Coupling of tilting Gaussian beam with Hybrid mode in the corrugated waveguide* Report number NIFS-474 (Jan. 1997)

Radial beam size 28.63 mm in diameter, Gaussian beam waist w_0 = 14.32 mm
R = 11398 mm
Z = 220 mm

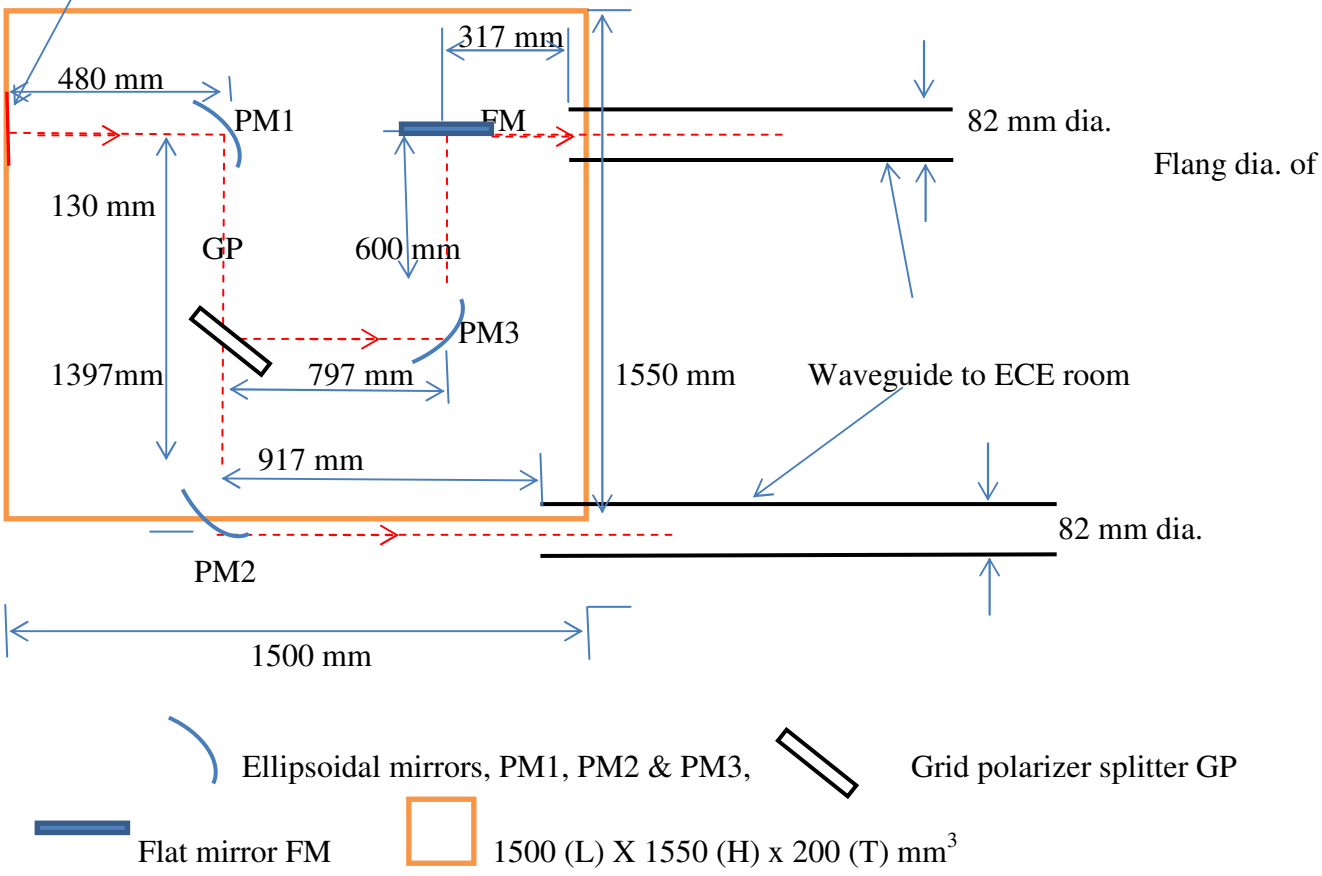

Size of the mirrors: EP1 = 145 mm, EM2 & EM3 = 145 mm and FM = 145 mm

Figure 6.9. The layout of the polarizer splitter box.

6.2.4.5 Transmission Lines

ITER ECE system will utilize four transmission line, two (X-mode & O-mode) for radial measurement and other two is for oblique measurement. The radial measurement is useful to determine electron temperature profile with good spatial and temporal resolution. The transmission line components include quasi optical components (i.e. focusing mirrors, plane mirrors etc.) and straight waveguide section and miter bends. The performance of the TL is crucial to ensure that the requirements for the diagnostic to measure the plasma parameters are met. Because of a wide range of requirements and natural constraints to the diagnostic performance, it is clear that not all measurements, as they are stated in the PR/SRD, can be met simultaneously.

In the case of ***core temperature profile,*** the ECE system is also called out to be utilized for "Advanced Control" (AC), which would require "real-time" analysis of the diagnostic data as well as the availability of "real-time" EFIT information. The required temporal resolution is 10 ms. In the area of high frequency instabilities (NTM amplitude), the diagnostic has also been identified as a primary contributor again for "Advanced Control".

In addition to the above primary roles, the system is also required to provide "Back-up" measurement capability (when possible) for the ***L-H transition indicator/ELM temperature transient***, and "Supplementary" capability for the following measurement parameters: plasma energy/poloidal beta, main plasma Prad/Pece, some runaway electon parameters such as runaway current after thermal quench and during failed breakdown, edge electron temperature profile and some high-frequency instabilities such as turbulence.

The Role of the 55F1 ECE diagnostic in the ITER program & Overview of the system requirements for 55F1 ECE Diagnostic from PR/SRD is described in table 3.1 & 6.1 respectively.

The requirements for the ECE TL are as follows:

- To provide as lower losses as possible over 70-1000 GHz, and with target of < 15 dB for the Te-profile relevant part of spectrum
- To be stable over time
- To maintain polarization
- To couple well to front end optics -> to yield optimum beam pattern.

In the TL concept presented at the CDR, the main (perpendicular) lines were using the circular corrugated waveguides (63.5 mm ID), whereas the oblique (10-degree) lines were using the rectangular smooth-wall waveguides (72 x 34 mm). This arrangement suits well the measurements below 350 GHz (which is the Bragg scattering frequency in the selected corrugated waveguide); however, to address other (though not primary) measurements with reasonably good performance, some modifications were proposed to the baseline. The general layout of the ITER ECE transmission lines is given in Fig. 3.1.

Although smooth-walled rectangular waveguide offers an advantage in terms of simplicity of construction, the disadvantages might outweigh this singular advantage. In particular, the major challenges involve coupling from the TE10 "tall-guide" mode in the rectangular waveguide to the fundamental free space (Gaussian) mode with circular cross section at both ends of the waveguide transmission line, and then maintaining the spatial localization of the received ECE emission, which is degraded by mode conversion. In smooth-wall rectangular waveguide, the Ohmic attenuation can be quite high, and the mode conversion in the E-plane mitre bends is exceptionally high. Both can be reduced by increasing the dimensions of the waveguide.

There is a multiplicity of engineering tradeoffs involved in the optimization of an ECE waveguide transmission line. Many different types of transmission lines might be considered including: corrugated circular waveguide, corrugated rectangular waveguide, smooth-walled circular and smooth-walled rectangular waveguide, dielectric lined circular waveguide, dielectric waveguide, as well as a lens relay system similar to that used by the Michelson and grating polychrometer ECE instruments on TFTR. In each case, there are a number of undesirable limitations that have to be considered. First of all, none of the above envisioned waveguide concepts can provide an attractive ECE transmission line with the desired characteristics over the entire frequency range of 70-1000 GHz. The natural prioritization is to provide the best possible performance over the low frequency

range of 70-300 GHz that is required for the electron temperature measurements, while accepting degraded performance for the higher cyclotron harmonics above 300 GHz.

In the discussion given by G. Hanson and J. Wilgen, Discussion on ITER TL options *(ITER_D_767FWW v1.0)*, it is assumed that the ECE emission that is collected via the optical viewing system is coupled into a single waveguide mode that propagates to the diagnostic hall where is it coupled into a single-mode detector, such as a fundamental waveguide mixer used by an ECE radiometer. This may also apply to a multi-mode instrument such as the Michelson, but perhaps only at the low end of the frequency range below 200 GHz. At the upper end of the frequency range where the Michelson instrument can accept multiple modes, and the front-end viewing system and the transmission line can propagate multiple modes, a different perspective may be needed, and the design criteria for the transmission line could differ.

Several conditions must be satisfied in order to provide adequate transmission line performance, including: 1) preservation of the polarization of the ECE radiation, 2) achieving the desired spatial localization of the ECE emission in the plasma via the optical viewing beam, and 3) relaying the ECE emissions to the measurement instrumentation in the diagnostic hall with acceptable transmission loss. For the purpose of these discussions, assume that: 1) the polarization needs to be preserved within 2%, 2) the ECE emission zone needs to be localized to a 6 cm diameter circular region in the plasma (omit degradation due to relativistic broadening effect), and 3) the waveguide attenuation should preferably be in the 6 to 12 dB range, should not exceed 10 dB in the 70-300 GHz frequency range, and should not exceed 20 dB above 300 GHz.

Preserving the Polarization

It is assumed that the polarization that is selected in the splitter box at the input to the ECE transmission line will be preserved during propagation along the transmission line, as the measuring instruments in the diagnostic hall (Michelson or radiometers) will be setup to receive a specific polarization. However, depending on the characteristics of the guide selected for the ECE transmission line, the polarization of the ECE radiation may be altered as it propagates along the waveguide.

As noted by Doane [Fusion Science and Technology **53**(2008)168], "corrugated circular waveguide has a significant advantage over smooth-wall circular waveguide, since ellipticity coupling from TE11 to its cross-polarized component can be large in smooth circular waveguide."

In the case of the smooth-wall circular waveguide, small elliptical distortions of the waveguide cross section can result in significant alterations of the polarization state of the ECE radiation The polarization rotation is due to the "bi-refringence of smooth-wall circular waveguide when deformed symmetrically" [Doane, Int. J. Electronics **61**(1986), p. 1111]. "… when two independent polarizations of a given mode have radial electric fields directed along the axes of maximum and minimum radius, …, then their phase velocities will be different. The relative phase shift of these polarization components then produces a rotation in the polarization of a mode whose radial electric field is initially oriented at some angle to these axes."

Note that smooth-wall square waveguide appears to present a similar situation, where bi-refringence of orthogonal polarizations can arise due to small variations in the two orthogonal dimensions of the square waveguide.

Localization of the ECE emission

Mode conversion in the ECE waveguide transmission line can act to compromise the desired 6 cm circular spatial localization, which is determined by the characteristics of the ECE optical viewing system.

How does an overmoded waveguide preserve the spatial localization of the ECE emission received from the plasma? A single waveguide mode couples to a unique antenna radiation pattern at both ends of the waveguide transmission line. In order to preserve the spatial localization associated with the viewing beam for a specific waveguide mode, mode conversion between waveguide modes must be avoided, and only that single waveguide mode should be allowed to couple into the measurement instrumentation located in the diagnostics hall.

In the case of corrugated circular waveguide employing the HE11 mode, the antenna pattern at both ends of the waveguide is nearly Gaussian, which provides a near perfect match with the existing ECE optical front-end viewing system, that is based on Gaussian optics. At the exit end of the waveguide transmission line located in the diagnostic hall, the HE11 mode also couples equally well to the the radiometer and Michelson instruments, rejecting ECE emission propagating down the waveguide via other modes. Mode conversion acts to spoil this near perfect arrangement. In the low frequency range below 300 GHz, where spatial localization is most critical for the electron temperature measurements, the mode conversion that occurs in the mitre bends couples to very high order modes that can only receive ECE emission at very large off-axis angles (with respect to the waveguide axis). Unfortunately many transmission line design options can incur signifiant mitre bend mode conversion at the low frequency end of the band. In the higher frequency range above 300 GHz, mode conversion due to waveguide curvature and/or axis tilt at waveguide joints dominates, resulting in the intermixing of the desired ECE emission content of the HE11 mode with that carried by the HE21, TE01 and TM02 waveguide modes. Note that none of these waveguide modes can match the spatial resolution of the HE11 mode, which provides a viewing beam that is peaked on axis. Therefore mode conversion is an important design consideration.

We should give tolerable polarization change.

Waveguide Attenuation.

If waveguide attenuation is excessive, it will not be feasible to provide an accurate calibration of the ECE measurements using the presently planned arrangement with the calibration hot sources located near the plasma. Based on calibration considerations, ohmic transmission line loss in the 6 to 12 dB range might be acceptable. However the losses should probably not exceed 10 dB in the 70-300 GHz frequency range, and should not exceed 20 dB above 300 GHz. For smooth-wall waveguide, both rectangular and circular, the transmission loss due to ohmic attenuation is relatively high. By comparison, corrugated waveguide has very low transmission loss (by two or three orders of magnitude), at least for frequencies below the Bragg frequency.

Since the ohmic attenuation loss of smooth-wall rectangular waveguide varies inversely with the E-plane dimension, the “tall-guide” polarization is often used to reduce the losses in long transmission lines. For tall-guide polarization in aluminum WR-187 (22 x 48 mm) waveguide, the expected attenuation values are 0.104, 0.145, 0.196, and 0.309 dB/m at frequencies of 100, 200, 400, and 1000 GHz respectively. For a 35 m ECE transmission line, the ohmic losses are estimated to 3.6, 5.1, 6.9, and 10.8 dB at frequencies of 100, 200, 400, and 1000 GHz respectively (neglecting ohmic losses in the MB mirrors).

Rectangular Smooth-Wall Waveguide Challenges

The biggest challenges posed by the use of rectangular smooth-wall waveguide are: 1) coupling to a circular Gaussian beam at both ends, 2) side lobes in the radiation patterns at both ends of the rectangular waveguide, 3) possible implications of the very large mode conversion in the E-plane mitre bends, and 4) accommodating the relatively high ohmic attenuation of the waveguide transmission line without compromising the performance above 300 GHz.

> Coupling to a circular Gaussian viewing beam requires near identical antenna patterns in both the E- & H- planes. Adequate coupling (98-100%) to the desired circular Gaussian; free space viewing beam requires tapering the dimensions of the rectangular waveguide, which could be accomplished using a transition to an aperture where the H-plane dimension is approximately 30% larger than the E-plane dimension, at both ends of the waveguide. Because the transition must provide good performance over a broad frequency range, 75-300 GHz range, in addition to being useable above 300 GHz, the transition could not be short.

> To achieve good spatial localization of the ECE emission requires >99% of power in the main lobe, so sidelobes must be minimized. In the case of smooth-wall rectangular waveguide employing the TE10 mode, the antenna pattern at both ends of the rectangular waveguide transmission line would have substantial sidelobes, particularly in the E-plane, which would not couple perfectly to the optical systems located at both ends. [*Note: for smooth-wall rectangular waveguide, at least 5% of the received power is via the sidelobes*]. One option for eliminating the sidelobes would be to corrugate the ends of the waveguide aperture to create a scalar horn that has negligible sidelobes.

> To maintain the spatial localization of the ECE emission, the ECE emission content of the TE10 mode cannot be allowed to intermix with other waveguide modes, which contain ECE emission from other regions of the plasma. In the 70-300 GHz frequency range, mode mixing in smooth-wall rectangular waveguide is dominated by mode conversion in the mitre bends, especially the notorious E-plane mitre bends which suffer from exceptionally large mode conversion. In order to minimize E-plane mitre bend mode conversion loss, the "tall guide" polarization must be used, where the E-plane dimension is larger than the H-plane dimension. Even so, the E-plane mitre bend mode conversion is **10-20 times** larger (by factor of b/lambda) compared with a corrugated circular waveguide mitre-bend of the same dimension. For example, for WR-187 guide with tall-guide polarization, the E-plane mode conversion loss is >11% at 100 GHz. The resulting mode conversion would result in the intermixing of the desired ECE emission content of the TE10 waveguide mode with that carried by the unwanted waveguide modes that are coupled at/by the E-plane mitre bends, mixing ECE emission from different regions of origin in the plasma. [*Since mode conversion in mitre bends couples predominantly to very high order modes, can mitigate this to some extent by taking precautions at the splitter box to assure that these modes do not receive any ECE emission from the plasma. To the extent that this can be accomplished, the mode conversion would then just be an additional power loss mechanism, in addition to the ohmic attenuation.]*

> Therefore, with smooth-wall rectangular waveguide, it would be challenging to achieve a situation where >95% of the measured ECE emission is localized within a 6 cm FWHM circular viewing beam pattern at the lowest normal field frequency range of 100-150 GHz.

> To obtain acceptable ohmic attenuation, the rectangular waveguide dimensions need to be relatively large. For example, WR-187 aluminum waveguide in "tall guide" polarization has an expected ohmic insertion loss of 4 dB at 100 GHz increasing to 11 dB at 1000 GHz, for a 35 m long transmission line. Unfortunately the large E-plane dimension, 1.87" (48 mm) results in quite high mode conversion above 500 GHz due to waveguide curvature and tilt at waveguide joints, mainly in the larger E-plane dimension. [*Note: Moderate amounts of attenuation in the transmission line can be beneficial, provided that it is not excessive.]*

> *[It might be noted that polarization information does not appear to be preserved by the rectangular waveguide, which may not matter as the ECE polarization information has already been separated at the splitter box. Since the rectangular waveguide sidewalls will naturally align with horizontal and vertical directions in order to accommodate the lack of rotational flexibility in the mitre bends, then the incoming X-mode ECE emission will have an E-field orientation slightly off-vertical due to the pitch angle of the magnetic field inside the plasma. So the ECE emission can be decomposed into mostly the "tall-guide" TE10 mode, and a smaller component of orthogonal "normal–guide" TE10. The two orthogonal components will propagate independently to the opposite end of the transmission lines at different velocities, and depending on the frequency, will not arrive in phase, resulting in elliptical polarization at the diagnostic hall. Additionally, the "normal-guide" polarization component will experience about twice the attenuation of the "tall-guide" polarization component, which basically means that the "tall-guide" polarization survives preferentially. Also note that for the orthogonal O-mode ECE emission, the waveguide orientation must be rotated 90-degrees (with respect to that for the X-mode emission) to provide the least attenuation to O-mode emission.]*

Contrast with Circular Smooth-Wall Waveguide Challenges

> By comparison, smooth wall circular waveguide doesn't require a change in the aspect ratio in order to couple to a near-circular Gaussian optic viewing beam. A tapered transition would not be required.

> Since the side lobes for smooth-wall circular waveguide are reduced by about 4.3 dB compared with rectangular waveguide, only about 2% of the power in the dominate mode is received via the sidebands (primarily E-plane). That might be acceptable.

> The possible impact of mode-mixing on the loss of the spatial location of the emission is significantly reduced because mode conversion in the E-plane mitre bends is not so extreme. That allows smaller diameter waveguide to be used, resulting in reduced mode conversion above 300 GHz due to waveguide curvature and tilt at waveguide joints.

> The ohmic attenuation of a smooth-wall circular waveguide transmission line is not very different from that in the rectangular waveguide

> Polarization rotation in smooth wall circular waveguide might be problematic due to the bi-refringence of the orthogonal polarizations arising from small elliptical distortions of the waveguide cross section, resulting in different propagation velocities.

Contrast with Circular Corrugated Waveguide Challenges

> Corrugated circular waveguide provides the best available match to the Gaussian viewing beam at the input, as well as to the Michelson instrument at the output.

> Since the radiation/antenna pattern for corrugated circular waveguide is very nearly Gaussian, it is therefore virtually free of side lobes.

> E-plane mitre bend mode conversion is reduced by a factor of 10-20 in corrugated waveguide, compared with rectangular smooth-wall waveguide. As a result, mode mixing of the ECE content with undesired modes is not an issue. That allows smaller diameter waveguide to be used, resulting in reduced mode conversion above 300 GHz arising from waveguide distortions such as curvature and axis tilt at waveguide joints.

> The ohmic attenuation of a corrugated circular waveguide transmission line is typically too small to be a concern, at least in the frequency range below the Bragg frequency. Assuming that the corrugations were optimized for the 70-300 GHz range, attenuation might still be an issue above 300 GHz.

> Polarization rotation in corrugated circular waveguide is greatly reduced compared with smooth-wall circular waveguide, and should not be a problem.

> Note 1: Corrugated waveguide for Gyrotron use at 460 GHz has been fabricated by using a tap. [Woskov, IRMMW-THz 2005, v2, pg.563.] Typically, the Bragg frequency is approximately 1.5 times the design frequency for high power use.

> Note 2: After fabricating the 600 GHz corrugated waveguide (254 micron pitch and depth) for the grating polychromator on TFTR, Cavallo concluded that “it should be possible to fabricate corrugated waveguide with a bandwidth of 120-1000 GHz [Cavallo, RSI **61**(1990)2396].

Dielectric Lined Circular Waveguide

Dielectric lined circular waveguide has many attractive features similar to corrugated waveguide, including propagation of a hybrid HE11 mode with low ohmic attenuation, and low mode conversion loss in E-plane mitre bends. However, since there are no periodic corrugations, Bragg scattering is not an issue. Only the depth of the dielectric layer must be selected to favor either the high or low frequency end of the ECE measurement range. For optimization in the 300-1000 GHz range, a quarter-wave layer of alumina at 600 GHz λ= 500 microns) would have a thickness of about 40 microns, which might be obtained by anodizing. Unfortunately such a waveguide would act much like a smooth wall circular waveguide at 100 GHz, where the dielectric thickness is almost negligible. A better option might be to optimize the dielectric thickness for the 100-300 GHz range, which requires about 120 micron thickness, and accept the resulting performance in the high frequency range. In this case, the performance at the high frequency end might be expect to exceed that of corrugated waveguide as Bragg scattering would not be an issue. Also, it might turn out to be easier to fabricate dielectric lined waveguide than corrugated waveguide.

Comment on Hollow Dielectric Waveguide

In his 1990 RSI paper, Cavallo includes the following comment regarding hollow dielectric waveguide [Cavallo, RSI **61**(1990)2396]:

> *"In the far infrared region of the spectrum (f>400) GHz), for linearly polarized single-mode propagation, hollow dielectric waveguide would appear to be the best choice for long distance transmission, (Losses for higher–order modes increase as the square of u_{nm}, the mth root of a Bessel function $J_{n-1}(x)$, so only the lowest-order modes can be propagated over significant distances.) It is relatively inexpensive, and can be evacuated to eliminate water vapor attenuation. "*

In that respect, there is a similarity with smooth-wall circular and rectangular waveguide in that the higher losses experienced by the higher order modes favors the selective propagation of predominantly the lowest order mode(s).

Conclusion

Taking the discussion above into account, the smooth-wall circular waveguide is a preferred solution for both lines-of-sight to enable simultaneous measurements of both X- and O-mode with acceptable level of losses. However, the R&D for the rectangular waveguide (72 x 34 mm), corrugated circular waveguide (ID 63.5 mm) and corrugated dielectric-coated waveguide options will be performed during the Preliminary Design Phase, to ensure that the TL for ITER ECE are chosen correctly to meet the primary measurement requirements and, to the best, requirements given as back-up or supplementary.

Estimation of transmission attenuation for the baseline transmission line

A smooth-wall circular waveguide (inner diameter or ID of 72 mm) is proposed for ITER ECE transmission line for both radial and oblique views as a current baseline design.

The ECE/black body hot source radiation is collected by the front-end optics and transmitted through vacuum window to the polarizer splitter box. The polarization of the radiation is selected in the polarizer splitter box and the radiation is transferred to corresponding transmission line waveguide. Further, the radiation is transmitted to receiver systems (i.e. Radiometer and Michelson interferometer). There is radiation attenuation during transmission. The estimation has been performed for ~43 m long smooth-wall circular waveguide with six miter bends. The value obtained from theoretical prediction has been doubled to account for unexpected additional losses and manufacturing/ installation imperfections. The total attenuation of the circular waveguide transmission line is given in Fig. 6.10 and compared to these for the corrugated circular (ID 63.5 mm) and smooth-wall rectangular (72 x 34 mm) waveguide options. A 43 m long corrugated waveguide transmission line attenuation is determined on basis of previous measurement of the corrugated waveguide transmission line attenuation. The attenuation for the rectangular waveguide transmission line is estimated by using theoretical expression and the calculated value has been again doubled.

Based on these estimations, the time required for calibration of ITER ECE systems has been evaluated.

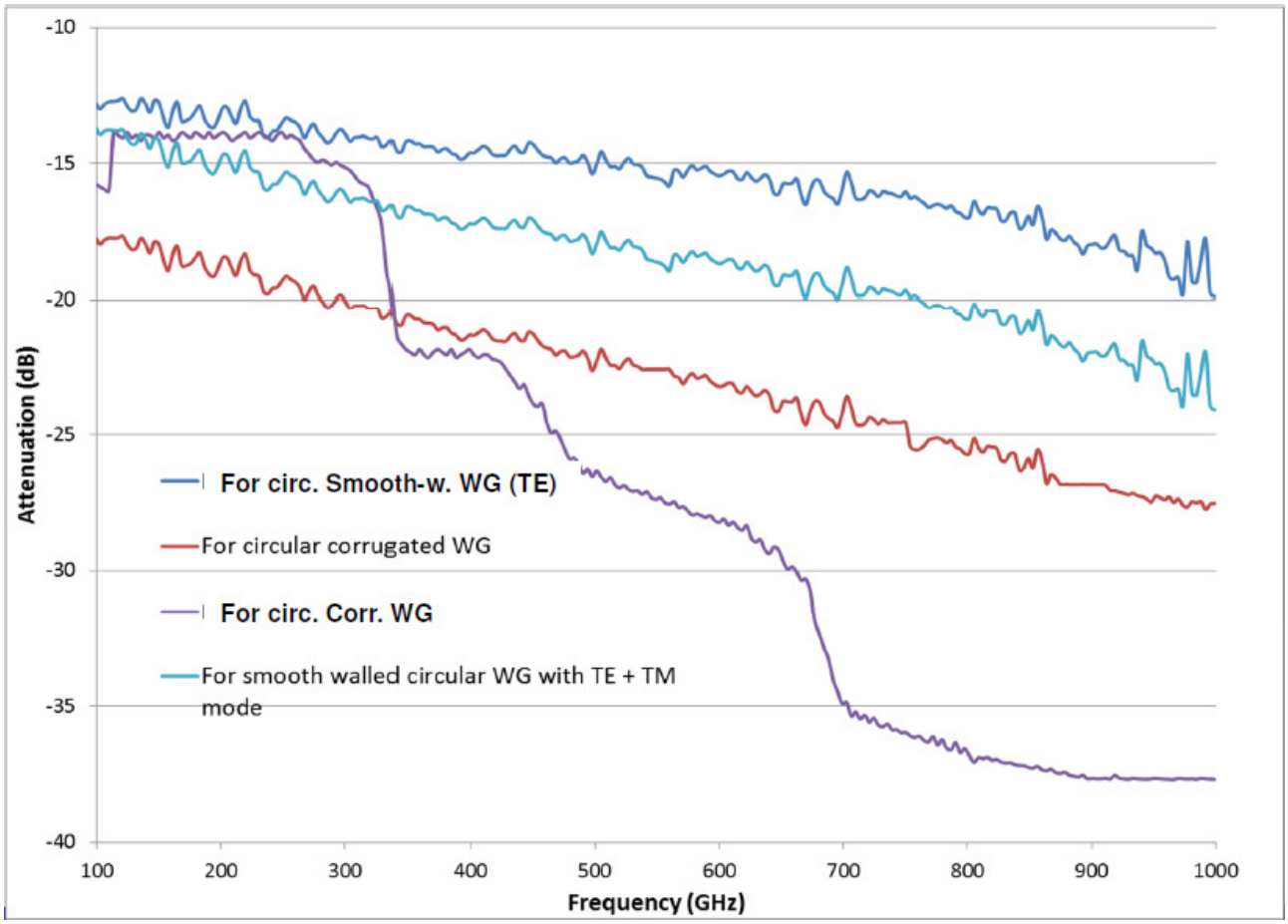

Figure 6.10. Estimated total attenuation of transmission line of all three waveguide options with three quartz windows, polarizer splitter box, 43 meter WG length, six miter bends and waveguide connection optics.

Alternative transmission lines

A possibility of using corrugated and smooth-wall rectangular transmission lines are to be investigated by IN DA for the PDR of the ECE system.

So far, the circular corrugated waveguide is used to obtain electron temperature profile in many ECE transmission line on various tokamaks, such as DIII-D [M. E. Austin et al. Review of Sci. Inst. **68(1)** 480 (1997)], JT-60U [N. Isei, A. Isayama et al. Fusion Eng. and Design, **53**, 213 (2001)], LHD [Y. Nagayama, K. Kawahata, et al., . Review of Sci. Inst. **77** 1021 (1999)], TCV [V.S. Udintsev *et al*., Fusion Sci. Technol. **52**, 161 (2007)], KSTAR [S. H. Jong et al. Review of Sci. Inst. **81** 10D922 (2010)]. Corrugated waveguide (CWG) has been also examined extensively for use in the reflectometry [W. A. Peebles et al., Proceedings of the 18th Meeting of the ITPA Topical Group on Diagnostics, Oak Ridge, 11–14 May 2010; D. Wagner, et al., Rev. Sci. Instrum. **68**, 431 (1997); R. R. Hanson et al., Rev. Sci. Instrum. **81** (2010)] and for ECH heating systems. It is known to be very stable, and it propagates HE11 mode which couples well to Gaussian optics.

On DIII-D, the corrugated TL has been designed to be used for the frequency range between 100 – 300 GHz. For the frequencies above 300 GHz, the Bragg scattering starts to degrade the performance of the TL. The Bragg scattering of high order modes, with large number of modes, causes continuum of losses. The measurement results for 15 m TL performed at DIII-D are presented in Fig. 6.11. The polarization scrambling in the corrugated waveguide after the polarizer

beam splitter results in the loss. This is one of the advantages of having the splitter box next to the window assembly, as no additional waveguide piece is inserted between the window and the polarizer and, thus, the polarization scrambling does not affect the measurement spectra at the back-end of the diagnostic. The disadvantage of this configuration is that the handling of the splitter box near the port plug flange is more difficult due to the occupation of the interspace and higher activation doses, compared to the Port Cell.

The theoretically estimate of Ohmic attenuation for lowest order hybrid HE_{11} mode in the corrugated waveguide is very low within the ITER ECE frequency range of interest. Only at certain frequencies, when the corrugation period becomes a multiple of half wavelength, the attenuation becomes very high due to Bragg reflection (Fig. 6 in [J. L. Doane, Fusion Sci. Technology, 53, 159 (2008)]). It appears that long (i.e. ~ 2 meters) section of corrugated waveguide with a pitch less than 0.38 mm is not possible to fabricate with required tolerance. Thus, the 'stop bands' (discreet spikes of high attenuation) are unavoidable above 394 GHz (λ = 0.76 mm). The ITER ECE radiometer measurement for the electron temperature profile is up to 355 GHz. Therefore, the temperature profile measurement is not effected due to the Bragg resonance. Further, the Bragg resonance due to period and depth of the corrugated waveguide depends on fabrication tolerance. There is broadening in the Bragg resonance line due to variation in period and depth. These give periodic pick in attenuation and sometime two peaks broader and merge to each other. This is not possible to control at high frequency. This is the main limitation of the corrugated waveguide use in high frequency (> 350 GHz) transmission line.

The smooth-wall rectangular waveguides were successfully used for ECE TLs at JET [E.A.M. Baker, *et al*., Overmoded millimeter waveguide transmission system for the JET ECE diagnostic, Proceedings of EC-4 4th international workshop on ECE and ECRH, Rome, 1984], A. E. Costley, *et al*., First measurements of ECE from JET, Paper presented at 4th Int. Workshop on ECE and ECH, Frascati (1984)] and at FTU tokamak [P. Buratti *et al*., A BROADBAND LIGHT COLLECTION SYSTEM FOR ECE DIAGNOSTICS ON THE FTU TOKAMAK, Infrared Phys. Vol. 34, p. 553 (1993)]. There is no Bragg scattering issue for the smooth-wall waveguides; however, at JET, the highest frequency for which the calibration factors have a small relative uncertainty below 2% is 350GHz and below 4% is 500 GHz, if the influence of water absorption lines is neglected. The waveguide attenuation measured at JET is given in Fig. 6.12. At FTU, measurement withing the frequency range of 70 – 900 GHz has been performed [P. Buratti, O. Tudisco and M. Zerbini, Infrared Physics Physics, Vol 34, 533 (1993)]. In this measurement, a square waveguide of 76 mm with three E-plane and two H-plane mitre bends are used for the transmission line. The total loss of this transmission line is 2.5 dB at 428 GHz. This is the resistive loss of the waveguide.

Thus, an R&D programme will be required both for the corrugated and smooth-wall waveguide TL to assess their performance (mode conversion loss, losses vs frequency and vs temperature).

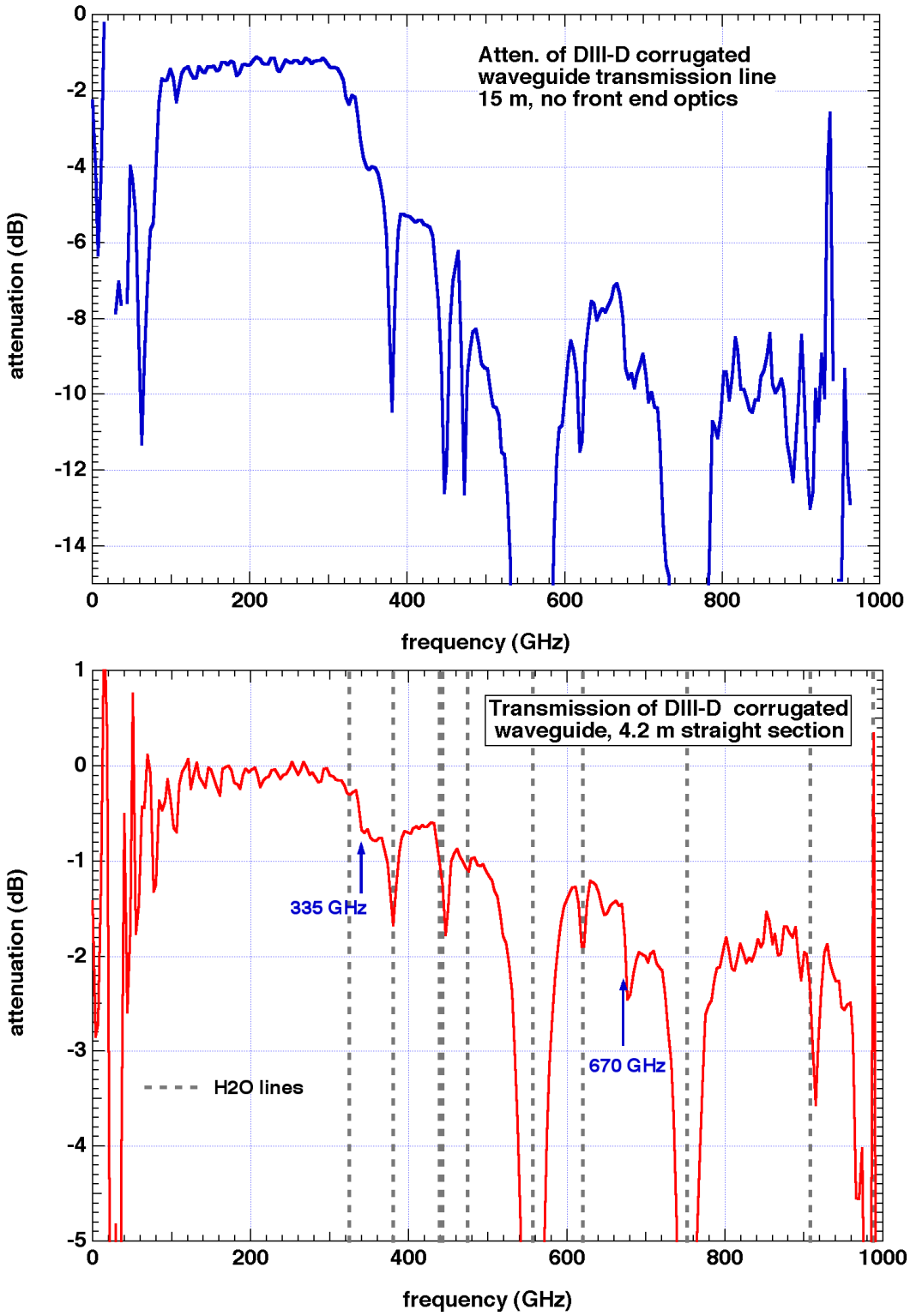

Figure 6.11. Attenuation of 15 m long DIII-D corrugated WG TL, without front-end optics (top); transmission of the 4.2 straight corrugated waveguide section (bottom).

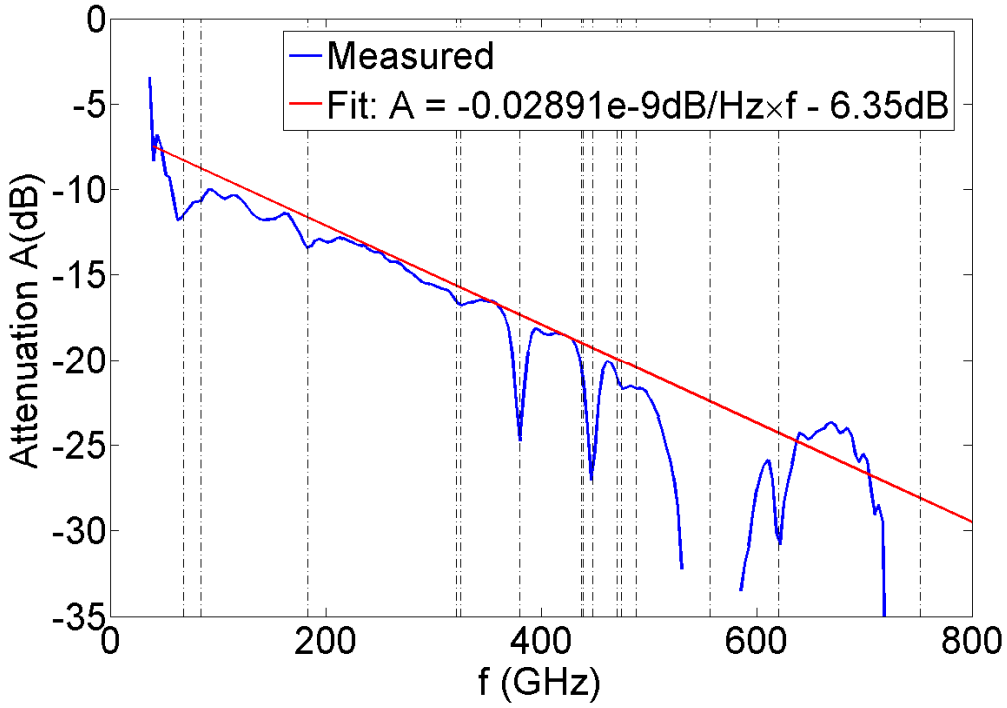

*S. Schmuck, RO of JET Michelson Interferometer (2009-2013), Stefan.Schmuck@ccfe.ac.uk

Figure 6.12. Attenuation of ~40 m long TL (rectangular waveguide) at JET.

6.2.4.6 Machine motion compensation in TL

The port plug flange will move radially, vertically and/or toroidally during machine warm-up, operation, and bakeout. This motion must be compensated for in the TL system. The polarization splitter boxes are mounted on the Interspace Support Structure. To deal with radial expansion, the output waveguides are allowed to slide along their centerline. To allow for toroidal and vertical motion, the waveguide will be designed to flex over several meters in the interspace region, and optics inside te splitter box are designed to be oversized with respect to the input beam. At installation, the waveguides will have to be aligned at the port plug flange in the cold position. Either the splitter box with output WG's can then be pre-stressed at the port interspace to align them with the window assembly, which would be at the operating temperature position. Or, a sliding vertical joint could be incorporated in the port cell to allow the WG to be aligned in the cold position all the way through the port cell. As the machine warms-up, the waveguides in the port interspace and in the port cell can be raised to maintain the required straightness, with this vertical motion taken up in the expansion joint. See sections 9.3 and 9.4 for further information.

6.2.4.7 Waveguide connection box

ITER ECE system has two radiometers (O-mode and X-mode) and a Michelson interferometer with four channels (two for O-mode and other two for X-mode). Thus, there are six measuring instruments that can operate simultaneously.

There are two types of measurement operations:

(1) Full magnetic field (B_{t0} = 5.3 Tesla), and

(2) Half magnetic field (B_{t0} = 2.65 Tesla).

The ITER Research Plan **ITER Research Plan (IRP) (2FB8AC v2.2)** specifies that the half-current/ half-field scenario is a necessary element of the development plan.

There are two front-ends radiation collectors proposed for ECE measurements. One is for radial measurement and other is for oblique (10^o angle to radial) measurement. By using two polarizer splitter units, the X and O-modes are selected from both the frontend radiation lines. Therefore, there are four transmission lines set up from the port interspace to the ECE room in the diagnostic hall. These four waveguide transmission lines (TL) are layed out at a ceiling of the ECE room. Among these, two TL are for oblique O-mode and X-mode measurement sightline (i.e. OO and OX). Other two TLs are for radial X-mode and O-mode measurement sightline (i.e. RX and RO) (see Fig. 6.13).
Here it is considered that the Michelson interferometer can simultaneously survey all 4 lines, and that radiometers are connected to the corrugated lines to obtain the electron temperature profiles, but could be switched to other two lines, too, if necessary. The measurements on the perpendiculat line-of-sight are used to derive electron temperature profile and to study phenomena related to the electron temperature. Hence, the radial measurements are detected in both modes by the radiometer as well as the Michelson interferometer. According to this requirement, the connection box is designed.

(1) Full magnetic field (B_{t0} = 5.3 Tesla) operation

Figure 6.13 shows a schematic diagram of a waveguide connection box. It consists of straight waveguide sections, two wire grid splitters and four miter bends. Two oblique measurement lines (i.e OX and OO) are fed to the Michelson interferometer (X-channel and O-channel) through miter bends (see Fig. 6.16). Other two radial beams (i.e RX and RO) are divided by the wire grid splitter G1 and G2. Then half beam power is input to corresponding radiometers (i.e X-mode radiometer and O-mode radiometer). And remaining power of both lines is entered to the O-mode and X-mode Michelson channels through miter bends M_3 and M_4. In this, six measurements are done simultaneously.

(2) Half magnetic field (B_{t0} = 2.65 Tesla)

For this measurement, there would be needed a change in the layout of connection box arrangement in the diagnostic room. The layout is shown in Fig. 6.14. Here, the radial X-mode line RX is disconnected from X-mode radiometer input and connected to the O-mode radiometer by using the waveguide section and miter bend. Before this connection, there is also a minor change which must be done at the input of the O-mode radiometer. The radial O-mode line is disconnected from input of the O-mode radiometer, the wire grid splitter is also removed from the RO path and a waveguide polarization-twister must be connected to the input of all the mixers of the radiometer to rotate a polarization of the incoming radiation beam. Therefore, there are five measuring instruments in this arrangement.

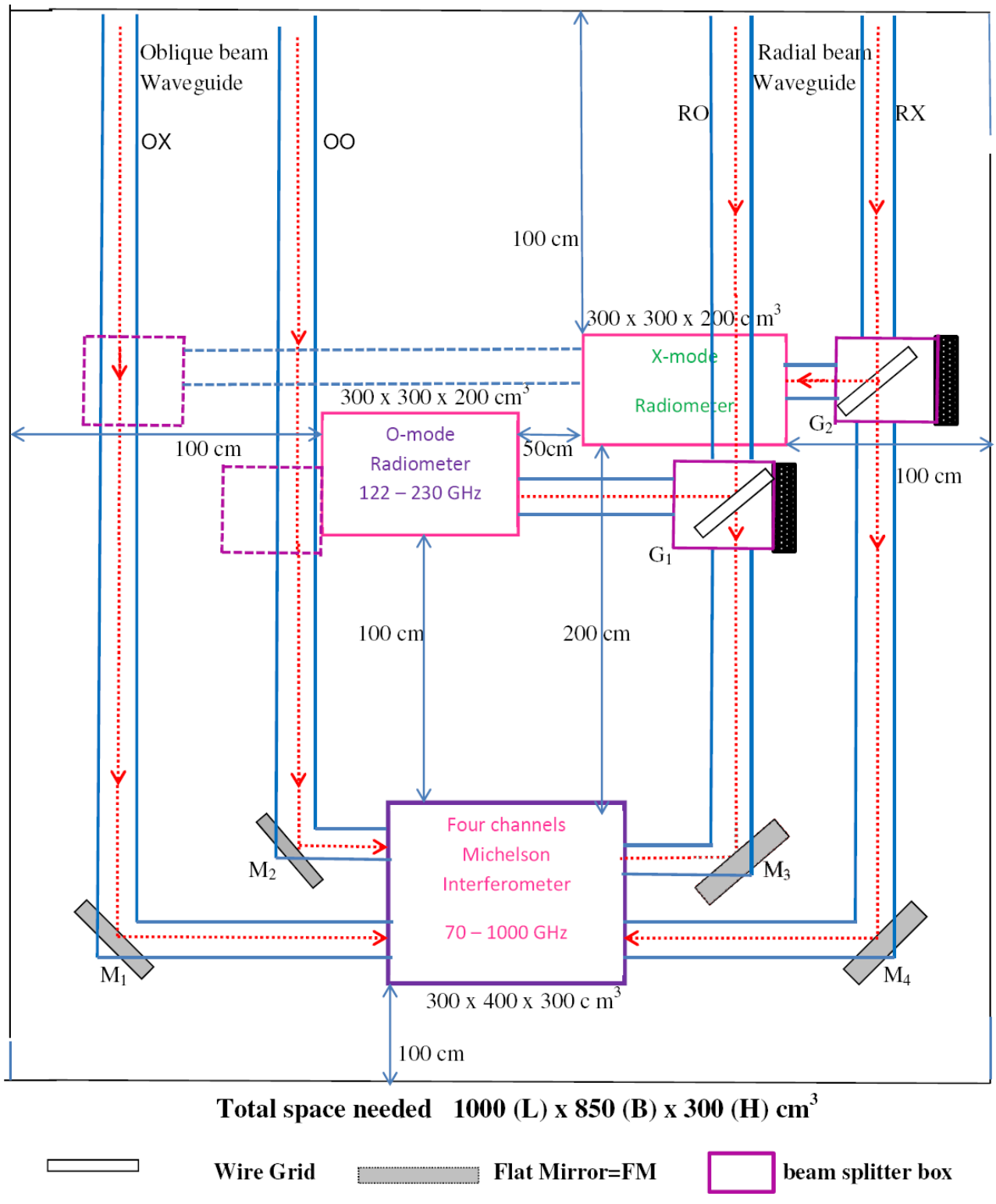

Figure 6.13. Connection box arrangement for full-Bt operation.

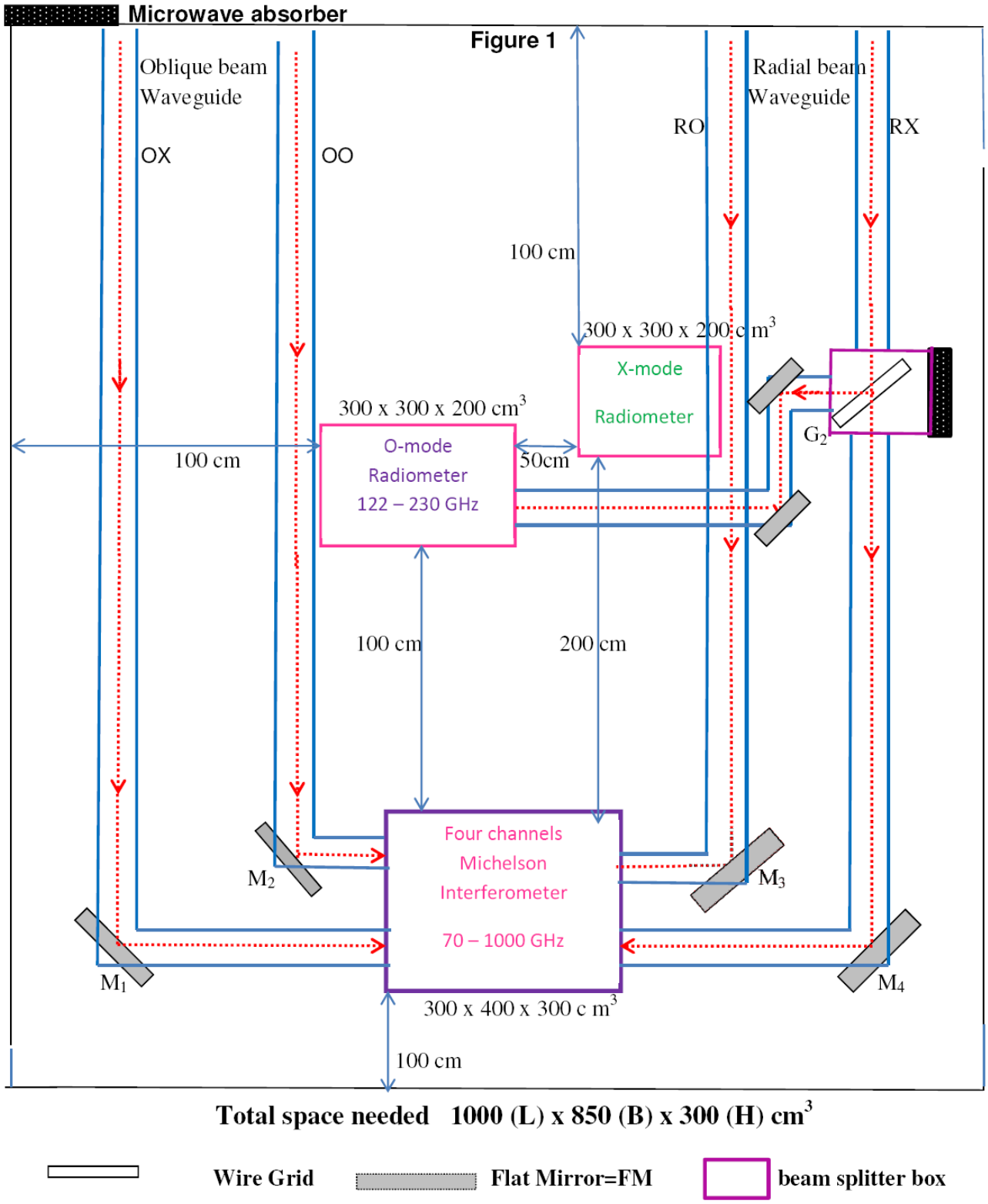

Figure 6.14. Connection box arrangement for half-Bt operation.

6.3 Description of proposed calibration and alignment concepts

The ECE system will require absolute calibration, alignment and verification measurements. These measurements will be part of the front end optics, TL, and instrumentation installation. Additionally, some calibration measurements must be made periodically, while other during each discharge. The Microwave Working Group has produced the report 'Requirements for calibration & testing of ITER microwave based diagnostic front-end components' [ITER_D_33ZRFR], which summarizes about the calibrations and testing needs for the ECE system.

Allowable calibration error for ITER ECE measurement

For ECE electron temperature profile measurement, the total error should be 5 % or less. The r.m.s. error should be 2.5 % or less. (The error of 5% is quoted as $\pm 2\sigma$ in the PR).

For power loss and spectral information, the r.m.s. error is also 2.5 %. For this, measurement from two views should be compared. Therefore, the r.m.s. error for each line of sight would need to be < 1.8 % rms (taken as: sqrt(0.5* (0.025^2)).

The statistical noise during plasma measurement depends on video band width (i.e. time resolution ~ 10 ms and the frequency resolution of the interferometer ~ 10 GHz). It is negligible for ITER ECE Michelson interferometer measurement. Hence the total r.m.s. error for each line of sight should not be exceeded 1.8% to cover both functions (profile measurement as well as power loss), but we note that the profile is a little more forgiving.

The calibration error depends on a number of factors of which the following three are significant contributors:

1) The error of the measurement of the hot/cold calibration source temperature;

2) The accuracy in the knowledge of the emissivity of the calibration source within interest of frequency range;

3) Statistical error during calibration.

One should estimate fractional error generated by each factor and determine accuracy of the ECE measurement instrument
The error into the measurement of the hot/cold source depends on three factors. First is temperature measurement accuracy of each thermocouple. This is ±0.5 ^{o}K; given by manufacturer of the thermocouple. Second in principle is the source surface temperature fluctuation during calibration. It is ± 2 ^{o}C out of 700 ^{o}C; specified in the ITER ECE calibration source design. However, this is automatically compensated when the average ΔT is calculated and can be neglected. Third is the surface temperature uniformity. This is ±10 ^{o}C of the surface temperature ~700 ^{o}C, specified in the ITER ECE calibration source design. Among all three errors, the error in the surface temperature uniformity dominates and gives ±1.5 % in the calibration. However, this is a systematic error that can be reduced during the hot source characterization. Assuming the temperature pattern is stable to 10%, the residual error will be about 1 K. The overall measurement error is then below 0.75 K r.m.s. or < 0.13 % r.m.s.
Typically, the accuracy in the knowledge of the emissivity of the calibration source is proximately ±1.2 % or better. This is achieved for the Alcator-C Michelson interferometer calibration source. A better value is expected for ITER ECE hot source.

The error due to above two factors is 1.2 % in r.m.s. Therefore, the statistical error in calibration data should be 1.35 % in r.m.s. to achieve total error of 1.8 % r.m.s. in the calibration process. The Michelson interferometer oscillatory nature is useful to reduce the random noise in the calibration and improve the calibration accuracy by long time integration of the measurement. The method to calculate required integration time is given in next section of the report. We calculated the integration time for 2% accuracy (1 % r.m.s) and shown in Fig. 4. This calculation is consistent with past experience of the DIII-D ECE Michelson interferometer, which was found to be less than 2% error for ITER ECE range of frequency.

Estimation of integration time required for calibration

For 2% accuracy (1 % r.m.s), the Signal-to-Noise ratio (SNR) equals to 100, and the integration time T_i is given by [Treffers, Applied Optics, 1997 and H. Hartfuss, EC-4 Workshop]:

$$T_i = 40000 \left(\frac{NEP}{P_s}\right)^2$$

Here, NEP is Noise Equivalent Power of the detector in Watt/Hz$^{-1/2}$, P_s is the calibration source power falling on the detector and can be determined by following expression:

$$P_s = K\,\theta_s\, f^2\, \Delta f\, E_t T_{tl}$$

In the latter, θ_s is the source temperature, f is the frequency of radiation, Δf is frequency resolution of the interferometer, E_t is the etendue, T_{tl} is the transmitivity from source to the detector and K = 2.44 x 10^{-41}. For the calculation, it is considered that NEP = 1 x 10^{-12} W/Hz$^{-1/2}$.
For ITER ECE Michelson interferometer parameters with frequency resolution of 10 GHz, source temperature of 973 K and etendue of 1.28 x 10^{-5} m^{2}Sr, the required integration time for the calibration is given in Fig. 6.15 for all three types of waveguide transmission line.

Note that, if one is targeting for 1% accuracy (0.5 % r.m.s.), the SNR is about 200. Thus, the calibration time will increase.

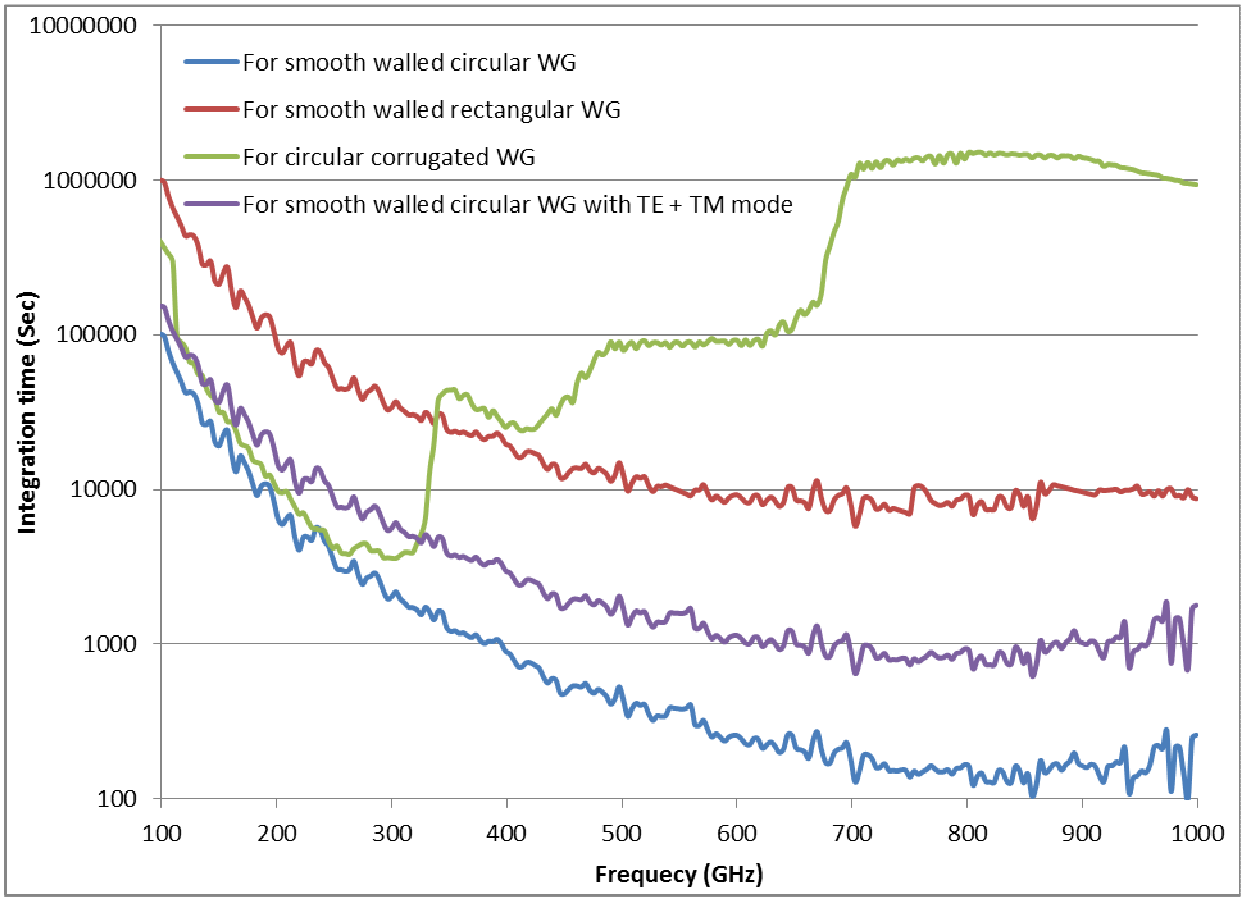

Figure 6.15. Required integration time for the calibration. It is observed that the required integration time Ti is low enough for the smooth-wall circular waveguide transmission line. Therefore, this type of waveguide is suitable for ITER ECE application.

6.3.1 Installation verification

Pre-testing of the in-port optics will be made in the Port Plug Test Facility (PPTF). Pattern measurements of the beam launched from the end of a polarizer splitter box will be made to determine mode purity (see example in Fig. 6.16). This may also be done at various locations along the TL during installation as needed. These measurements will need to be performed at least three/four desecrate frequencies in the ECE temperature profile measurement band 110 – 360 GHz. Additional measurements for each TL will be performed transmission attenuation and polarization scrambling through the full TL. Finally, the specific alignment or pointing of front-end optics will be verified using lasers, and the in-vessel coordinate measurement system used to measure the exact front-end aperture locations.

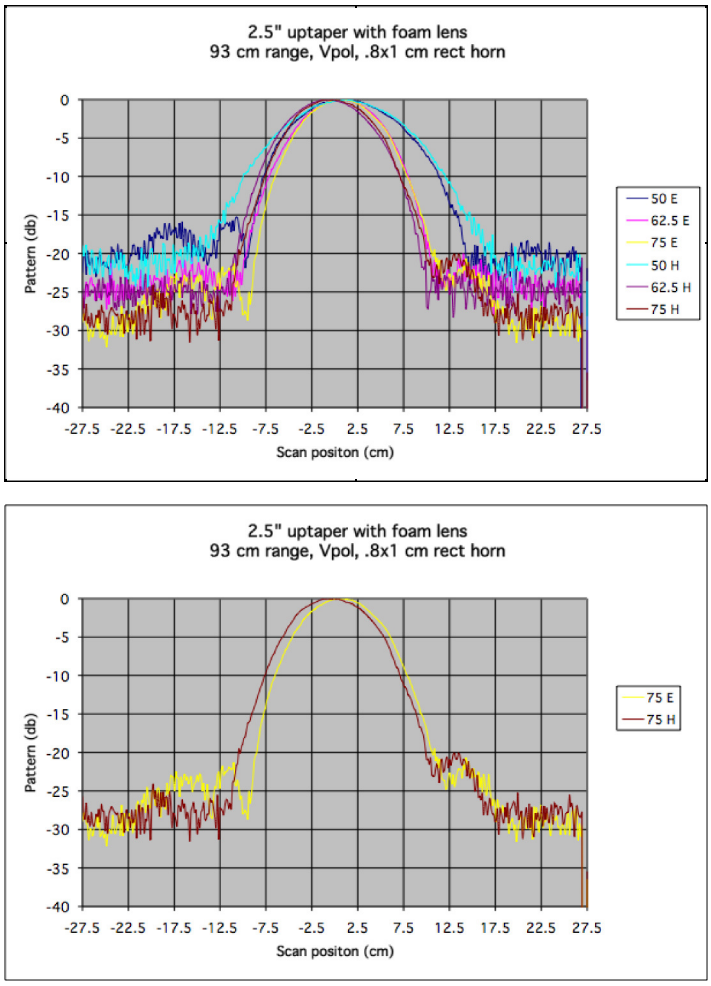

Figure 6.16. Examples of beam pattern measurements from the end of a corrugated waveguide for the LFS reflectometry TL. Deviation from the predicted HE11 mode pattern indicates higher order modes in the launched signal.

6.3.2 In-situ calibration

One of the electron temperature measurement diagnostics for ITER is based on measurement and interpretation of electron cyclotron emission. The required instrumentation detects radiation from 100 GHz to 1 THz. Since the measurement depends critically on the absolute intension of the radiation, a calibration source is included to monitor the evolution of the transmission of the front-end, in-vessel optics and the transmission of the waveguide.
The calibration source is needed for in-situ absolute intensity calibration of the front-end components of the diagnostic. The source is a blackbody emitter, and will be needed for a two-temperature calibration of the system sensitivity. The details of the hot source are given in Section 6.2.4.2 and in the Annex 6.2.1.

An additional but very infrequent end-to-end calibration of the diagnostic would require a dedicated calibration tool (hot source) remotely inserted by an articulated arm (so-called Multi-Purpose Deployer, or MPD) inside the vacuum chamber. This can be done during the scheduled shutdown; the results of the calibration can be used to check the calibration factors obtained by routine built-in calibration sources. Note that the procurement of this dedicated tool is currenly not in the scope of this diagnostic and may be considered during the operational phase.

In addition, the proposal to integrate an additional source for checking the stability of the

radiometer is under consideration. It would be similar to the front-end calibration source and installed in the transmission line.

6.3.3 Calculation of Signal-to-Noise ratio for the ECE Michelson interferometer transmission line

Calculation of Black body hot source intensity can be performed using the following assumptions:

$$I_{BB} = \frac{f^2 KT}{2c^2} \qquad (6.3.1)$$

Here, f (in Hz) is a radiation frequency, K (= 1.38 x 10^{-23} J/k) is the Bolzmann constant, T is the source temperature and c (3 x 10^8 m/s) is a speed of light.

Calculation of etendue for frontend optics is an important step for the power calculation. The optical arrangement is given in Fig. 6.17.

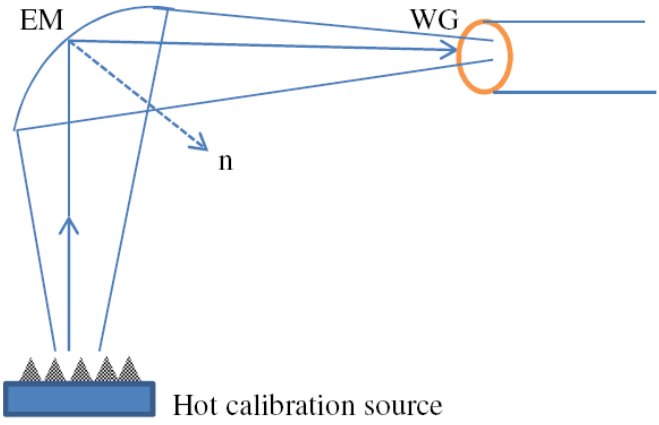

Figure 6.17. An arrangement to calculate the etendue for front-end optics.

The distance between the source and an elliptical mirror and mirror to the waveguide is considered to be 2.1 m. The size of the EM mirror is 0.2 m. The size of the radiation beam which falls on the entrance of the waveguide depends on the radiation frequency and can be derived using the following relation:

$$\omega_0' = \frac{\omega_0 f}{Z_R} \qquad (6.3.2)$$

Here, ω_0 = 0.0286 m is the size of the input beam, f = 2.1 m is focal length of the EM, and

$$Z_R = \left(\frac{\pi \omega_0^2}{\lambda}\right) \qquad (6.3.3)$$

For frequency of 115 GHz, the Gaussian beam size is calculated to be 0.06 m wide. The etendue can be calculated using the following equation:

$$Et = dA_m * \frac{dA}{f^2} \omega_0' \cos(45^\circ) \qquad (6.3.4)$$

In this equation, dA_m is the area of the EM mirror surface which is 0.0314 m^2, $dA_{\omega'0}$ is the area of the radiation beam at entrance of the waveguide which is 2.83 x 10^{-3} m^2, the focal length f is 2.1 m, and cos(45^o) is 0.7071.

Thus, the etendue is calculated to be 1.4235 x 10^{-5} Str. m.

The power at the entrance of the waveguide can be calculated by multiplying etendue by the equation (6.3.1), so one gets P = 4.33 x 10^{-11} W.

Let's assume that the etendue at the input of the detector is greater than the etendue at the front-end optics.

Fop the transmission attenuation, following the approach described in section 6.2.4.8, one gets 13.8 dB for the frequency of 115 GHz. The fraction of power transmission due to this attenuation is calculated to be 0.042. The total power which is detected is 4.33 x 10^{-11} x 0.042 = 1.81 x 10^{-12} W, assuming the Hot Source temperature of 600 K.

The Signal-to-Noise ratio can be estimated as follows:

$$SNR(f) = \frac{P_{cal}}{NEP}\sqrt{\frac{T_{int}}{4}} \qquad (6.3.5)$$

Here, P_{cal} is calibration source power, NEP = 1.25 x 10^{-12} is the Noise Equivalent Power of the detector. T_{int} is integration time to achieve required SNR value.
For SNR = 10, T_{int} is 190.77 s. If the Hot Source temperature is 1000 K, T_{int} is 64 s.
Similar calculations for the radiometer yield the required calibration time of about 9.7 hours (the noise temperature of the radiometer is 10 eV).

The assessment for Michelson for higher frequencies has yielded the following calibration times:

- for the frequency of 150 GHz with the TL loss of 15 dB, T_{int} is 312 s. If the temperature of the Hot Source is 1000 K, one gets 112 s;
- for the frequency of 400 GHz and 21 dB loss, T_{int} is 1783 s, or 0.5 days for 1000 K Hot Source temperature

The maximum mode number that can be detected is calculated following the scheme given by Fig. 6.18.

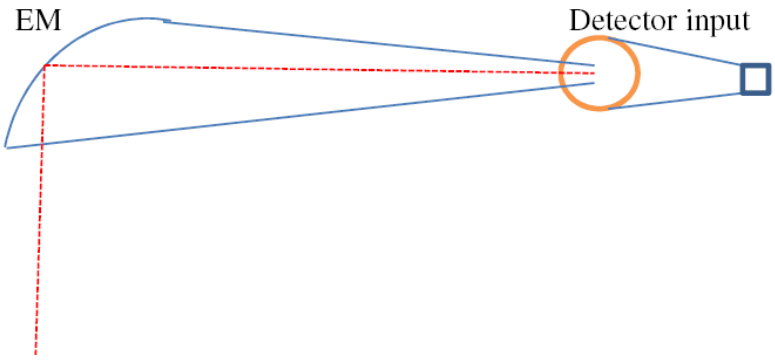

Figure 6.18. The detector input optics arrangement to calculate the etendue for detector optics.

The size of the EM mirror is 150 mm and the detector size for Michelson is assumed to be 20 mm in diameter. The focal length of the mirror is 300 mm. The etendue for detector optics is calculated by using equation (6.3.4) for these mirror parameters. It is found to be equal to 4.4 x 10^{-5} m^2.Str.

Therefore, the maximum number of modes which is coupled to the detector is Et/λ^2. For frequency 115 GHz, it is int(6.47) = 6.

6.3.4 TL line-length measurement and alignment

The length of the TL will change from the cold position to the hot position for plasma operations. The TL length will change as the temperature in the port cell, gallery and diagnostic lab changes during the day.

The TL length can be measured by use of a linear encoder on the radial (and vertical, if present) expansion assemblies (that can be a part of the polarizer splitter box assembly) to measure the exact change in length. Additionally, the deployment of thermocouples along the TL from the interspace to the diagnostic lab will allow the temperature profile of each TL to be determined in real time. The use of the linear encoder data and the temperature data will allow accurate prediction of the total length change from the cold calibration position to the operating position, and any additional changes during a shot.

The strain gauges located along the TL in the port interspace, port cell, gallery and the diagnostic area will allow to monitor the bends in the long waveguide runs to account for the mode conversion losses in the TL.

An ‘in-waveguide’ measurement (like in the reflectometry systems) can also be potentially enabled but more difficult to implement. This measurement will utilize reflectometer-like measurement technique to measure the distance to a known reflection in the TL. An obvious known reflection could be a primary window assembly or a shutter. A shutter can be located on the diagnnostic hall side of the expansion assemblies to measure the TL length of the ‘fixed’ system. These measurements would not likely be made during a discharge, but could be down just before and/or just after. An additional reflection point can be the intentional introduction of a reflection at the 2nd miter bend in the port plug. This may be a small groove or a high frequency grating in the miter bend reflector. Note that this type of measurement will require an additional mm-wave source and RF/IF circuit integrated in the back-end of the diagnostic. The detailed assessment of various possibilities will be done during the preliminary design phase.

6.4 Stray radiation protection

The ECE transmission lines are expected to receive significant amounts of millimeter wave (MMW) power due to unabsorbed ECH power and emission from the plasma. The expected power loads could be 100's of watts or more during plasma startup (see Annex 18.2 for details). Power loads from plasma emission from ELMs, fast electrons and unabsorbed ECH power can be in the 10's of Watts based on experience from other machines. The MMW power in the TL can damage electronics, passive WG components and Quasi-optical (QO) components. A detailed review of the risks from Stray Radiation and the possible techniques for protecting from these threats can be found in the Microwave Working Group report 'Stray radiation protection of ITER microwave based diagnostics', **ITER_D_33PKHG v1.0.**

To protect the ECE system, a layered approach to attenuating or eliminating ECH and stray radiation power is required (see Annex 6.4.1). This layered approach will utilize shutters in the WG to block stray radiation during plasma startup and late in the ramp-down phase. Additionally, the shutter may be connected to stray radiation sensors to close the shutter if increased MMW radiation levels are detected. On request, the signal from these stray sensors can be supplied to the Central Interlock System (CIS) and to the PCS. It is desirable to have shutter speeds of <1 ms, but presently speeds of >10 ms are available.

To obtain fast protection of microwave diode components, active devices, such as PiN switches or Ferrite isolators, will be used. These have switching times of <1 μs and can provide over 20-dB attenuation. Ferrite attenuators may be preferable because when combined with TM mode filters, they can attenuate both in band and out of band (over-moded) signals.

6.5 Description of data-acquisition and software concepts

Diagnostic should use all approaches that exist now on different machines to best performance. This is a rough outline of what the data acquisition demands might be for the ITER ECE system.

O-mode Radiometer systems:

There are four down convertor systems. These give total 52 channels for the O-mode radiometer. All these channels require minimum 18 bits data channels @ 10 kHz for slow measurements and @ 100 kHz and @ 1MHz for fast measurement in window in time span of one ITER plasma operation. The duration of window depend on physics phenomena under study. Table 6.7 gives the desired specifications for the O-mode radiometer. The final channel separations and the final frequency range coverage will be agreed by the PDR.

Table 6.7. Target specifications for the O-mode radiometer.

Parameter	Value	Comment
Frequency range	122 GHz – 230 GHz	
Channel separation for 122 – 139 GHz	1 GHz of 18 channels	F-Band waveguide ; 1 mixer
Channel separation for 141 – 169 GHz	2 GHz of 15 channels	D-Band waveguide ; 2 mixer
Channel separation for 172 – 218 GHz	3 GHz of 16 channels	G-Band waveguide ;3 mixers
Channel separation for 222 – 230 GHz	4 GHz of 3 channels	1 mixer
Duty cycle	Continuous	
Video BW	DC – 1 MHz (as per requirement)	Further integration to be performed digitally
Dimensions (L x W x H)	3 x 3 x 2 m (tentative)	Only for receiver system

X-mode Radiometer system:

There are sixteen down convertor system with 36 channels. All these channels require minimum 18 bits data channels @ 10 kHz for slow measurements and @ 100 kHz and @ 1MHz for fast measurement in window in time span of one ITER plasma operation. The time window duration depend on physics phenomena under study.
The measurement frequency bandwidth to be covered is in the range between 244 – 355 GHz. The anticipated channel coverage set for core and edge measurements at 5.0 T for 2X-harmonic for the X-mode radiometer is given as follows, following CDR proposal:

- 32 channel core set:

– Frequency range: 234-306 GHz,
– Channel spacing: 2.25 GHz,
– B_{IF} = 2 GHz,

- 16 channel high resolution set:

– Channel spacing: 375 MHz,
– B_{IF} = 250 MHz,
– Switchable to other mixers.

The final channel separations and the final frequency range coverage will be agreed by the PDR.
The ECE is meant to operate as a single diagnostic. To this end the software to run the Hot Sources (US DA) and to run the X-mode radiometer (US DA) must be interoperable with the (IN DA) contribution.

Michelson interferometer:

For ECE measurement in fusion plasmas, a polarized interferometer is used to observe the wide range of frequencies. One of the most successful types of FTS instruments is a Martin-Puplett type of Michelson interferometer. At JET, Michelson ECE measurement has three lines-of-sight with two orthogonal linear polarizations (X and O-mode). In this, one is for radial measurement done by

a rectangular waveguide and two oblique (at about 9.5^o and 20.5^o respect to the radial direction) measurements done by a combination of fixed mirrors, feeding the nearly radially oriented smooth circular waveguides. All three antennas are located approximately equatorial plane on the low field side and connected to a multi-channel Michelson interferometer through 60 meter long transmission line. Each oblique antenna signal is split into O-mode and X-mode and fed to Michelson with quasi-optical arrangement. The optical layout is same for all channels. This is a so-called Martin-Puplett interferometer with four helicodal sectors on circular rotating wheel mirror of radius 150 mm. The combined output beam is measured by He cooled InSb detector. The interferometer gives interferogram with ~ 5 ms time resolution and output spectrum covered from 1st harmonic to 4th harmonic (~ 75 – 350 GHz for magnetic field of B_H of 3 T).

The division of the incident wave is achieved by a polarizer beam splitter made up of arrays of parallel metal wires. An interferogram is generated by combining two beams at the beam splitter after reflection one beam from a fixed and other beam from a moving mirror. The spectral intensity is obtained by Fourier transformation of the interferogram.

Proposal for ITER Michelson interferometer design

There are three important features for the design driver of the Michelson interferometer for the ITER ECE spectrum measurement. One is the rapid scanning mechanism that decides the time resolution of full spectrum measurement. Second is the isolation from atmosphere to avoid water vapour absorption of the mm-wave radiation. Third one is a throughput of the interferometer. Absolute calibration of the Michelson interferometer by the hot/cold black body source technique depends on the throughput of the interferometer. The interferometer with high throughput can be absolutely calibrated within moderate time scale. These three features need to be optimized in the design of the ITER ECE Michelson interferometer.

In the "old" (2001) ITER ECE baseline, two Michelson interferometers (for O- and X-mode) were included. The scheme of the "old" design is given in Fig. 6.19.

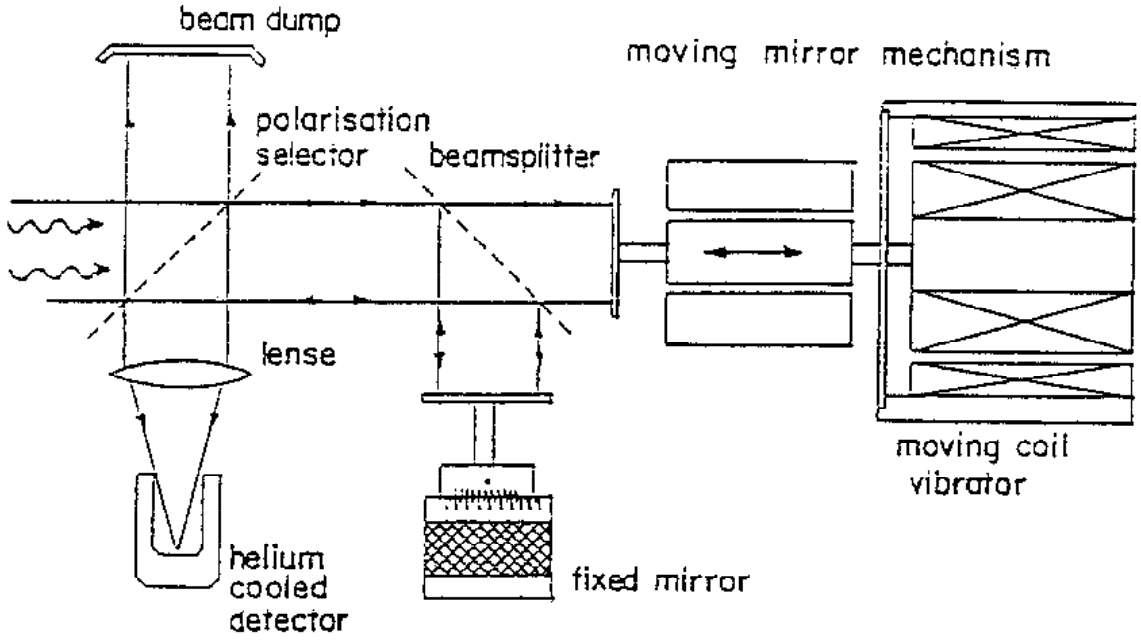

Figure 6.19. "Old" (2001) design of Michelson interferometer for ITER ECE.

The future design of the ITER ECE Michelson will give improvement in the state-of-the art in ECE spectra measurement method. The use of all reflection optics for coupling between waveguide transmission line and the interferometer give good throughput. The vacuum tight modular design and an in-vacuum rapid scanning mechanism are suitable for the ITER ECE measurements up to 1 THz.

With above design features of ITER ECE Michelson interferometer, the following specifications are proposed:

Spectral range (GHz) : 70 – 1000
Frequency resolution : 5 GHz
Linear path scan (mm) : 40
Path difference sampling (μm) : 20
Scanning repetition rate : 10 ms
Sampling frequency of the recording system: 200 kHz
Instruments throughput > 0.4 x 10^{-4} m^2Sr (see Fig. 6.18 and the text below).
Number of Michelson interferometers: 2 (one for O-mode and another for X-mode)*
Duty cycle: continuous

*Note that the space reservation for extra Michelson instruments is planned in the diagnostic building and in the port cell. The latter one is a risk mitigation action if the TL losses will disable the reasonable calibration time for instruments located in the diagnostic area. This enabling feature is decoupled from the Procurement Package and from deliverables by IN DA as they will be specified in the Annex B.

Existing available technology of optical components (like reflecting mirrors, wire grid polarizers etc.) can cover ITER ECE required spectral range 70 to 1000 GHz.

Typical Detector Performance

- Spectral Bandwidth : 60 to 1200 GHz.
- System Optical Responsivity: > 2,000 V/Watt.
- System Optical N.E.P, : < 1.25 x10^{-12} Watts $Hz^{-1/2}$
- Maximum power handling capacity : 10 μW
- Upper level of dynamic range (3 dB) : 1 μW
- Total dynamic range : > 29 dB
- Frequency Response (-3 dB) : 0 to 750 kHz
- Active Area : 25 mm^2
- Typical Operating Resistance : 5-10K ohms
- Operating Temperature : 4.2K

Coupling optics and Michelson optics layout

A circular smooth-wall waveguide of 72 mm inner diameter is proposed for ITER ECE transmission line for both radial and oblique views. Two transmission lines (i.e. one for radial and other for oblique measurements of O-mode) are kept near input of the O-mode Michelson interferometer and same arrangement is also for X-mode Michelson interferometer input. There are coupling optics placed between the transmission line waveguide and the input of the Michelson interferometer. For optimum coupling between waveguide to optical mirror, there is relation between dimensions of the waveguide (i.e. radius, a, or longer side, a) to the beam waist radius (w) at the input of the waveguide. One can use this relation for dimension calculation of the optical

components. For smooth-wall circular waveguide, an optimum coupling is 87%, and the ratio of the beam waist radius (w) to the radius of the waveguide is 0.76. Therefore, the beam waist radius (w) is calculated to be 27.36 mm for the ITER ECE proposed waveguide transmission line.

The coupling optics and the Michelson interferometer optical layout are shown in Fig. 6.20. The layout consists of two Gaussian beam telescope constructed by using four ellipsoidal mirrors. First three mirrors have same focal length (~ 33 cm) with diameter of ~11 cm, and last mirror has a focal length of 12 cm (with same diameter). The beam size from the waveguide output to the detector input is calculated by using Gaussian beam optics theory. This size is useful to decide the size of the optical components. The size of the optical components should be more than 4 times the radius of beam for optimum coupling (~ 99%).

Other possibility for the transmission line waveguide types has also been investigated for the CDR. In this proposal, there were two types of waveguide at the input of the interferometer, compared to the one type of waveguide in the present baseline. One is circular corrugated waveguide of diameter 63.5 mm and other is rectangular smooth walled waveguide of dimension 72 x 34 mm^2. The same relation for optimum coupling is used for both types of waveguides. These are: w/a = 0.64 for circular corrugated waveguide with coupling coefficient of 0.98 and w/a = 0.3 for smooth walled rectangular waveguide with coupling coefficient of 0.85.

Note that, during the PDR phase, one of the priority activities would be to follow up the state-of-the-art of FTS systems and to propose the solid design at the Preliminary Design Review. In additional to the FTS instruments proposed in the current baseline (which is reported in the current note), the Michelson interferometer with four channels output from four detectors (as presented at the CDR) and four-channel Mach-Zehnder interferometer are clear candidates to investigate as R&D tasks. The MZ option may also include the in-waveguide instrument with waveguide diplexers which are being currently developed by KIT. The latter has been discussed to be able to measure up to 1 THz; however, the manufacturing tolerances, as well as alignment, are critical issues to solve. The extended discussion on different pros and contras of the above-mentioned instrumentation is reported in this document: Note on Candidate Fourier Transform Spectrometers for ECE Measurements on ITER *(ITER_D_4DQA8H v1.3)*. Because of the broadband frequency operation, water vapour removal is a problem which will require a careful attention during the design of the FTS instrumentation. The design of the TLs and the integration of the ECE back-ends into the tokamak complex and into the diagnostic areas will enable smooth switch from one type of instrument to another without any major issue.

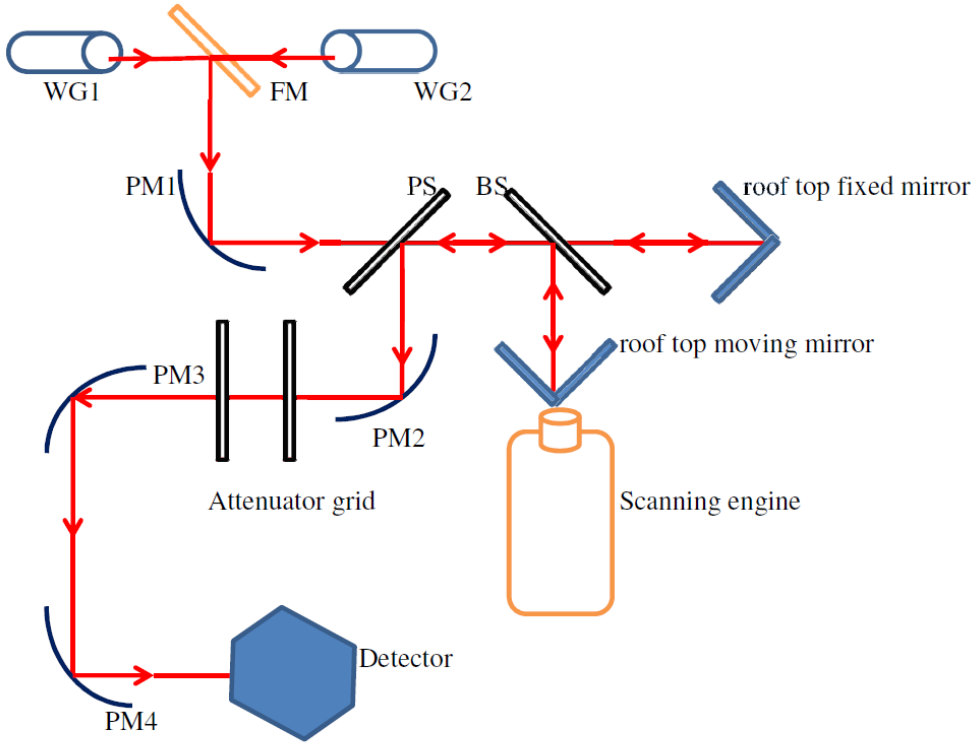

WG - circular waveguides, FM - flat mirror, PM - parabolic mirrors, PS - polarizer selector, BS - beam splitter.

Figure 6.20. Layout of Michelson interferometer optical components for the current baseline.

Transmission Line, Power and ECH monitoring:

In addition to actual data signals, it is anticipated that there will be monitoring of:

a) Transmission line temperatures
b) Transmission line movements/expansion
c) Measurement of ECH power in transmission line for protection

Most of this data can be taken at low data rates (100's of kHz), apart from the ECH protection data, which will require fast acquisition for use with a fast protection system.
Assuming 2 frontend waveguide and four transmission lines waveguides; in the baseline design, this implies:

1) 60 Slow data channels, at 10 channels per waveguide, so 60 channels at 100 kHz.
2) 12 faster data channels for ECH protection and interlocking, so 12 channels at 10 MHz.

The signal survey for ITER 55F1 ECE diagnostic is summarized in Table 6.8.

Table 6.8. The signal survey for ITER 55F1 ECE diagnostic.

Number of PSH (Plant system hosts) if not 1 (standard) : ……..

Physical Signals ONLY

FAST CONTROLLERS

1. ADCs (please enter number of channel and modify sampling rate and resolution if needed)
   a. 10 kHz, 18-bit ……100
   b. 100 kHz, 18- bit ……..100 (window)
   c. 1 MHz, 18- bit ……..116 (Window)
   d. 10 MHz, 16- bit ……..0
   e. 100 MHz, 14-bit ……..0
   f. 1 GHz, 12-bit ……..0
   g. Other (specify) ……0
2. Cameras (specify image size and frame rate)
   a. Visible ……...0
   b. IR ……..0
   c. VUV ……..0
   d. X-Ray ……..0
   e. Other (specify) ……..0
3. Other Measurement equipment
   a. Mass Spectrometer ……..0
   b. Optical Spectrometer ……..0
   c. Dosimetry ……..0
   d. Lasers ……..0
   e. Signal Sources (calibration)……0
   f. Signal Source (probing) ……0
   g. Microwave receiver ……..12
   h. Pneumatic system ……..0
   i. Other 1 (specifiy) ……0
   j. Other 2 (specifiy) ……0

SLOW CONTROLLERS

Sensor signals (please indicate if special requirements not compatible with S7 Simatic)

1. Temperature ……4
2. Pressure ……..0
3. Flow ……0
4. Level ……0
5. Vibration/Acceleration ……..0
6. Position ……0
7. Displacement ……0
8. Strain ……4
9. Other 1 (specify) ……..0
10. Other 2 (specify) ……..0

Actuator signals (specify whether digital or analog)

1. Shutter ……..2
2. Mirror ……0
3. Valves ……0
4. Motors (specify type) ……0
5. Other 1 (specify) ……0
6. Other 2 (specify) ……0

6.6 Summary of risk analysis and proposed mitigation plans

This section aims at setting out the feasibility risks for the LFS Reflectometer diagnostic identified during the CDR preparation. It identifies the technical problems that have the potential to adversely affect the ECE system on the meeting of the system requirements.
This work is based on the approach of the MQP Risk Management Plan (v2.1) 22F4LE (https://user.iter.org/?uid=22F4LE&version=v2.1&action=get_document). For each risk, an approach has been chosen between three possible choices: to mitigate, to avoid and to accept. Then, the possible actions in this approach have been described.

The results are detailed in the ECE diagnostic risk table [Annex 6.6.1, ITER_D_6KXF4U - ECE system risk table]. Risks are classified into five types:

- Design and Manufacturing
- Transportation
- Installation
- Operation
- Maintenance.

High Risks in Design and Manufacturing phase have been identified as follows (Risk score before and after the mitigation is indicated):

- **Waveguides**, miter bends etc not manufactured to design specs, or **design specifications do not provide predicted performance**: **16 ➔ 8** (after mitigation)
- Design specifications for front-end aperture size, tilt angle and/or separation do not provide predicted performance for plasma measurements: **16 ➔ 8**
- Low reliability of the shutters in the PP to protect the hot source: **16 ➔ 8**
- Poor preformance of the hot source: **16 ➔ 8**
- **Primary Vacuum Window** design and implementation **fails to meet safety** and/or vacuum requirements. -- **16 ➔ 4**
- **Primary Vacuum Window** design and implementation **fails to meet** microwave transmission/reflection **performance requirements**. **16 ➔ 8**
- **Secondary confinement boundary window** (Port Cell/Gallery and Gallery/Diag. Bldg) designs and implementations **fail to meet safety** and/or vacuum requirements -- **16 ➔ 4**

7 System performance assessment

In this Section the expected performance of the proposed ECE diagnostic conceptual design is discussed in relation to the specified measurement requirements. In addition, the major challenges to implementation are described together with identification of potential showstoppers.

7.1 Summary of measurement requirements

The measurement parameters for the ECE system are quite broad as illustrated in the Table 6.1. In the case of ***core temperature profile,*** the ECE system is also called out to be utilized for "Advanced Control" (AC), which would require "real-time" analysis of the diagnostic data as well as the availability of "real-time" EFIT information. The required temporal resolution is 10 ms. In the area of high frequency instabilities (NTM amplitude), the diagnostic has also been identified as a primary contributor again for "Advanced Control".

In addition to the above primary roles, the system is also required to provide "Back-up" measurement capability (when possible) for the ***L-H transition indicator/ELM temperature transient***, and "Supplementary" capability for the following measurement parameters: plasma energy/poloidal beta, main plasma Prad/Pece, some runaway electon parameters such as runaway current after thermal quench and during failed breakdown, edge electron temperature profile and some high-frequency instabilities such as turbulence.

The following sections discuss the issue of measurement prioritization and provide specifications for the diagnostic consistent with current expectations. This is followed by a discussion of major technical challenges facing implementation on ITER.

7.2 Measurements prioritization

Based on the above measurement requirements a prioritization analysis has been performed using a limited set of criteria. Prioritization is important in establishing a focus for development of a conceptual system design as well as accommodating constraints set by cost and space limitations.

The following three criteria were utilized in the assessment:

(1) IMPORTANCE of the proposed measurement parameter to the ITER mission

- This criterion is *independent of measurement technique* and focuses on the parameter to be measured

- The ITER Research Plan was employed to assess the importance of specific measurements

(2) RELATIVE VALUE of the measurement as performed by ECE system when compared to *alternative* techniques

- This criterion *assumes that the measurements can be made successfully*

- Listed ITER measurement specifications used as part of the process

- Unique capabilities are given significant credit

(3) CHALLENGE, ease or difficulty of actually measuring the specified target measurement parameter using the ECE diagnostic system

It should be noted that assessments were performed for both the early lower performance operating phase, as well as for operation during the planned Q= 5 to10 burning plasma phase. The analysis produced a clear primary measurement prioritization as illustrated below:

1. Core electron temperature profile;
2. NTM amplitude δT /Te;
3. Edge electron temperature profile and ELM temperature transient indicator;
4. Power loss due to ECE and the wall reflection coefficient determination;
5. Temperature fluctuation measurements due to MHD and high-frequency modes and instabilities;
6. Measurement of non-thermal electron population parameters and contribution to the EDF determination.

As can be seen the overall highest priority in a variety of ITER operating phases was identified as the **Core electron temperature profile** and **measurement of the NTM complex amplitude δT / Te.** It was concluded that for these measurements:

(1) ECE diagnostic could provide the required temporal and spatial information;

(2) the core profile represents the least measurement challenge for ECE system;

(3) the measurement couples well and contributes to other desired core phenomena measurements such as the L-H transition and the ELM temperature transient, as well as contributes to the poloidal beta estimation;

(4) ECE contributes to the feedback system to stabilize NTM by ECH or any other methods by using different heating methods and q-profile tailoring.

Based on the above prioritization, the conceptual design of the ECE system has therefore been driven to deliver optimum signal quality for determination of the core temperature profile during the burning plasma phase of the ITER operation, and to deliver the information about the NTM evolution in real-time to the PCS. However, for operational scenarios similar to Scenario 2, it is also expected that many of the measurement requirements indicated in Table 6.1 will be available during the plasma current flat top.

The expected measurement capabilities are described below.

(1) Real-time, continuous temperature profile data for active control:

- Requires real-time processing;
- Neural nets, field-programmable gate array (FPGA) based analysis, etc.

(2) **Optimized temperature profiles, ELM temperature transient, L-H transition – performed post-discharge. Continuous temporal evolution:**

- Store analysed electron temperature profile data. Dump majority of raw I/Q data;
- Time shared digitizers to allow memory transfer;
- L-H transition, ELM temperature transient data are available whenever required;
- Some portion of I/Q raw data can be stored for independent software analysis assessment.

(3) Multichannel ECE radiometers (spatial and temporal resolved) MHD/TAE data stored continuously:

- Possible sharing of O-mode radiometer for X-mode 2^{nd} harmonic measurement for half toroidal magnetic field operation;
- Requires waveguide connection arrangement for this.

(4) Michelson interferometer four-channel data stored continuously:

- Analysis will provide electron temperature profile with poorer (than radiometers) spatial and temporal resolution but with broad frequency bandwidth;
- Allows estimate of runaway/non-thermal electron study.

The above measurement capabilities are extremely impressive and unique for a single diagnostic system but it should be understood that there are some fundamental limitations inherent in the baseline design that require some discussion. In addition, prior to generating a Measurement Specification Table it is important to present a number of definitions related to ECE measurement accuracy.

7.3 Design Constraints

The adoption of a limited number (2) of fixed measurement lines (driven by space constraints and cost) introduces *some* restrictions to the operational range of the diagnostic. Typically, scenario modelling indicates that the plasma height is held relatively constant during the plasma current flat top but, can vary significantly (tens of centimetres) during ramp up & ramp down. Plasma height also varies with operating scenario. For example:

- Recent H-mode scenarios, Z ~ 520mm;
- Original Scenario 2, Z ~ 680mm;
- L-mode, Z ~ 504mm
- Half-field scenario, Z~ 660mm
-

It should also be understood that large variations in plasma shape (e.g. during startup/ramp down) can limit performance and availability. The height of 437 cm in the port plug reference layout is acceptable and will meet the measurement specifications. However, it is not optimal for all plasmas, and further optimization may be possible during the port plug redesign.

The limited number of measurement lines also serves to limit the available system redundancy. For example, failure of the front-end optics or the calibration shutter such that the ECE radiation cannot reach the radial measurement line. Then the electron temperature will be measured by the redundant/oblique ECE measurement line. However, by using microwave interferometry, CTS, or reflectometry transmission lines can provide alternate means for system redundancy. The X-ray crystal spectrometer (core high resolution) can also provide backup measurement capability.

Simultaneous measurement of electron temperature profiles, the ELM temperature transient, L-H transition, MHD/TAE/turbulence measurements, poloidal flow, etc. will be challenging. The measurement of the ELM temperature transient and provision of an L-H transition monitor require CONTINUOUS data availability. The collection of data in variable time windows is an effective and useful technique for high frequency, fast evolving MHD modes such as TAEs.

7.4 Spatial Resolution

Electron temperature measurement spatial resolution depends on the ITER plasma parameters, the front-end radiation collection system and the instrumental frequency resolution. In the following, we will discuss each parameters effect on spatial resolution.

In the original design, a Gaussian telescope was employed as front-end optics for radiation collection. This scheme will not be useed in reduced size ITER design. ITER ECE US group worked on front-end optics evaluation and proposed a new design [see Annex 7.4.1]. The new

design consists of a single focusing mirror located 152 cm from the plasma edge and a flat mirror between the splitter box aperture and focusing mirror. This arrangement provides a width of less than 6 cm for the outer minor radii for both first harmonic O-mode and second harmonic X-mode range of frequencies and accomplishes the ITER ΔX requirement of a/30 = 6.7 cm in the measurement. These front-end optics and their focusing properties define the poloidal and toroidal resolution of the ITER ECE measurements. But the radial resolution is determined by ECE frequency broadening effects, primarily due to the relativistic broadening. The effects of relativistic broadening were investigated for a typical ITER scenario using ECE simulation codes. The calculation was performed for plasma with a central electron temperature of 25 keV and density 1 x 10^{20} m^{-3}, the ITER core measurement requirement of $\Delta X < 6.7$ cm is only met for roughly the outer half of the plasma minor radius. For extreme ITER operating parameters, $T_e(0) = 40$ keV, the ECE simulation showed that the 1st harmonic O-mode frequencies can still provide measurements on the outer midplane with resolutions of 7 – 13 cm. Simulation at half –field ($B_t = 2.52$ T) and $T_e(0) = 12$ keV (i.e. the first operating phase of ITER) indicate that good T_e profile measurements. Calculations for edge region (r/a > 0.85) showed the relativistic broadening limits the spatial resolution. The width of the emission layer was found to be 1 – 4 cm except near the last closed flux surface – only there is the 0.5 cm specified in the ITER requirements approached. A target ΔR of 1 cm implies Δf of 280 MHz (IF bandwidth) for edge profile measurements.

The relativistic broadening effect on spatial resolution is summarized in following Tables 7.1 and 7.2.

Table 7.1 Width of Emission Layer for 1st Harmonic O-mode, Scenario 2

R_maj(cm)	620	640	660	680	700	720	740	760	780	800
Freq.(GHz)	148	144	139	135	131	128	124	121	118	115
Width(cm)	8.9	9.2	9.3	9.1	8.6	7.9	7.0	6.2	5.5	4.8

Table 7.2 Width of Emission Layer for 2nd Harmonic X-mode, Scenario 2

R_maj(cm)	620	640	660	680	700	720	740	760	780	800
Freq.(GHz)	297	287	279	271	263	256	249	242	236	230
Width(cm)	114	67	27	8.6	7.8	6.9	6.0	5.1	4.4	3.9

As seen in the tables, the ECE resolution along the viewing sightline ranges from 4 to 9 cm. This means that Te-profile features smaller than this will be obscured by the averaging effect. An important question then arises for using ECE in ITER to measure MHD modes, which need to be detected before they grow to a large size. In recent work it has been shown that, due to the low rotation in ITER, an island growing to only 5 cm in width will lock and disrupt the plasma.2 It needs to be determined, then, if the ECE measurement on ITER can detect islands smaller than 5 cm. To do this, we have undertaken a simulation of an MHD mode in ITER and its measurement by ECE taking relativistic broadening into account.

In order to simulate the effect of relativistic broadening on the ECE temperature measurement of an MHD mode, a set of Te profiles was created with a flat spot whose width varies in time, representing a magnetic island rotating with its X and O points in front of the ECE line of sight. The starting Te (R) is the ITER Scenario 2 profile and for the creation of the Te (R, t) points an island center and maximum width w_{max} are specified.

For the ideal measurement, i.e. one with perfect resolution, to a good approximation the maximum ΔTe is simply the half width of the island times the local gradient in Te:

$$\Delta Te, max = w/2*(dTe/dR). \qquad (7.4.1)$$

The width of the flat spot is varied sinusoidally from 0 to w_{max} and back to 0 with a regular and arbitrary time step. The Te-profile outside of the flat spot is set by making the change in Te fall off to zero at the profile center and edge with the cube of the radius from the widest point of the island. The resulting profiles for the extreme points of the oscillation, the X and O-points, are shown in Fig. 7.1.

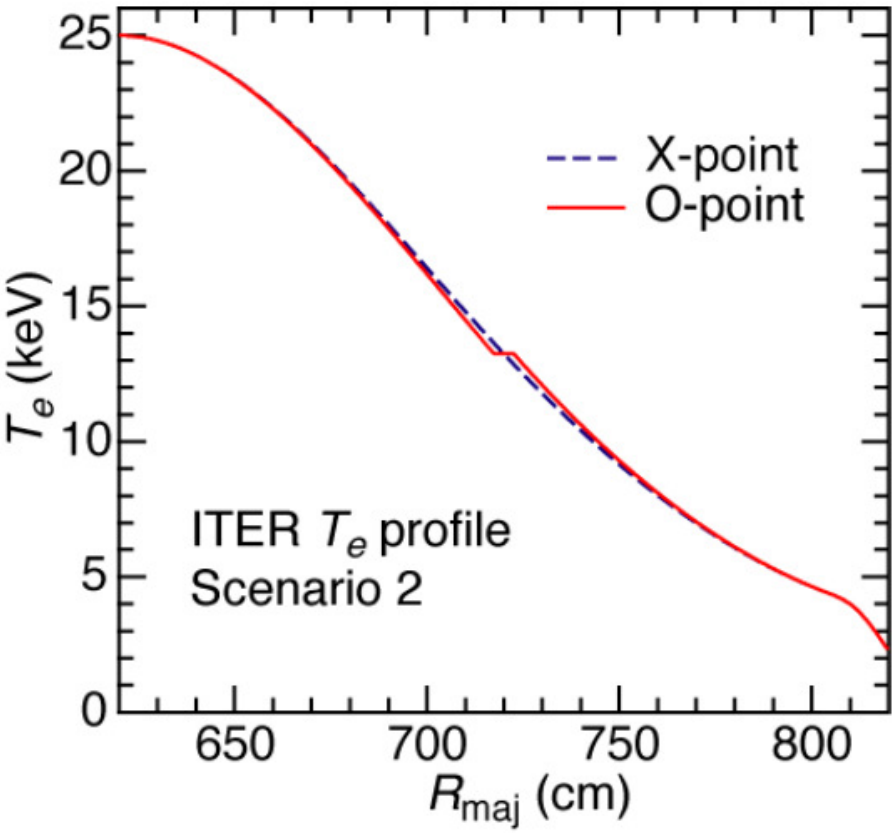

Figure 7.1. Two Te-profiles used in the MHD island simulation. The profiles are those for the X- and O-points of the island in the view of the ECE antenna.

The effect of relativistic broadening on ECE measurement of MHD islands in ITER is shown to be modest [see Annex 7.4.1]. The greatest reduction in measured ΔTe is about 35% and for island widths of 2 cm and larger, the decreased amplitude still exceeds the noise limit of a properly designed radiometer. For islands as small as 1 cm and located closer to the core, the measurement of ΔTe will be more challenging, but FFT techniques can probably be employed to detect signals buried in noise. The reason for the relatively small consequence of relativistic broadening is due to the generally broad effect of an MHD island on the electron temperature profile; the island perturbs the profile over a fairly wide radius outside of the O-point. Also, the relativistically broadened line is approximately Gaussian, hence the emission is fairly concentrated around the peak. In addition, as can be seen in Eq. 7.4.1, the ΔTe depends directly on the Te gradient and the island steepens the gradient as the O-point passes. The difficulties come for measuring MHD deep in the core. The smaller gradients there result in diminished ΔTes, but also the relativistic broadening can be quite large. For these reasons, the detection of any MHD modes in the core of ITER will be difficult. On the other hand, edge oscillations in ITER H-mode plasmas should be easily detectable, relatively speaking, due the steep gradient there and the lower Te values which will give smaller relativistic broadening.
Figure 7.2 gives expected ΔTe/Te from rotating MHD islands for perfect (ideal) measurement and relativistic broadened cases for different island widths.

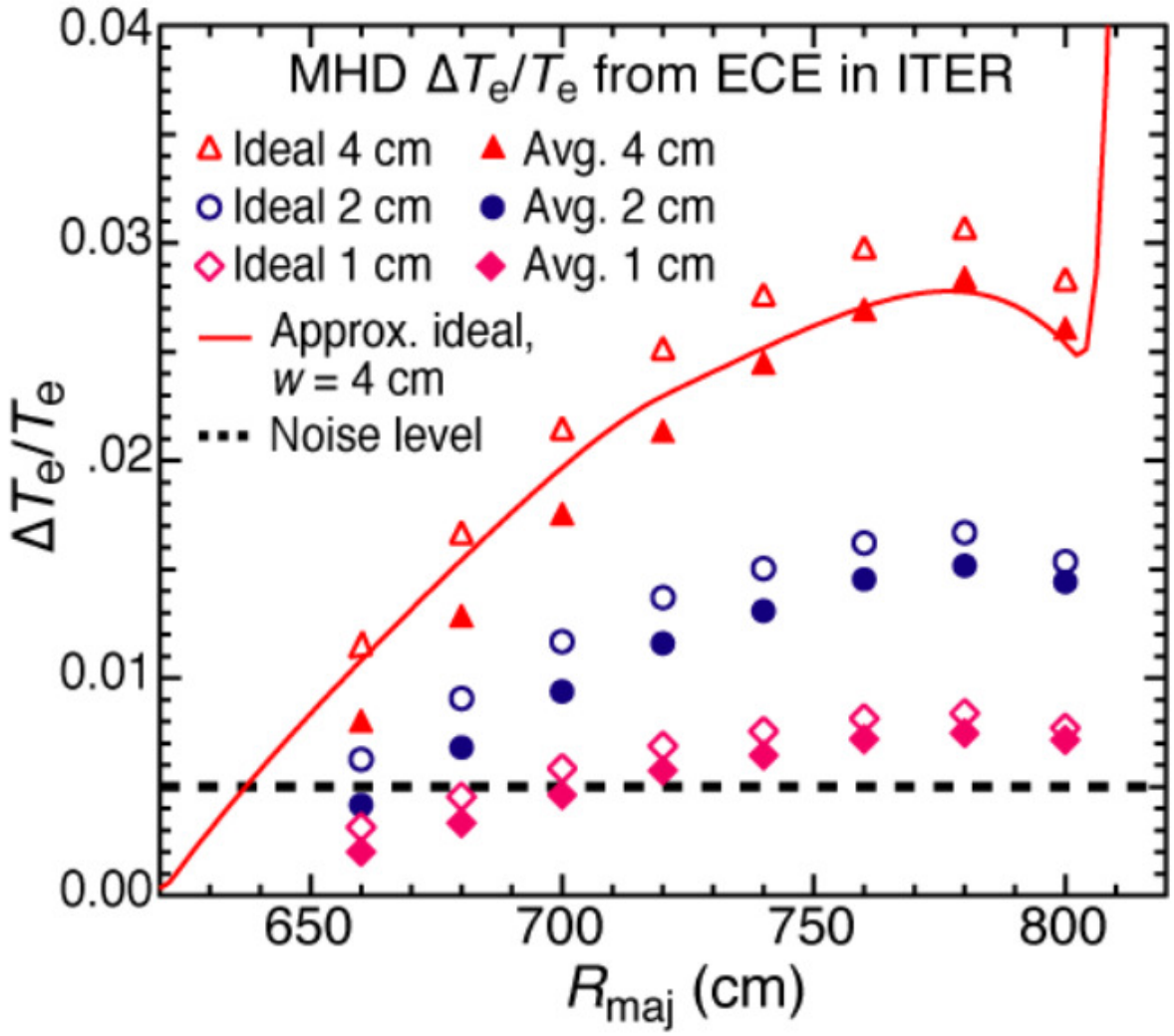

Figure 7.2. Plot of expected ΔTe/Te from rotating MHD islands for perfect measurement case (Ideal - open symbols) and relativistic broadened case (Avg. - solid symbols) for 1, 2, and 4 cm island widths. The solid curve is the approximate ideal ΔTe/Te (see Eq. 7.4.1) for a 4 cm island. The dashed curve is the assumed noise limit of the ECE radiometer measurements.

7.5 Temporal Resolution

For ECE electron temperature measurement by a radiometer, the time resolution depends on time response of the radiometer IF detectors, a video amplifier bandwidth and sampling rate of a digitizer. The time response of the IF detector is 1 μs and the video amplifier bandwidth can be adjusted between DC to 1 MHz according to measurement requirement. The digitizer sampling rate also can be kept more than 1 MHz.

For detailed analysis of events such as ELMs and the L-H transition continuous (Δt ~0.1ms) acquisition of electron temperature data is desired. This can be achieved through the use of an ECE radiometer data acquisition system which can be continuously digitized through sequential sharing of memory modules. The ECE radiation data recorded in digitizer memory is periodically transferred to offline storage. During this transfer period data acquisition is transferred to a second digitizer. This can be repeated as necessary.

The above operating scenario for the ECE system allows for continuous, real-time, profile acquisition. In addition, more accurate analysis of the stored ECE data (at various frequencies) can also be performed post-discharge at any discharge time. Also, more precise *software* ECE radiation

analysis of selected I/Q data can be performed post discharge to obtain the highest quality profile data

Finally, it should be noted that as the ITER database expands, the adoption of neural network analysis techniques may also prove particularly beneficial and reduce the data acquisition requirements.

The other ECE measurement system, the Michelson interferometer, has poor time resolution (~ 5 – 10 ms) dependent on the speed of the mirror scan.

7.6 Measurement accuracy and errors

The stated measurement requirement accuracy in Table 6.1 for the electron temperature profile is typically 10%. Meeting these targets may be challenging. Table 7.1 gives the functional specifications for the ECE diagnostics suite.
It should also be noted that the uncertainty in ECE measured electron temperature depends on the absolute calibration accuracy. Because of the rather unique measurement characteristics of the ECE diagnostic the description of accuracy has been divided into two areas – the so-called "precision" and "systematic error" of a measurement. The term "precision" refers to the statistical variation recorded while performing repeat measurements. This parameter therefore does not refer to an absolute error but more to the reproducibility of a measurement i.e. does the system consistently measure the *same* correct/incorrect value. The term "systematic error" is used in reference to *absolute errors* introduced by things such as calibration error, EFIT uncertainty, plasma start position errors, etc. So, to summarize, the "precision" of the ECE measurement of temperature profile relates to how reproducible the measurement is even with all of the flaws associated with calibration, etc. The "systematic error" of the profile measurement would relate to the fact that an incorrect EFIT or calibration (as examples) caused the plasma start position to be offset by ~2 cm even though the determined profile was very reproducible.

There are two types error introduced into ECE measurement. One is the random error due to the nature of blackbody emission and other is systematic error due to calibration. Generally the random error is negligible so, measurement error is dominated by the calibration error. The calibration error mainly depends on the following three factors:

1) The accuracy to which the surface temperatures of the calibration sources are known.
2) The error in the emissivity of the calibration source.
3) Stability in receiver sensitivity for long term operation.

One shall estimate the fractional error introduce by above each factor and determine the accuracy of the ECE measurement instrument.
The measurement accuracy of the surface temperatures of the calibration source depends on thermocouple temperature measurement accuracy (~ ±0.5 ^{o}K, the thermocouple meter manufacturers specify), radiation temperature uniformity over surface (i.e. ±5%, given in critical parameter of the ITER ECE hot source) and radiation temperature stability (i.e.±1.5 ^{o}K, specified in the critical parameters of the ITER ECE hot source design). Among all these three errors, the error in the radiation temperature uniformity is dominated.
If the remaining above mentioned two errors can be kept within in ±5%, we can achieve the measurement accuracy of the ITER ECE diagnostic.

Calibration errors are not a significant issue on present devices. A major new challenge on ITER is that the calibration may change *during* the long-lived ITER discharges due to dimensional changes

from thermal expansion, etc. This requires an in-situ, real-time calibration. A vacuum compatible in vessel hot body source is be used to provide the absolute calibration of the ECE system.

As an example, let us consider the calibration of a Michelson interferometer, one of the principle ECE instruments to be used on ITER. By design, a Michelson is very stable, and due to the oscillatory nature of its operation, it is inherently amenable to multiplescan averaging for calibration. This provides a means for statistical analysis of the calibration data. Figure 7.3 shows calibration data for the DIII-D Michelson interferometer, the upper plot an overlay of eight calibration spectra (10k scans each) and the lower plot the normalized standard deviation of those eight spectra. The standard deviation reflects the minimum uncertainty of the calibration due to the inherent noise of the system. For this case it varies from about 10% for the lowest frequency of interest to less than 2% for high frequencies. This bodes well for achieving, for most of the desired frequency range, accuracies of 5% as stipulated in the functional specifications. Other factors affecting the calibration are: accuracy of the calibration source temperature and gains of supplemental amplifiers. It should be possible to determine the temperature of a hot calibration source to within a few degrees, so for example if we know the temperature of an 800 °C source to within 2°C, that is an uncertainty of 0.25%. Similarly, the gain of a quality amplifier can be known to within a fraction of a percent.

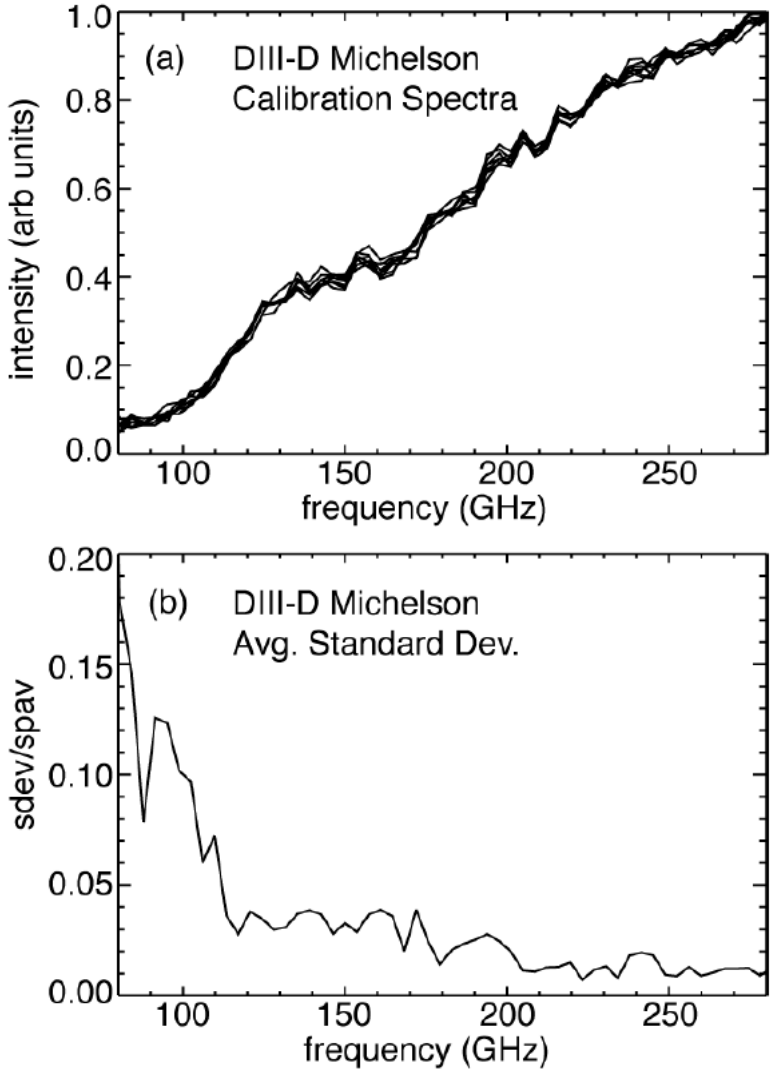

Figure 7.3. (a) Michelson interferometer calibration spectra (8 averaged 10k scans overlaid), and (b) average standard deviation.

Outside of the calibration itself, other factors affecting accuracy are the stability of the instrument, mainly the detector sensitivity, and the stability of the transmission system, the waveguide plus the coupling to the instrument and plasma. For the Michelson interferometer the detector tends to be very stable as it sits on the cold plate of a LHe cryostat; the sensitivity remains constant for long periods of time. For the DIII-D instrument, regular measurements of the instrument sensitivity indicated a change of less than 2% over a six month period. Regarding the transmission line, the DIII-D corrugated waveguide system is mounted to rigid structures in the machine hall and there is minimum movement during plasma discharges. The waveguide is not connected to either the Michelson or the tokamak vessel; however, at both ends the optics are "under filled", except for the very lowest frequencies, and this makes the coupling very insensitive to small movements of the components. Again, it has been shown on DIII-D that alteration of the front-end optics brought about by an unplanned vessel vent in the middle of a experimental campaign and resulting in small displacements of order a millimeter, changed the calibration by less than 2% percent. On Alcator C-Mod, which also uses a Michelson interferometer and broadband calibration source, calibration curves for the whole system, including a long quasi-optical beamline, have been found to be stable to typically < 5%, over periods of several years. Frequent recalibration is thus unnecessary. Hence for the Michelson interferometer, all uncertainties are in the range of 2% or less.

For the total accuracy, the uncertainties for each component add in quadrature, so for example, for three components with 2% accuracy (calibration, instrument, and transmission line) plus two with 0.5% accuracy (amplifiers and source temperature) the total accuracy is 3.5%. From these arguments we find the specification of 5% total accuracy to be reasonable.

For the ITER heterodyne radiometer, the variabilities in calibration and instrument sensitivity will be pretty much the same. One difference is the stability of the radiometer itself. It is known that the components of a radiometer can be highly sensitive to changes in position and temperature such that just adjusting the tightness of a connector or allowing the IF amplifier's temperature to change by a few degrees can cause a significant change in sensitivity, as much as 5-20%. Therefore it will be critical that the ITER radiometer be built as a temperature-controlled unit that can be left undisturbed for long periods of time. But also, it will be prudent to include a local noise source as part of the radiometer to allow relative calibration of the instrument by itself should the need arise. Cross-calibration of spectra and temperatures to Michelson interferometers can also be performed; this is common on current experiments.

7.7 ECE diagnostic: System Specifications

As mentioned previously, the stated measurement requirements should be available at any time and for any discharge condition. A purpose of the Table 7.1 is to provide a guide to the required quality of the instruments. It is in some ways a “wish list” which is based on reasonable assumptions about what is achievable.
The ECE is required to provide **Core electron temperature profile measurement** and **NTM temperature perturbation (δT/Te) measurement** for Advanced Control. The original measurement requirements reported in Table 15 specify only time resolution of 10 ms, but not the system latency with which data is delivered to the Plasma Control System (PCS) (see also ITER_D_ABR2ZV). In order to effectively control the plasma, PCS requires data representing the core temperature profile to be delivered with latency (delay) no greater than 2.5 ms (this defines a latency cycle), from the detection of the signal and the delivery of the required auxiliary data from PCS, assuming that a control cycle time is about 10 ms. PCS will provide necessary auxiliary data arising from other diagnostics and or modelling, mapped to the diagnostic sightline as reported by the diagnostic in its self-description. At present auxiliary data include: electron density profile,

magnetic field profile and their errors. Any additional details or requirements for this data exchange will be agreed between IO and DA during the detailed design phase and recorded in the interface sheets with PCS.

For core electron temperature profile measurement by ECE, the high temperatures foreseen in ITER (30 – 40 keV) will affect the spatial resolution, due to the large relativistic and Doppler broadening, which will lead to a widening of the radial extension from which a given frequency in the ECE spectrum is emitted. The target of a/30 would be possible only in regions with a low enough value of Te (typically r/a > 0.5 for Te(0) = 30 keV on ITER). The relativistic downshift at the high temperatures in ITER is substantial and will strongly limit the access to the plasma. It is important to remark that the high temperature scenarios considered for ITER (Te(0) up to 40 keV) would degrade the spatial resolution of Te due to a further widening of the emission layer.

Note that, for the measurement of the core and edge temperature profile, 10 ms temporal resolution as specified in the PR is adequate, whereas for the MHD/ TAE mode structure reconstruction, faster sampling is required. ECE radiometers can achieve much faster sampling than specified in the PR, so the target is set to 1 μs. For ELM evolution study, one has to sample at < 10 μs to follow up the crash and the recovery of the temperature after the event, so 1 μs sampling target is justified.

ECE will play a key role in the targeting of ECH heating to control neoclassical tearing modes (NTMs). The ECH deposition widths for the NTM stabilization are in the range of 30 – 70 mm. The island with the width of w > 20 mm is detectable by ITER ECE. Thus, assumption for ECE channel separation of 20 mm or smaller at NTM radii is adequate for the mode detection and localization. The response time of the feedback system once the mode is tracked is in the order of tens of ms. It is anticipated that it will take about 20 ms to begin moving the ECH steering mirror and then some time to lock onto the mode. The total response time might be 30 – 50 ms or even longer to lock onto the mode and begin suppressing it with ECCD, depending on how far the mode rational surface is away from where the mirror is pointing at the time. The growth time of the NTM is in order of 100 ms, and the target resolution of the diagnostic expressed in terms of sampling rate could be in the range of 0.1 – 1000 kHz. Response to the NTM in ECE measurements is limited by the intrinsic resolution of the instrument which includes the relativistic broadening and the antenna pattern. Also, the signal-to-noise ratio limits the minimum island size to about 2 cm for a dT_e/T_e ~1%. The latency needed for the NTM feedback is estimated to be 1 ms which is sufficient to match the response time of the feedback system. To improve the NTM detection and make the ECH feedback more effective, correlation with another ECE line-of-sight or with magnetic diagnostics will be used to increase the sensitivity of the measurements. For islands as small as 10 mm and located closer to the core, the measurement of ΔTe will be more challenging, but FFT techniques can most likely be employed to enhance signals relative to noise.

Table 7.1. The proposed set of specifications for ECE diagnostic.

MEASUREM.	PARAMETER	CONDITION	RANGE or COVERAGE	Time or Freq. Res.	Spatial or Wave No. Res.	ABS. ACCURACY	STAB. Of MEAS. *
04. Plasma energy	Beta_p	Ip > 3 MA	0.01 - 5	0.1 ms	Integral	5% for beta_p =1	1%
23. Te profile	Core T_e	r/a < 0.9	0.5 – 15 keV	10 ms for profile/ target 1 μs for modes structure	2 – 5 cm increasing with T_e	5%	1%
			15 – 40 keV	10 ms for profile/ target 1 μs for modes structure	5 – 13 cm increasing with T_e	5%	1%
	Edge T_e	r/a > 0.9	0.05 – 8 keV	10 ms for profile/ target 1 μs for modes structure	1 – 5 cm increasing with T_e	5%	1%
			8 – 10 keV	10 ms for profile/ target 1 μs for modes structure	5 – 6 cm increasing with T_e	5%	1%
14. H-mode, ELMs and L-H mode transition indicator	ELM T_e transient & L-H pedestal formation	r/a > 0.9	0.03 – 10 keV	1 μs	1 – 6 cm; limited by physics	5%	1%
15. Runaway electron	Maximum electron energy	-	up to 100 keV	10 ms	no spatial resolution	20%	20%
	Runaway current	Post thermal quench	(0.05-0.7) x I_p	10 ms	no spatial resolution	-	30% rel.
		Failed breakdown	0 – 1 MA	10 ms	no spatial resolution	50 kA	-
27. High frequency instabilities (MHD, NTMs, AEs, turbulence)	$\Delta T_e/T_e$	r/a < 0.9	$\Delta T/T \geq 1\%$ sensitivity decreasing with bandwidth	0.1 – 1000 kHz	Radial resolution 10 – 20 cm depending on temperature; (m,n) < (2,1),(3,2) for NTM	20%	1% (depends on thermal noise, thus on Bv and Bif)
		r/a > 0.9	$\Delta T/T > 1\%$ sensitivity decreasing with bandwidth	0.1 – 1000 kHz	Radial resolution 4 – 10 cm depending on temperature	20%	1% (depends on thermal noise, thus on Bv and Bif)
05. Radiated power	Radiated power in ECE band	Default	70 – 1000 GHz	20 ms/ 5 ms depending on the FTS instrument assessment	Normal and oblique to outer flux surface	20%	10%
	Radiation temperature vs frequency	-	70 – 1000 GHz	20 ms/ 5 ms depending on the FTS instrument assessment	Normal and oblique to outer flux surface	5%	1%

**** The stability of the measurement in this table is understood in terms of stability of a measurement over the time period of a discharge, high linearity of the instrument response, and low noise.***

For TAE measurements, the measurements do not need to go up to 2 MHz, as stated in the PR. It is unlikely that there will be significant AE activity above 0.5 MHz.
For the maximum electron energy of non-thermal (runaway) electrons, it is obvious that the ECE system will never measure up to 100 MeV. The anticipated upper energy limit is up to a few hundreds of keV, probably less. The exact number will be evaluated for the PDR of the diagnostic, and the front-end design must enable the measurement up to the limits set up by physic constraints.

The power budget for the radiometer baseline design for different frequency bands is given in Table 7.2.

Table 7.2. Power budget for different frequency bands for ITER ECE radiometer.

Components name	Radiometer with frequency range			
Loss/Gain	F-Band 122 – 139 GHz 1 down convertor 18 channels with 1 GHz channels separation	D-Band 141 – 169 GHz 2 down convertor 15 channels with 2 GHz channels separation	G-Band 172 – 218 GHz 3 down convertor 16 channels with 3 GHz channels separation	Millimeter wave 22 – 230 GHz 1 down convertor 3 channels with 4 GHz channels separation
Transmission line loss (dB)	-10.7	-10.7	-10.7	-10.7
Splitter unit	-6	-6	-6	- 6
Directional coupler	0	-3	-6	0
Band pass/High pass filter	-1	-1	-1	-1
Mixer conversion loss in down conversion step	-8	-8	-8	-8
Two stage IF amplifiers	80	80	80	70
IF section Power splitter	-14.6	-13.8	-14	-2.8
Band pass filter	-1.5	-1.5	-1.5	-1.5
Total gain	**38.2**	**36**	**32.8**	**40**
The sensitivity of the radiometer for detector sensitivity of 1000 V/W	6.6×10^{6}	4×10^{6}	2×10^{6}	1×10^{7}
Noise temperature (eV)	7.4	8.7	9.9	7.4
Noise power (W)	5.9×10^{-10} for B_{if} = 500 MHz	1.4×10^{-10} for B_{if} = 1000 MHz	2.4×10^{-9} for B_{if} = 1500 MHz	2.4×10^{-9} for B_{if} = 2000 MHz

7.8 Constraints related to satisfying the measurement requirements

The baseline ECE conceptual design is currently limited to the integration of 2 lines of sight into Equatorial Port 9. This means that there are only two front-end ECE collection optics designated to satisfy the measurement requirements.

Operation of the diagnostic during the current ramp up and down is likely to be restricted in order to avoid interference and potential damage resulting from the 20 MW, O-mode 170 GHz electron cyclotron heating (ECH) and possibly the 2 MW, X-mode 60 GHz collective scattering systems. As mentioned earlier, the relativistic electron temperatures (> 20 keV) in ITER will affect on the spatial resolution. This is illustrated in Fig. 7.4 below, both for the X-mode and O-mode measurement frequency. The assumed electron density is flat in the standard Scenario 2 profiles.

Peak electron temperatures approach 25 keV. This causes significant modifications which limit the spatial resolution and accuracy of measurements.

It should be noted that there is harmonic overlap in the ECE harmonic frequency. The ECE measurement capability is mainly limited by harmonic overlap due to relativistic frequency downshifting in high temperature ITER plasma. Harmonic overlap occurs because of large variation in toroidal magnetic field across the plasma, which allows two or more harmonics to resonate at the same frequency in different parts of the plasma cross section. The first harmonic X- mode lies below the cut-off and therefore, it is not available for measurement. Figures 7.5a and 7.5b show the effect of downshifting of higher harmonics which cause harmonic overlap and thereby result in limited access of first harmonic O-mode and second harmonic X-mode for temperature measurement.

Other potential constrain for ECE temperature measurement is mode scrambling. A simulation study inferred that in the range of 310-380 GHz, the second harmonic O-mode intensity is considerably in excess of the X-mode intensity, so even a 5-10% conversion of O mode into X-mode prior to polarization separation, could distort the temperature profile in the outboard side by more than 10%. In the inboard region, the distortion in the apparent temperature can be more than 40%. It has an effect on the derivation of Te which has to be determined by more appropriate error analysis.

In the global power balance, the power loss from the plasma due to ECE remains relatively small. Electron cyclotron radiation loss increases with the electron temperature, $P_{EC} \sim n_e^{0.5} T_e^{2.5}$. For the case of high electron temperatures, $T_e > 30$ keV, and moderate electron densities, $n_e \sim 7\text{-}6\ 10^{19} m^{-3}$, optimal for the maximal current drive (CD) efficiency in the long pulse operation, the role of the EC radiation becomes more pronounceable in comparison with the heating from fusion alphas. Even so, the EC net loss is typically < 20%. For ITER operation scenario with $ne \sim 6\ 10^{19}\ m^{-3}$, and high temperatures, $T_e(0) \sim 25$ keV, required for long pulse operation, it equals to $f_{EC} \equiv Q_{EC}/(Q_\alpha + Q_{aux}) \sim 9\%$, see EPS 2011 Proceedings or in [*Kukushkin, Minashin, Polevoi, ITER_D_47R2CM, https://user.iter.org/?uid=47R2CM*]. The total P_{rad} for typical ITER operation is estimated to be about 50 MW, in which P_{ECE} does not exceed 10 MW.

If plasma is Maxwellian and optically thick ($\tau >> 1$), its emission can be described by the equation for black body radiation:

$$I_{BB}(\omega, T_e) = \frac{\omega^2}{8\pi^3 c^2} k_B T_e, \qquad (7.8.1)$$

where k_B is the Boltzmann constant, T_e is the electron temperature. One should realize, however, that the plasma in a tokamak is not always optically thick, especially at high harmonics.
In these cases, it is also necessary to mention that microwaves can be reflected from the tokamak walls, so the wall reflection coefficient ρ_{refl} should be added to Eq. (7.8.1):

$$I(\omega, T_e) = I_{BB} \frac{(1-e^{-\tau})}{(1-\rho_{refl} e^{-\tau})} = \frac{\omega^2}{8\pi^3 c^2} k_B T_e \frac{(1-e^{-\tau})}{(1-\rho_{refl} e^{-\tau})}. \qquad (7.8.2)$$

To get an estimate of the P_{ece} from ECE diagnostic, one should measure the spectra (radiatin temperature vs frequency) and the wall reflection coefficient also as a function of frequency. On different tokamaks, the wall reflection coefficient varies from 0.6 to 0.9, depending on the wall

material and geometry. Therefore, if one assumes the accuracy of the wall reflection coefficient measurement to be 10%, it will give an uncertainty in the P_{ece} determination of several MW, depending on the scenario. The radiation temperature vs frequency and the wall reflection coefficient vs frequency will be supplied to the PCS for the further analysis by codes, to make an estimation of the power loss due to the ECE.

The oblique view was not one of the topics of the original statement of work. It became relevant during port integration of the ECE diagnostic. Comparing radial and oblique ECE views would reveal deviations from Maxwellian. The measurement and comparison must be done across multiple harmonics and simultaneous measurements are required in both polarizations. This places a stringent requirement on instrumentation. All of the Michelsons included in the proposed instrumentation (i.e. two O-mode and two X-mode measurements) are in fact required for this measurement. An oblique view for the ECE diagnostic will show whether emission is consistent with Maxwellian. If not, we can gain sufficient information on the distortion to construct a model for it and to provide the means for determining the true electron temperature. If the distribution is Maxwellian (and to some degree if it is not), the view will be useful. It can provide a redundant measurement possibility in case of mechanical or other failure in the radial view, and signal any changes in system calibration.

The ECE diagnostic is critical to ITER. As other parts of this DDD indicate, much is expected of the diagnostic. The goal of providing redundancy was a key consideration in our selection of a moderate oblique angle (10 degrees). An example of Te profiles which might be produced from the two views for Scenario 2, using second harmonic, is shown in Fig. 7.4. While frequency spectra (left figure) are shifted, it is straightforward to correct for the radius of maximum emission.

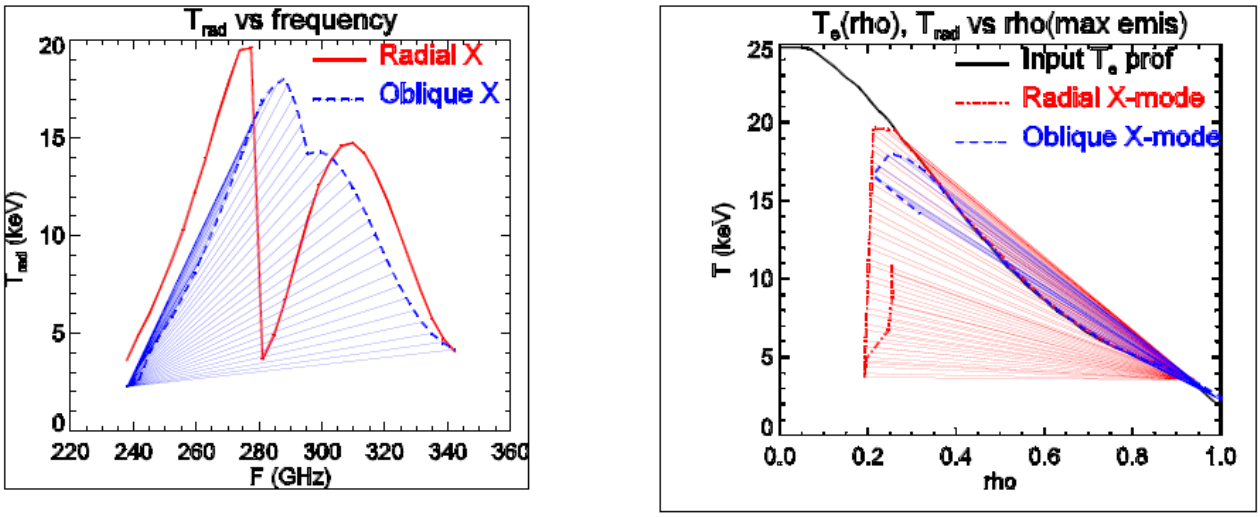

Figure 7.4. An illustration of the use of the oblique view as a redundant view.

Figures 7.5 and 7.6 illustrate the emission widths for ECE frequencies and the profiles of O-mode and X-mode absorption coefficient for various harmonics.

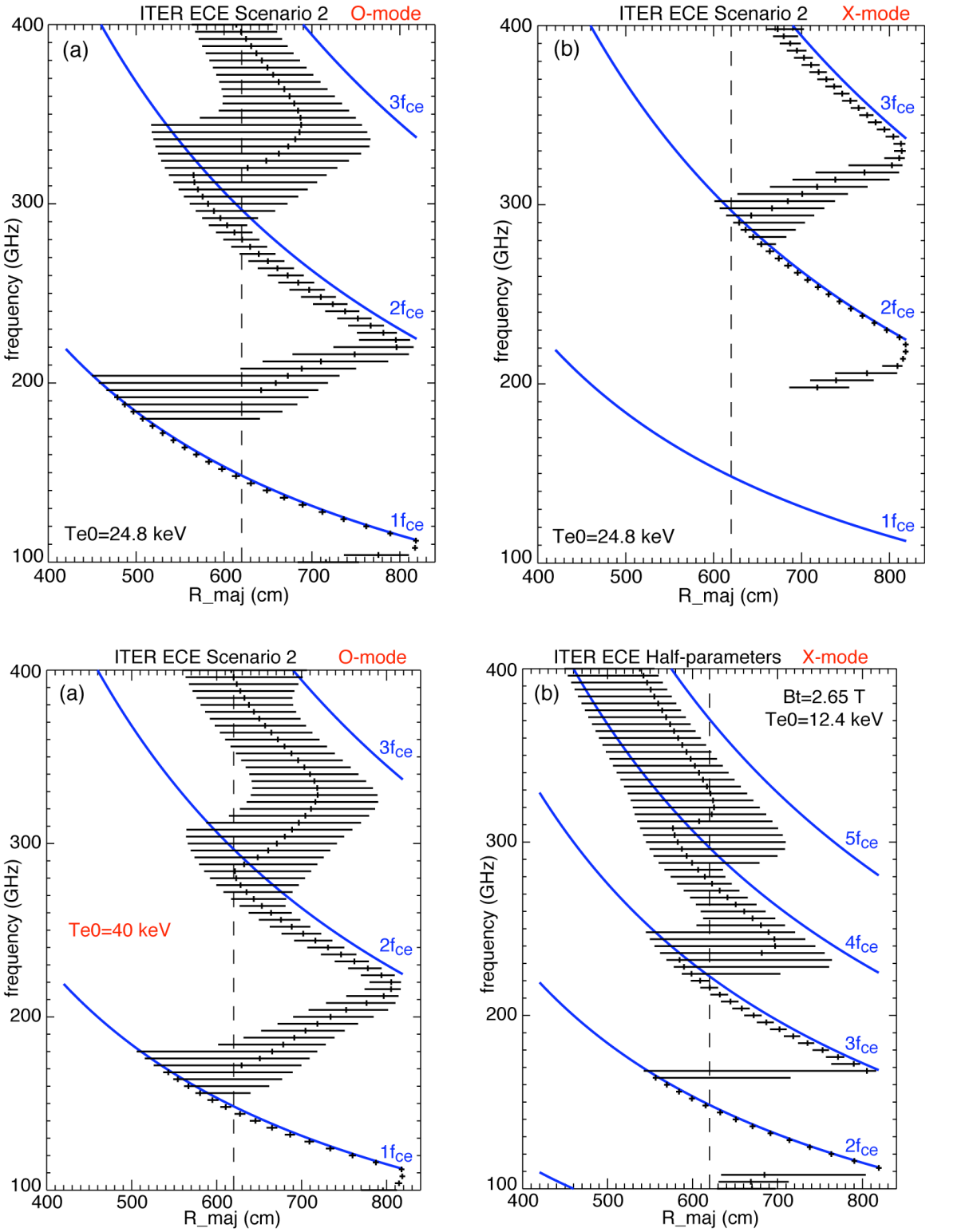

Figure 7.5. Emission widths for ECE frequencies covering harmonics 1-3 for ITER Scenario 2 for (a) O-mode and (b) X-mode polarizations The width of the horizontal lines indicates the radial extent of the 5-95% emission level for that frequency for full field (5.3 T) operation and half field (2.65 T) operation.

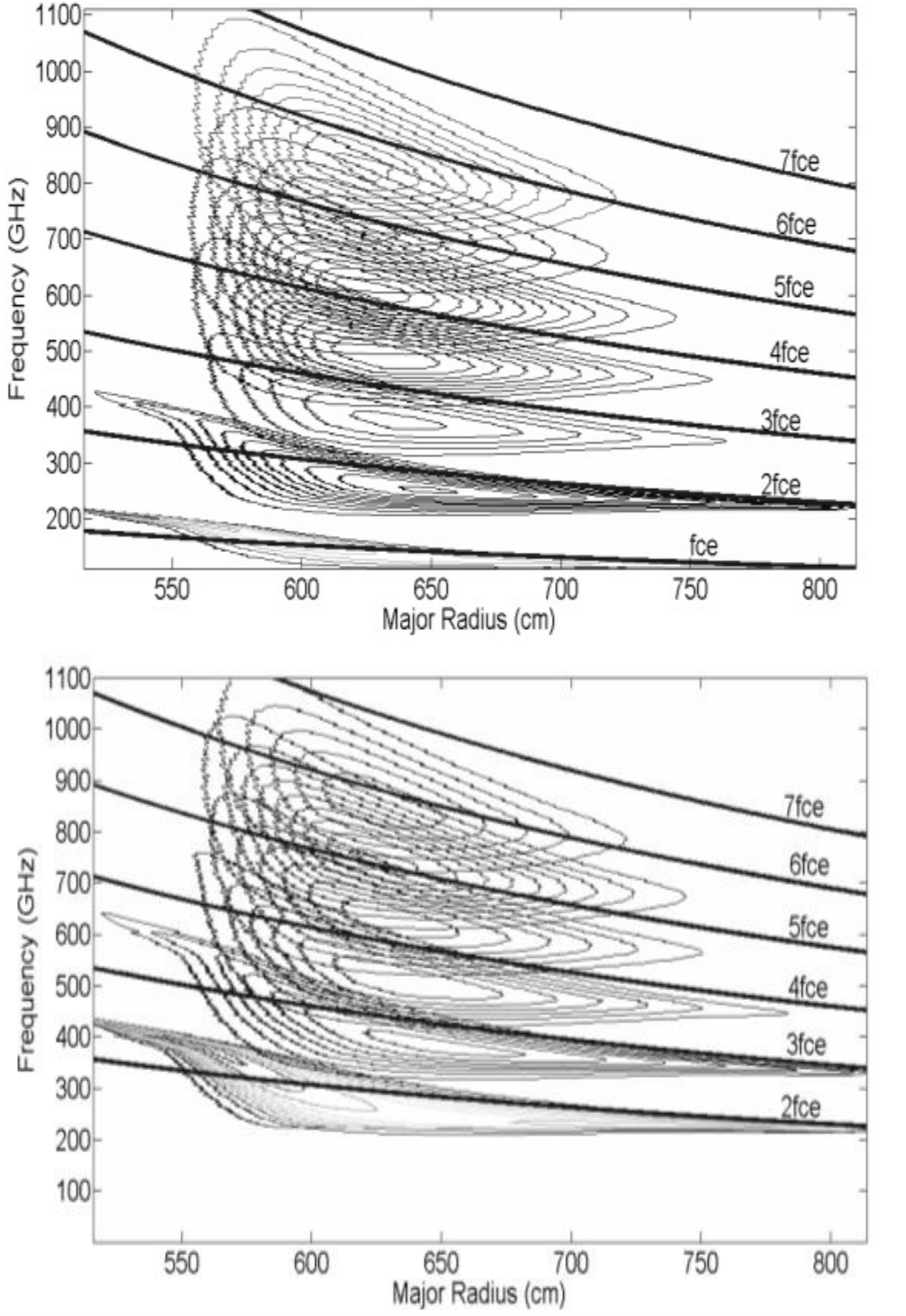

Figure 7.6. (a) & (b) represent the profiles of O-mode and X-mode absorption coefficient for various harmonics, respectively.

7.9 Challenges to operation of the diagnostic

The anticipated challenges to successful operation of the ITER ECE diagnostic are listed below. These are potential issues stemming from plasma and wave propagation physics and ITER discharge conditions. This is outside of the mechanical and instrumental challenges –it is assumed the ECE systems operators will have solved or dealt with all problems in these areas.

1. Inability to extract Te measurements due to presence of non-Maxwellian electron distribution function. ITER discharges will be high temperature, low collisionality plasmas with a large amount of ECH power that can pump a high energy tail on the distribution function. Although the reabsorption of non-thermal emission by the bulk electrons will mitigate this problem, the potential exists for emission radiation temperature that does not match the bulk temperature.

2. EC emission encountering cutoffs due to high electron density. Current ITER simulations using reasonable transport models do not show this occurring in most scenarios; however, if the particle confinement should turn out to be better than in existing devices, the blocking of the first harmonic O-mode and second harmonic X-mode is certainly a possibility, leaving the third harmonic, which with the strong overlap with higher harmonics makes Te measurements very difficult.

3. Excessive ECH stray radiation that interferes with measurements or damages instruments. Although plans to have notch filters to block the stray ECH are in place, depending on the power level and coupling to the ECE antenna, sufficient power to interfere with the instruments is possible. For the radiometer, the narrow ECH frequency would ostensibly only effect one channel, but the stray power could also bias the mixer and affect a whole bank of channels. For the Michelson, the large number of modes and high sensitivity means that a even a small amount of power can spoil the interferogram.

4. Presence of plasma instabilities that create intense bursting radiation at ECE frequencies. In present-day tokamaks, it is not unusual for bursting radiation during discharges with Edge Localized Modes (ELMs) to interfere with ECE measurements. ITER is not supposed to have ELMs, but similar bursting emission has be seen in non-ELMing discharges with an Edge Harmonic Oscillation (EHO) and this mode is currently being strongly promoted as an ITER operating scenario. The bursts mainly affect the edge radiometer channels, but the mixer biasing problem can occur also. For the Michelson, the spiky bursts obviously will spoil the interferograms and make it difficult to obtain a valid spectral measurement.

5. Plasma height out of range. Pains have been taken to chose the Z height of the ECE antenna to couple well to a range of vertical plasma heights but the extreme Z height cases will likely result in the view missing much of the plasma core.

8 System Arrangement

8.1 Block diagrams

In Section 8.1.0, the conceptual layout of 55F1 ECE diagnostic breakdown is shown (Fig. 8.1). Thereafter the Process Flow Diagrams with the electrical diagrams, vacuum diagrams, cabling & transmission route through Buildings are reported.

8.1.0 Engineering Plant Breakdown

The mm-wave Radio Frequency (RF) ECE signal from the plasma is detected by the receiving front-end antenna (which is a quasioptical arrangement) and coupled into the polarizer splitetr box where it is split into O-mode and X-mode signals. The mm-wave received signal is delivered to the diagnostic areas where it is split into different bands, converted into IF frequency ranges and then detected by video detectors. The resulting signal (in V) is then sent to CODAC or PCS.

8.1.1 PFD and SLD electric diagrams

The guideline document to prepare schematics (Process Flow and Cabling diagrams) can be found in the CAD Manual chapter 14 (IDM_D_35CY6V).

8.1.1.1 Process Flow Diagram

The 55F1 ECE diagnostic vacuum process flow diagrams are shown in Fig. 8.2. The full specification is given in Annex 8.1.1 (ITER_D_6KV3XY - 55.F1.00- Process Flow Diagram for ECE).

8.1.1.2 SLD Electrical Diagram

SLD Electrical Diagram for the ECE diagnostic is given in Annex 8.1.2 (ITER_D_6KTSNE - 55.F1.00- Cabling Diagram for ECE). Note that more detailed design must be provided before the PDR.

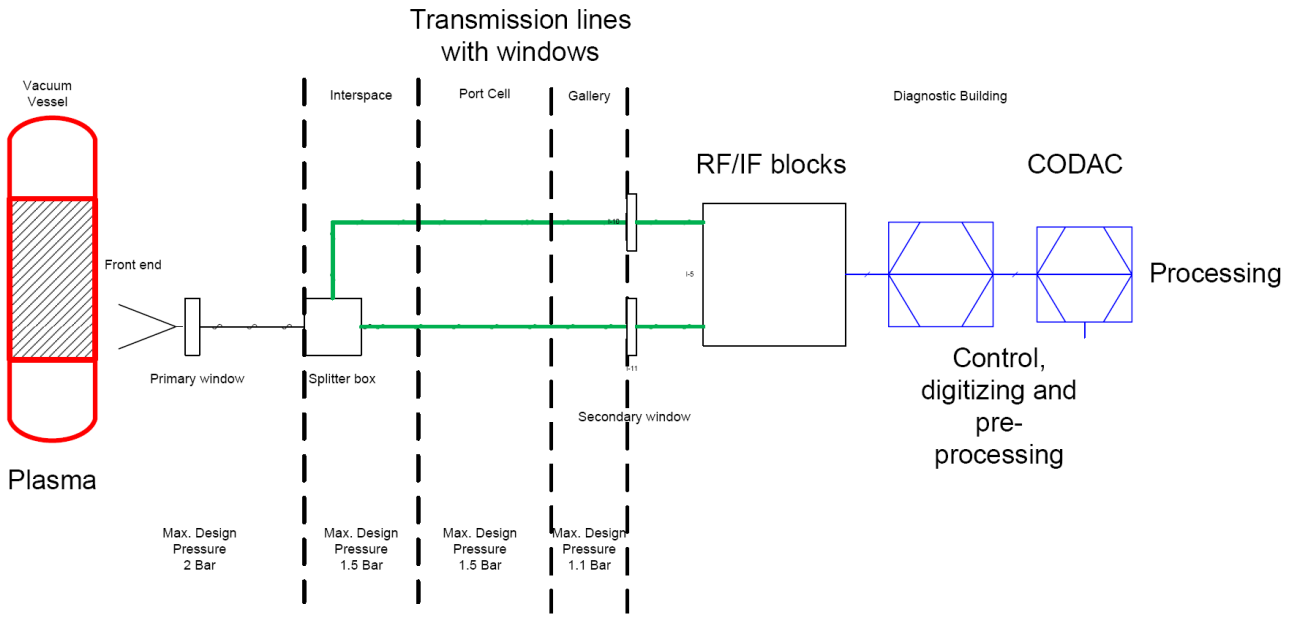

Figure 8.1. 55F1 ECE diagnostic Plant breakdown.

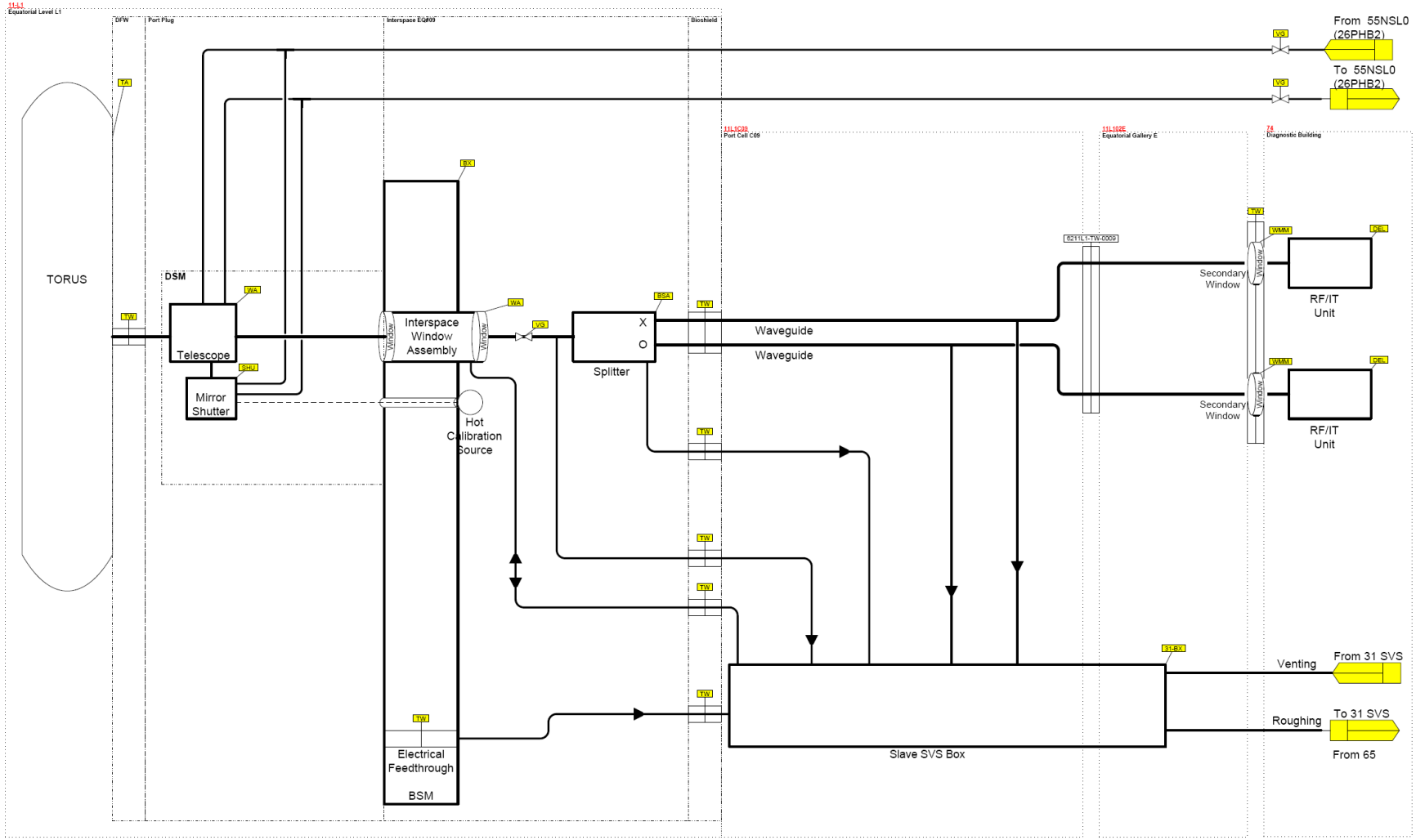

Figure 8.2. 55F1 ECE system PFD.

8.1.2 Vacuum requirements and classification for 55F1 ECE Diagnostic

TABLE 8.1 Vacuum classifications of components for 55F1 ECE Diagnostic.

Port	Port No	PBS No	Diagn component	Quantity	VQC	Vac Service type	Each - interspace volume m^3	REMARK
Equatorial	9	55.F1	**ECE**	1				
Equatorial	9	55.F1	Shutter (port-plug)	2	VQC 1B			Port-Plug
Equatorial	9	55.F1	Wave guides and Antenna (in port plug)	1	VQC 1B			
Equatorial	9	55.F1	Diagnostic windows Assembly(N07)	2	VQC 1A	Window	0.001	Primary Window
Equatorial	9	55.F1	Wave guides	2	VQC 3B	Interspace	0.8	Interspace
Equatorial	9	55.F1	Quartz Vacuum Window (Safety Window)	4	VQC 3A			Safety Window
Equatorial	9	55.F1	Microwave Detector	tbd	VQC N/A			Diagnsotic Building

The schematics arrangement of ECE diagnostic is given in Fig. 8.3.

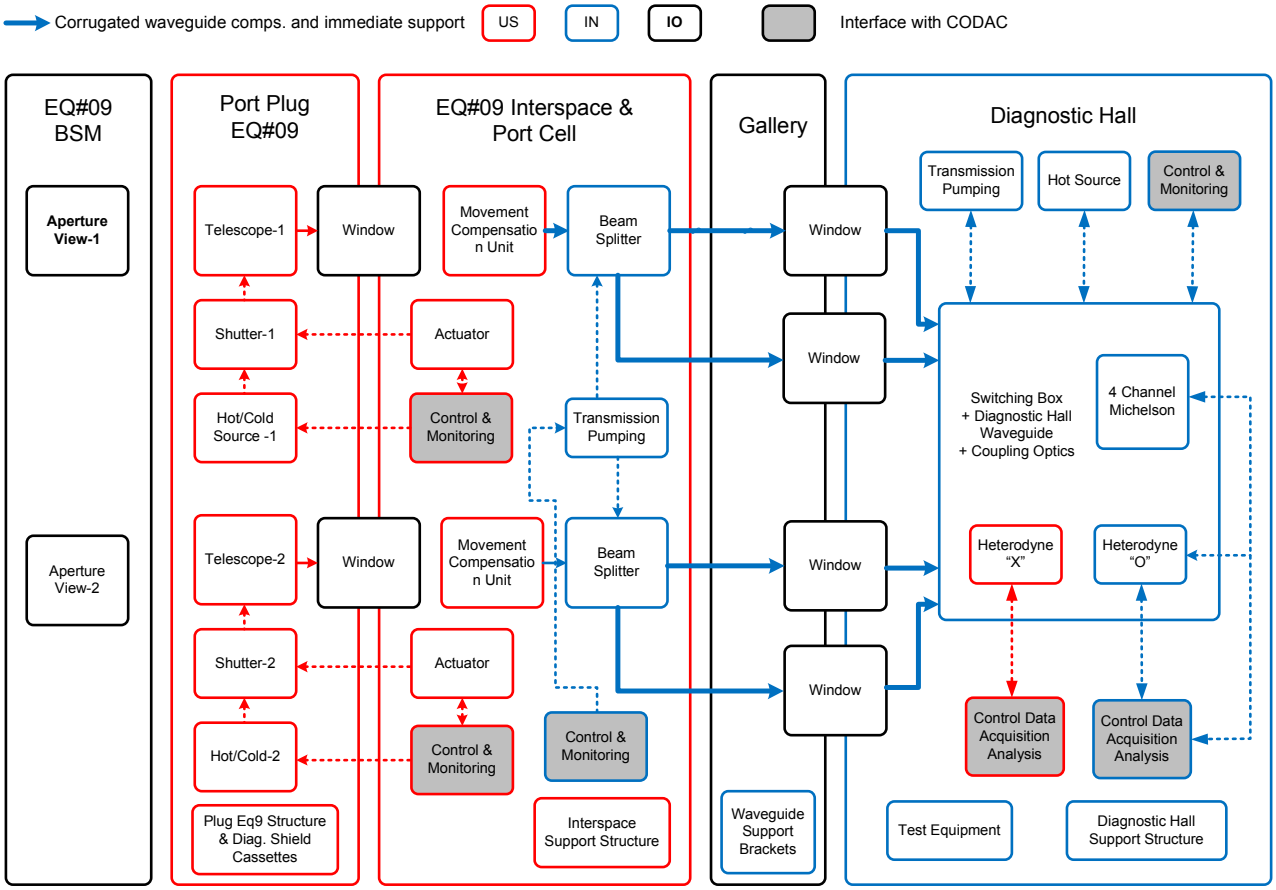

Figure 8.3. Vacuum system for 55F1 ECE diagnostic (schematics) with responsibilities divided between IO and DAs involved in development of ITER ECE diagnostic.

Above mentioned arrangement has been agreed for the ECE diagnostic by Diagnostic Division & Vacuum Group & safety group during meeting arranged at 519/019 on 4th October, 2011.Attendees of this meeting were Shaun Hughes, Leonid Topilski, Max Austin (US DA), Hitesh Pandya (IN DA), Kaushal Patel, Udintsev Victor.

- ECE diagnostic will interface torus vacuum, through double walled diagnostic window. Space in between these two walls will be monitored by service vacuum system.
- Diagnostic window facing torus vacuum, hence its vacuum classification is VQC 1A & safety classification is SIC-1.
- Wave guide connecting to diagnostic window and diagnostic hall will be under the rough vacuum. There is possibility to connect this wave guide to service vacuum system for evacuation as well monitoring purpose. Currently it is under study.
- Even wave guide can be connected to dedicated roughing pump, if SVS will not available for the evacuation of wave guide.
- Wave guide will isolate diagnostic hall by placing an addition single walled window.
- Purpose of this single walled window is to prevent diagnostic hall from tritium exposure in case of any failure event.
- IO (Vacuum Group) is responsible to provide suitable connection for SVS to diagnostic window.
- IO will supply USDA & IN DA, company name, catalogue number of the necessary vacuum equipment (valve, gauge, controller, double bellow etc.)
- IO will supply USDA & IN DA the drawings of the flanges needed for connection of the pumping system and interspace monitoring system.

Memo has been issued mainly to clarify applicable safety & VQC guidelines for the conceptual arrangement of ECE diagnostic. (Ref: ITER_D_6P3MQW - Confinement Barrier Strategy for ECE Diagnsotic)

From the Vacuum Handbook, the quick summary for vacuum vessel requirements can be compiled:

- The pumping system of the Vacuum Vessel (~1330 m^3) shall be capable to evacuate vessel, from 10^5 Pa to 10 Pa within first 24 Hrs.
- A base pressure of less than 10^{-5} Pa (for hydrogen isotopes) shall be achieved after wall conditioning prior to plasma operation
- A base impurity pressure of less than 10^{-7} Pa (the sum of partial pressure of impurity gases) shall be achieved after wall conditioning prior to plasma operations.
- The vacuum vessel and all components within or containing vacuum shall meet the requirement of the ITER Vacuum Handbook.

Other Applications of Vacuum Handbook:

- Valves used for ITER Vacuum Vessel Isolation (VQC 1A) should be bakeable to 250 ^oC in accordance with the requirement of ITER Vacuum Handbook and be of all metal construction. (Ref. ITER_D_2EPFG4 - Appendix 7 Valves)
- Welding vacuum boundaries and its outline procedure for qualification, approval and testing is described in the Appendix 1 of the ITER Vacuum Handbook. (Ref. ITER_D_2FMM4B - Attachment 1 Welding)
- Design, construction and fabrication of Diagnostic Windows Assembly should follow ITER vacuum guidelines. (Ref. ITER_D_2DXZZ3 - Appendix 6 Windows)
- MI Cable used for signalling should comply with ITER vacuum guidelines. (Ref. ITER_D_2ETNLM - Appendix 10 Vacuum Cables.)

Material-Out Gassing/Leak rate:

Selected material must satisfy certain criteria as mentioned in the ITER Vacuum guideline:

- All material used in 55F1 ECE should be design & constructed in accordance with the requirement specified in the ITER Vacuum Handbook.
- List of the accepted material is available in the Appendix of ITER Vacuum Handbook. (Ref. ITER_D_27Y4QC - Appendix 3 Materials)
- MI Cable used for signalling should comply with ITER vacuum guidelines. (Ref. ITER_D_2ETNLM - Appendix 10 Vacuum Cables.)
- Design, construction and fabrication of Diagnostic Windows Assembly should follow ITER vacuum guidelines. (Ref. ITER_D_2DXZZ3 - Appendix 6 Windows)
- Out gassing rate must be meet ITER Vacuum requirement. (Ref. ITER_D_2EXDST - Appendix 17 Guide to Outgassing Rates and their Measurment)
- Material used in the manufacture of the LFS Reflectometry component shall have the following properties:
  Maximum steady state out gassing rate at 100 ^{o}C,
  Hydrogen isotopes: 1 x 10^{-7} Pa m^3 s^{-1} m^{-2}
  Other Impurities: 1 x 10^{-9} Pa m^3 s^{-1} m^{-2}

Following material has been proposed for the construction of ECE Diagnostic.

TABLE 8.2. Proposed material for ECE diagnostic

PBS	Diagnostic System	Material	Description of material	Location	VQC		Possible Issue	Remark
55.F1	ECE Diagnostic	Stainless Steel (ITER Grade)	Mirror & Shutter	A - Invessel & In-Port	VQC 1B	Yes	No	
55.F1	ECE Diagnostic	Silicon Carbide	Calibration Source	A - Invessel & In-Port	VQC 1B	Yes	No	
55.F1	ECE Diagnostic	Quartz	Window Material	A - Invessel & In-Port	VQC 1A	Yes	No	
55.F1	ECE Diagnostic	Aluminium (ITER Grade)	Waveguide - Tube	B-Portcell & Intespace, C-Gallery, D-Diagnostic Area	VQC 3B	Yes	No	

Service Vacuum System:
Service Vacuum System comprised of subsystems mentioned below:

- Roughing System: ≤ 10 Pa Vacuum to all Clients,
- Guard Vacuum System: ≤ 10^{-2} Pa Vacuum to Clients needing it.
- Leak Detection System: Detection and localization services to all clients and its subsystems.
- Venting system: Venting to all clients and backfill services to those needing it.
- Pressure Monitoring: monitoring interspaced pressure to the client those need it.

SVS distribution boxes service covers most the tokamak area, mainly located in port cell. Diagnostic windows of Reflectometry LFS will interface with nearest Service Vacuum System Client Distribution Box. Interface between windows of ECE diagnostic and SVSCDB shall comply with ITER vacuum guidelines, i.e. tubing size, demountable connections etc (see ITER_D_2EV3R6 - PFD - SVS distribution box concept).

Routing of the tubing structure would be finalized for the PDR.

8.1.3 55F1 ECE diagnostic components in Reinforced Concrete Buildings

In general, Diagnostic systems extend from the Sensors/ Detectors/ Antennas inside the Tokamak to the electronics in the Diagnostics Cubicles. Therefore, each Diagnostic has significant interface with PBS-62 (Reinforced Concrete Buildings) mainly with Tokamak Building 11 and Diagnostics Areas (which are located in Diagnostics Building 74, Assembly Hall Building 13 and Tritium Building 14). The following arrangement is envisaged for ECE:

- ECE needs some cubicles in the Diagnostic areas: in particular, in Building 74 for the waveguides which are routed from Equatorial Port 9. The waveguides are making use of penetrations in the interface wall between the Tokamak Building and Diagnostics Building.
- In the enclosure area, the RF and IF equipment for ECE shall be installed. The post-processing and I&C interfacing equipment should be located in the cubicle area (see Fig. 8.4).

The estimation of number of cubicles required and electrical power requirement are given in the Diagnostics Cubicles database **Diagnostics Cubicles (ITER_D_33VTKU)**. The CAD description of waveguides routing to the diagnostic areas is given in Section 9.

Figure 8.4. Top view of Diagnostics and Tokamak building in Equatorial level.

Interface with buildings has considered the location, weight, dimensions, seismic load, heat load and Fire load of the systems (see corresponding table in the IS 55-62).

The estimation of the number and allocation of embedments required to support the Interspace Support Structure (ISS) which carries the ECE waveguides in the Port Interspace are given in Annex 8.1.3.

8.1.4 SSEPN requirements for 55F1 ECE diagnostic

All Diagnostic equipments and cubicles in the port cells and in the diagnostics building will require electrical power. All cables, including those for power, signal and control, should be kept laid inside cable trays. Therefore each Diagnostics has an interface with Steady State Electrical Power Network PBS 43 and, via 55NE, with PBS 44. Details of requirements for the 55F1 ECE from PBS 43 and PBS 44 are similar to those of the 55F2 LFS reflectometry and are given in Annex 8.1.4.

8.1.5 CODAC, PCS and CIS requirements for 55F1 ECE Diagnostic

The block-diagrams below (Figs. 8.5 – 8.8) are given as examples to demonstrate the data flow required to fulfil the measurement requirements indicated in Table 6.1. Table 8.3 summarizes the contribution of various diagnostics to the measurements provided by ECE. Requirements from CODAC/I&C (PBS 45) are treated in Section 11. For real-time control, there is an interaction with the Plant Control System (PCS; PBS 47).

Relations with Central Interlock System (CIS; PBS 46, not shown on diagrams here) are required for the protection from the ECH stray radiation. They will be assessed for PDR.

TABLE 8.3. Contribution of various diagnostics to the measurements provided by ECE diagnostic.

Contribution Primary - well suited to the measurement Back Up - provides similar data to primary, but has some limitations Supplementary - validates or calibrates, but is not complete in itself			A.05	B.01	B.02	B.07	B.13	C.01	C.02	C.05	C.06	E.05	E.07	E.12	E.13	E.14	E.15	F.01	F.02	F.09	G.01
Role		Diagnostic Role	Diamagnetic Loop	Radial Neutron Camera	Vertical Neutron Camera	Radial Gamma Ray Spectrometer	Vertical Gamma Ray Spectrometer	Thomson Scattering (Core)	Thomson Scattering (Edge)	Toroidal Interferometer/Polarimeter	Poloidal Polarimeter	X-Ray Crystal Spectrometer (Core)	Radial X-Ray Camera	CXRS based on DNB (Edge)	X-Ray Crystal Spectrometer (Survey and Edge)	Hard X-Ray Monitor	Beam Emission Spectroscopy	Electron Cyclotron Emission	Reflectometer (Main Plasma, LFS)	Reflectometer (Main Plasma, HFS)	IR Cameras, Vis/IR TV (Midplane)
1a1	Machine Protection																				
1a2	Basic Control																				
1b	Advanced Control																				
2	Physics Evaluation																				
Measurement, Parameter																					
4	Plasma energy, beta-p	1a1						S										S			
14	H-mode, ELMs and L-H mode transition indicator, ELM Te transient	2							S					S			S				
15	Runaway electrons, Emax/I, after thermal quench/failed breakdown	2		S	S													S			
23	Electron temperature profile, Core Te	1b										S	S								
23	Electron temperature profile, Edge Te	2											S		S			S			
27	High frequency instabilities, TAE dT/T	2																S			
27	High frequency instabilities, NTM dT/T (complex, 100 ms integ.)	1b																			

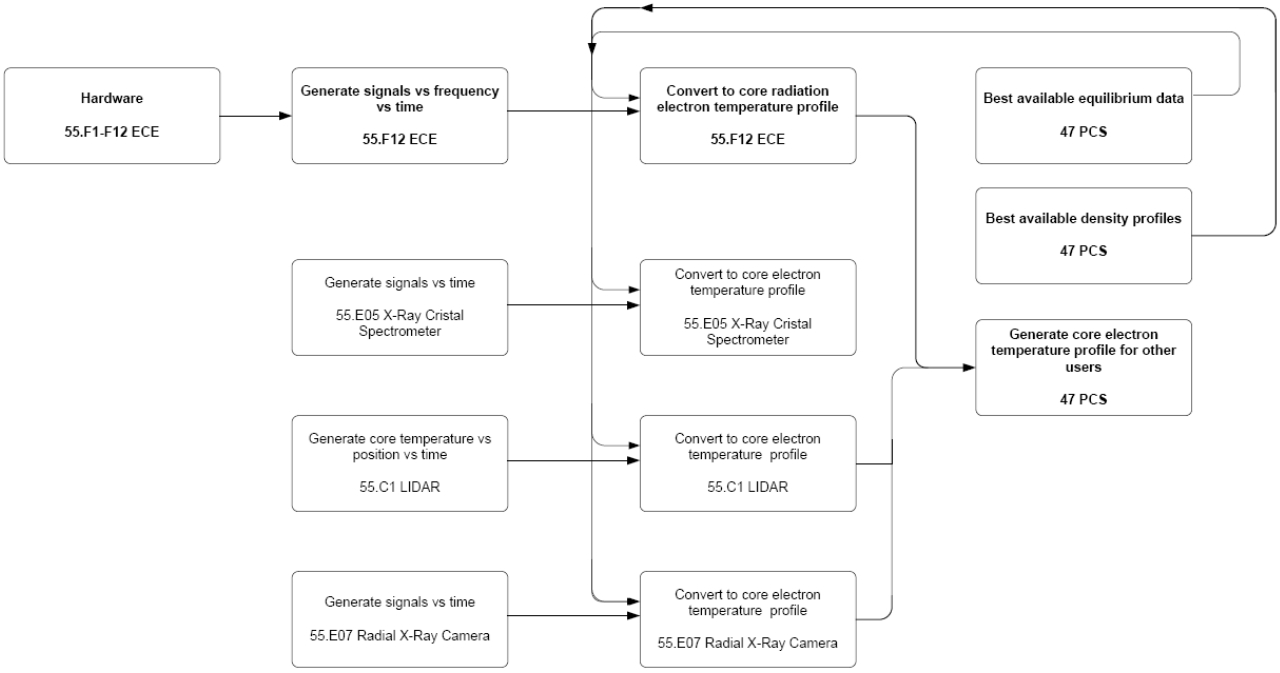

Figure 8.5. Example of the functional outline for measurement 23-052 (Core Electron Temperature), 1b – Advanced Control. ECE diagnostic has a primary role in this measurement. Other diagnostics which contribute to this measurement are also shown. For real-time processing, the data is fed to PCS.

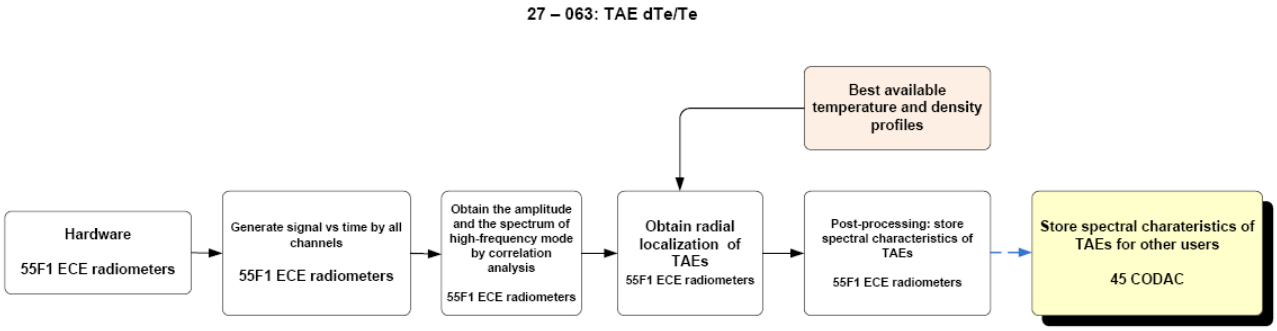

Figure 8.6. Example of functional outline for measurement 27-063 (TAE dTe/Te), 2 - Physics. No interface with PCS is needed but interface with CODAC could be envisaged. ECE diagnostic has a supplementary role in this measurement.

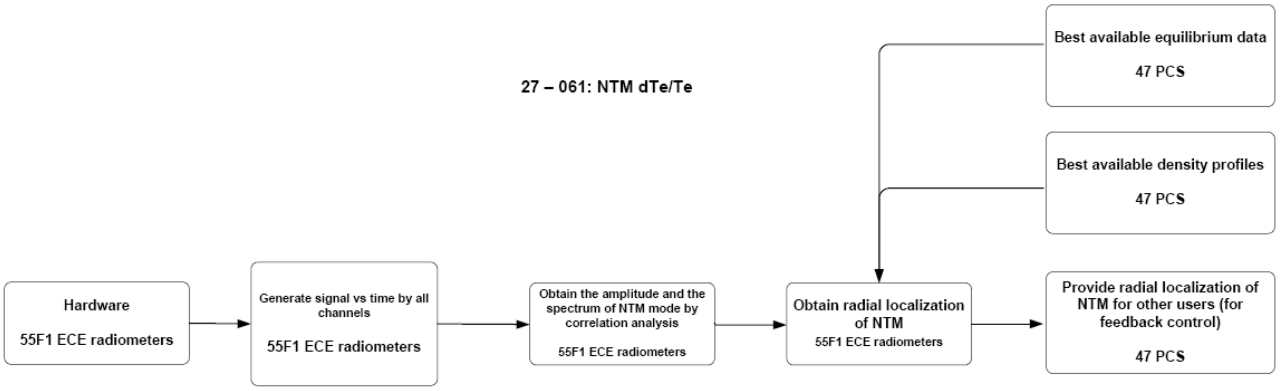

Figure 8.7. Example of functional outline for measurement 27-061 (NTM dTe/Te), 1b – Advanced Control. Interface with PCS is identified for real-time processing. ECE diagnostic has a primary role in this measurement and is the only one to deliver NTM dTe/Te.

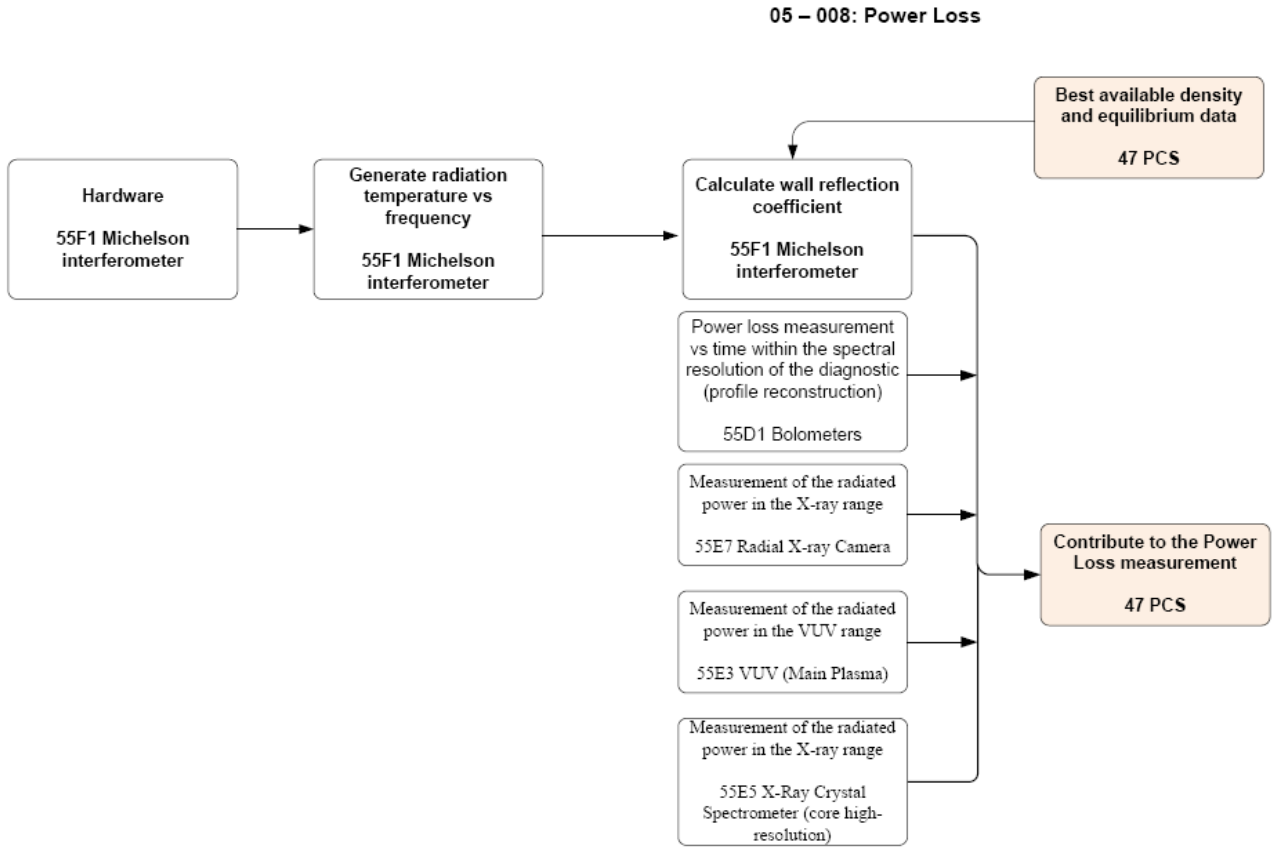

Figure 8.8. Example of functional outline for measurement 05-008 (Main Plasma Power Loss), 1a2 – Basic Control. Interface with PCS is identified for real-time processing. ECE diagnostic has a supplementary role in this measurement.

9 Component Design Description

CAD models of the ECE will be available in the ENOVIA US database for the Equatorial Port 09 System Integration which will be held on December 2nd 2011.

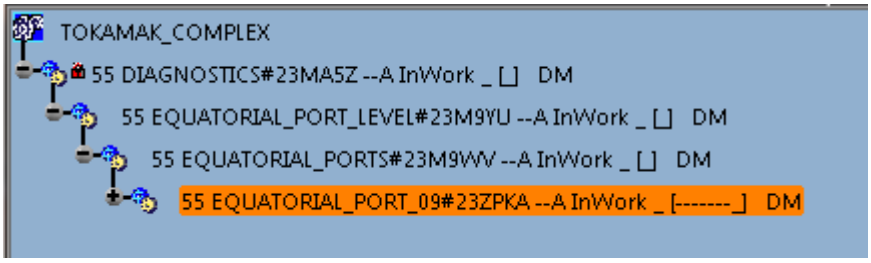

Figure 9.1. Enovia VPM tree for diagnostic systems in Equatorial Port 09 in which will be stored the ECE system (55F1).

9.1 Integration in the Port Plug

The system is installed in the Equatorial Port 09 area (building 11, level 1, sectors 4 and 5), which includes the equatorial port 9 itself, port cell and port gallery.

The Port Plug is split into 3 vertical drawers (DSMs). These drawers will have to integrate:

G1 - Eq Vis/IR TV	=>	EU
C5 - TIP	=>	US
E5 - XRCS Core	=>	US
F1 - ECE	=>	US / India

It has been defined that the ECE system is integrated within the central drawer.

This arrangement leads to the implementation given in Fig. 9.2.

For further details on the Equatorial Port Plug structure and the DSM designs, refer to the following documents:

https://user.iter.org/?uid=3U8JU7 – Generic Diagnostic Equatorial Port Plug Structure DDD;
https://user.iter.org/?uid=44U4SK – Generic Diagnostic Shield Module DDD.

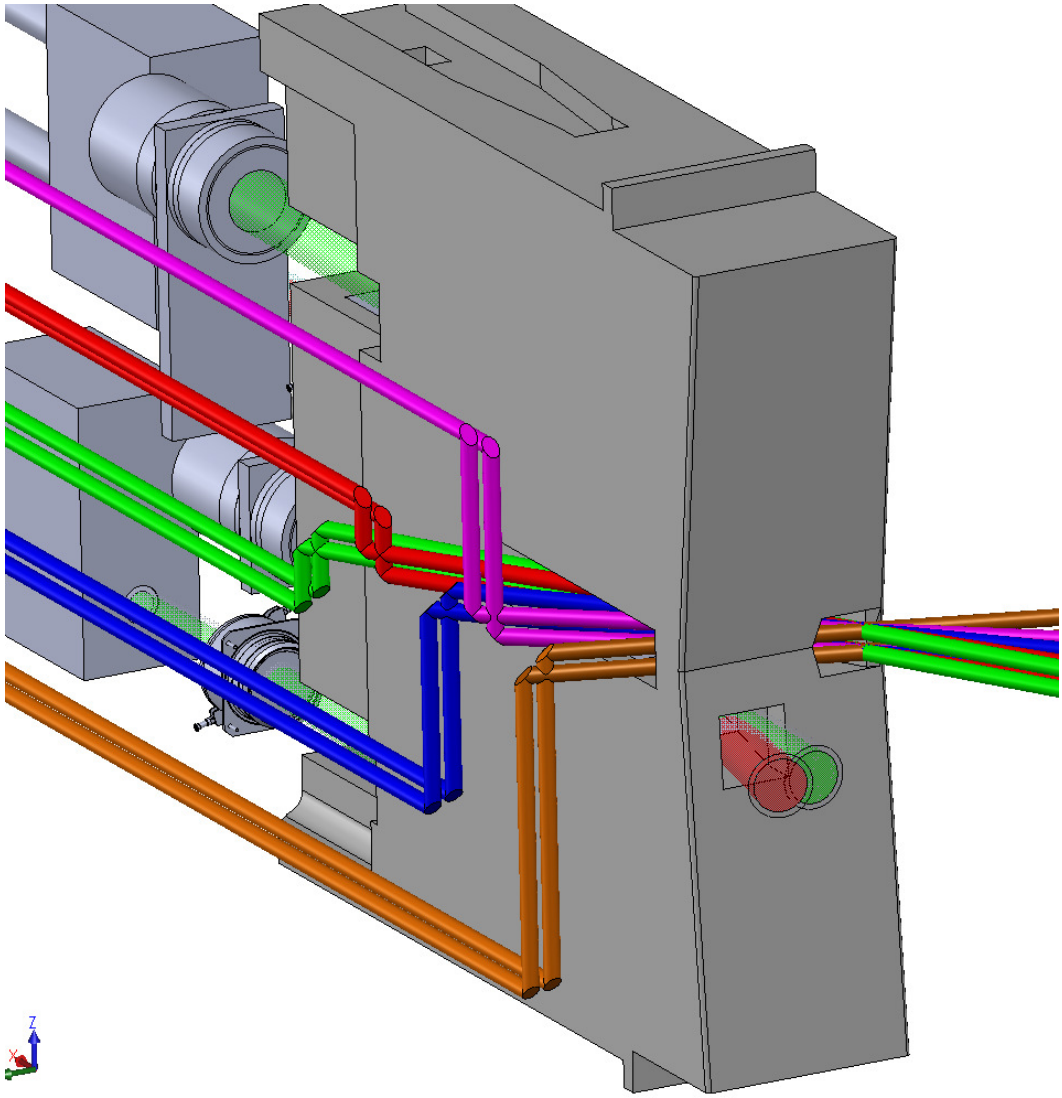

Figure 9.2. ECE arrangement in the Equatorial Port plug 09 central drawer viewed from the plasma.

9.2 Front-end arrangement

The baseline antenna system utilizes 2 lines-of-sight for the 55F1 ECE diagnostic. The ECE system is allocated the central drawer in EQ9 (see Section 9.1 and Fig. 9.2 therein). Figure 9.3 shows the proposed front-end implementation into a drawer. All drawer and diagnostic components have been cleaned and baked to meet VQC-1A standards. The allocation of mirrors is designed to assure that under most conditions; at least one pair line-of-sight will be able to measure Te-profile.

The front-end feature a single focussing ellipsoidal mirror as the first element, with a simple turning mirror as the second element to create the required labyrinthian design that prevents streaming of neutrons directly through the port plug. The ellipsoidal mirror focusses an aperture or beam waist at the back of the port plug to a beam waist near the low-field side edge of the plasma. The motivation in the design is for simplicity to minimize the risk of failure in operation. The plasma-facing mirrors may require active cooling to deal with the surface distortions. Arrangement similar to the cooling of the ECH launcher mirrors can be adapted int the design, if necessary.

There is also a shutter to switch between plasma view and calibration by the Hot Source. The shutter can be actuated pneumatically, electrically or mechanically: in the latter case, a mechanical feedthrough with double-bellow arrangement can be proposed.

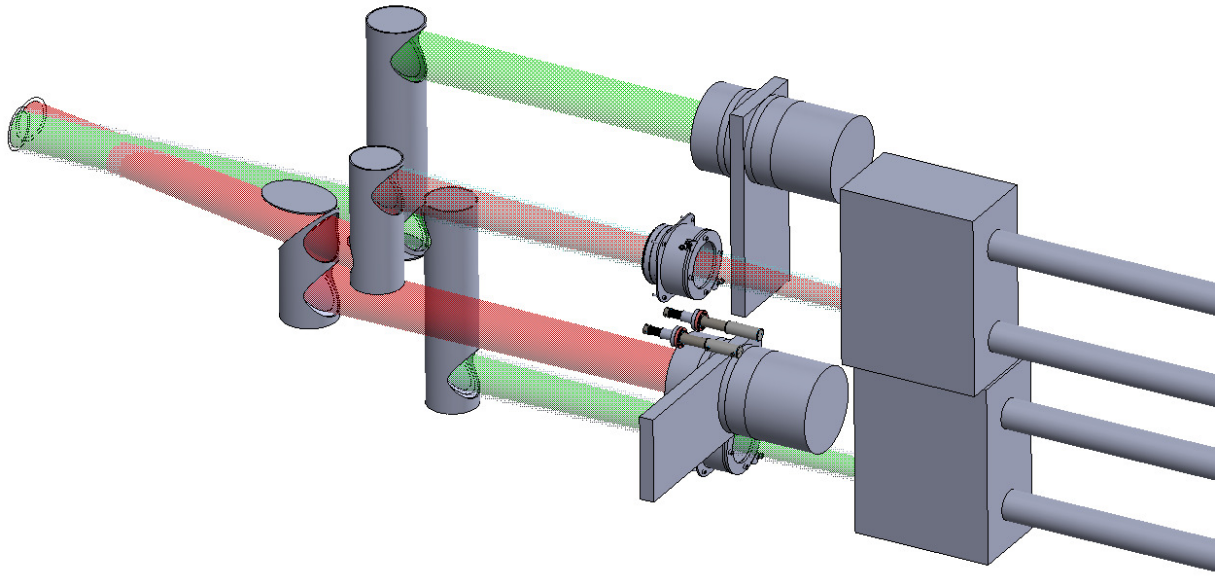

Figure 9.3. Front-end of the ECE Diagnostic in the Equatorial Port Plug 9.

9.3 Polarizer splitter box arrangement on the Interspace Support Structure

The polarizer beam splitter boxes are mounted on the Interspace Support Structure (ISS) to view the beam that goes from the in-port optics through the double-window assemblies. The space between the optics and the double-window assembly is pumped out by the rough pumping system and isolated from the interspace/ port cell atmosphere by a bellow assembly. The evacuation pipe is connected to the roughing pump located in the Port Cell. The port plug flange will move radially, vertically and/or toroidally during machine warm-up, operation, and bakeout. The alignment of the polarizer splitter box is foreseen for the operation temperatures; it is pre-stressed at the room temperature. Also, the optics in the splitter boxes are designed to be oversized, to accommodate for the vertical relative movement of the port flange with windows with respect to the splitter box. Some fine adjustments are possible for the box itself and for optics inside. The output waveguides are designed to take the radial movement, with respect to the beam axis. Figure 9.4 shows the arrangement for the polarizer splitter boxes and the hot source assembly on the back of the Equatorial Port 9. Figure 9.5 gives an example of the feedthrough with double-bellows (SVS-monitored) for 55F2 LFS Reflectometry waveguide which can be used to allow the radial movement of the output waveguides in the polarizer splitter box.

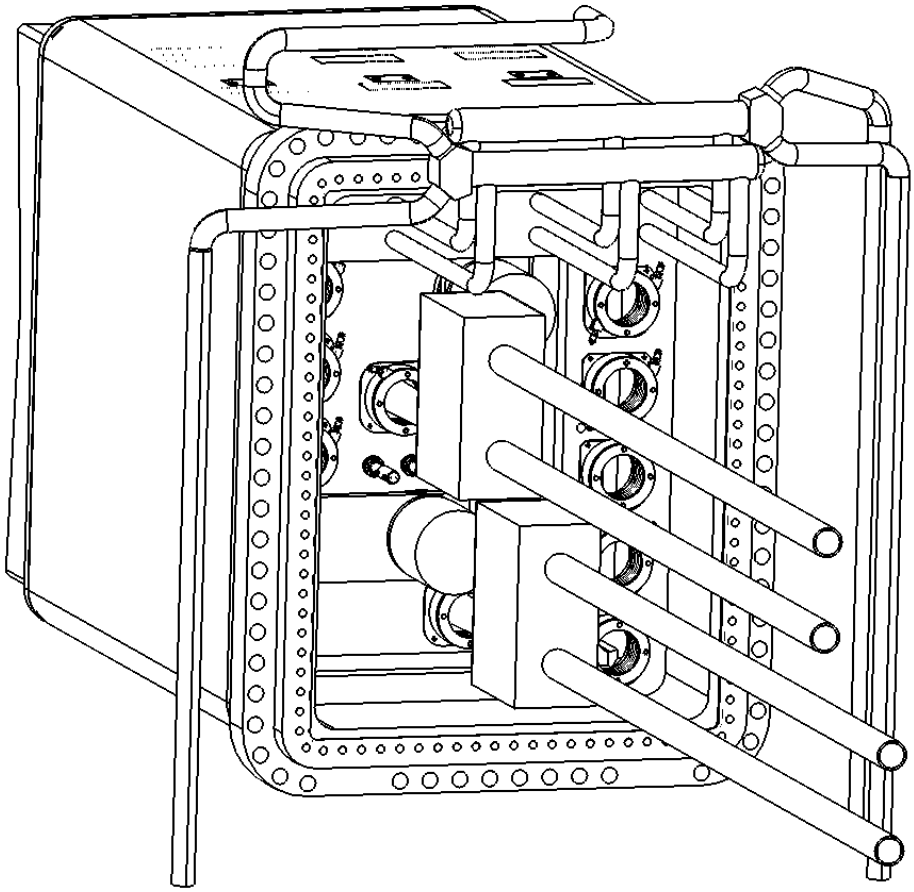

Figure 9.4. The arrangement for the polarizer splitter boxes and the hot source assembly on the back of the Equatorial Port 9.

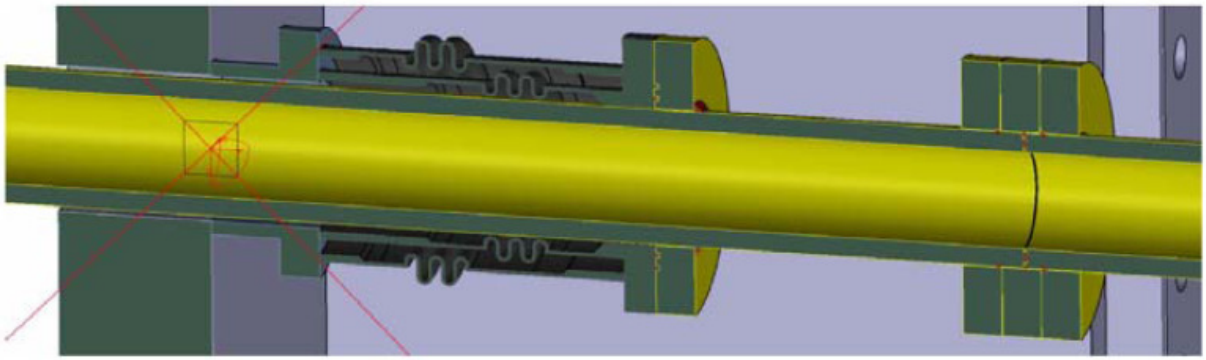

Figure 9.5. Concept of the feedthrough with double-bellows (SVS-monitored) for LFS Reflectometry waveguide. Similar concept can be used to allow the radial movement of the output waveguides in the polarizer splitter box for 55F1 ECE diagnostic.

9.4 Ex-Vessel Waveguides

The apertures, pipes and waveguides with their shielding are supported by the Interspace Support Structure (ISS), which is fixed to the building (Fig. 9.6).
The port-plug facing 55F1 ECE waveguide sections are planned to be installed on to the Interspace Support Structure. The Interspace Support Structure is foreseen to be brought as one part, with all apertures, pipes and waveguides already mounted on it. Radial thermal motion will be taken up by a sliding waveguide joint will be used in the polarizer splitter box. Furthermore, there are doglegs that are intoduced to the TL in the Port Cell, thus allowing for compliance in the radial direction. The long waveguide run also helps to compensate for the vertical movements. In the Port Cell, the waveguides are partly supported by means of the Port Cell Support Structures (PCSS) (Fig. 9.7). Generally, the integration in the port cell is driven by the size of each diagnostic. Two main frames are foreseen to handle the equipment in the port cell. Each one of these frames is designed to be compatible with the Remote Handling Cask Air trolley.

The waveguides are clamped regularly on the ISS and PCSS, thus preventing sagging and additional mode conversion losses. The «zero-gravity» waveguide supports are being currently developed; the basic concept can be found at WWW.PHSIND.COM (Variable Spring Catalogue), © PHS Industries, Inc (Fig. 9.8).

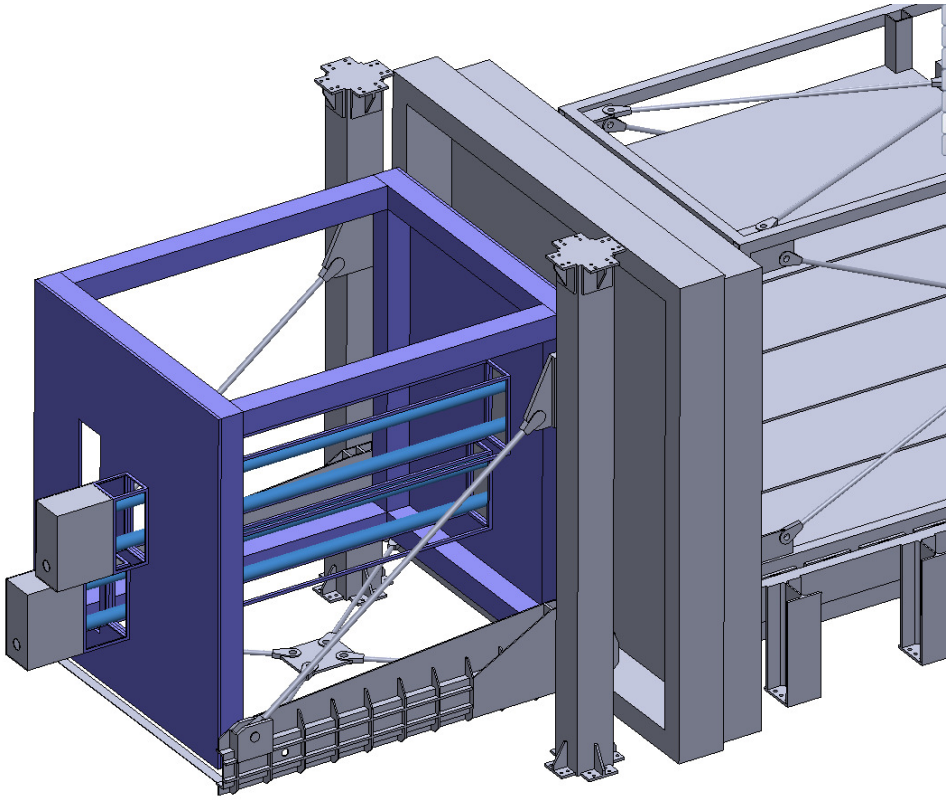

Figure 9.6. Front view of the ISS in the Equatorial Port 9 with ECE transmission line.

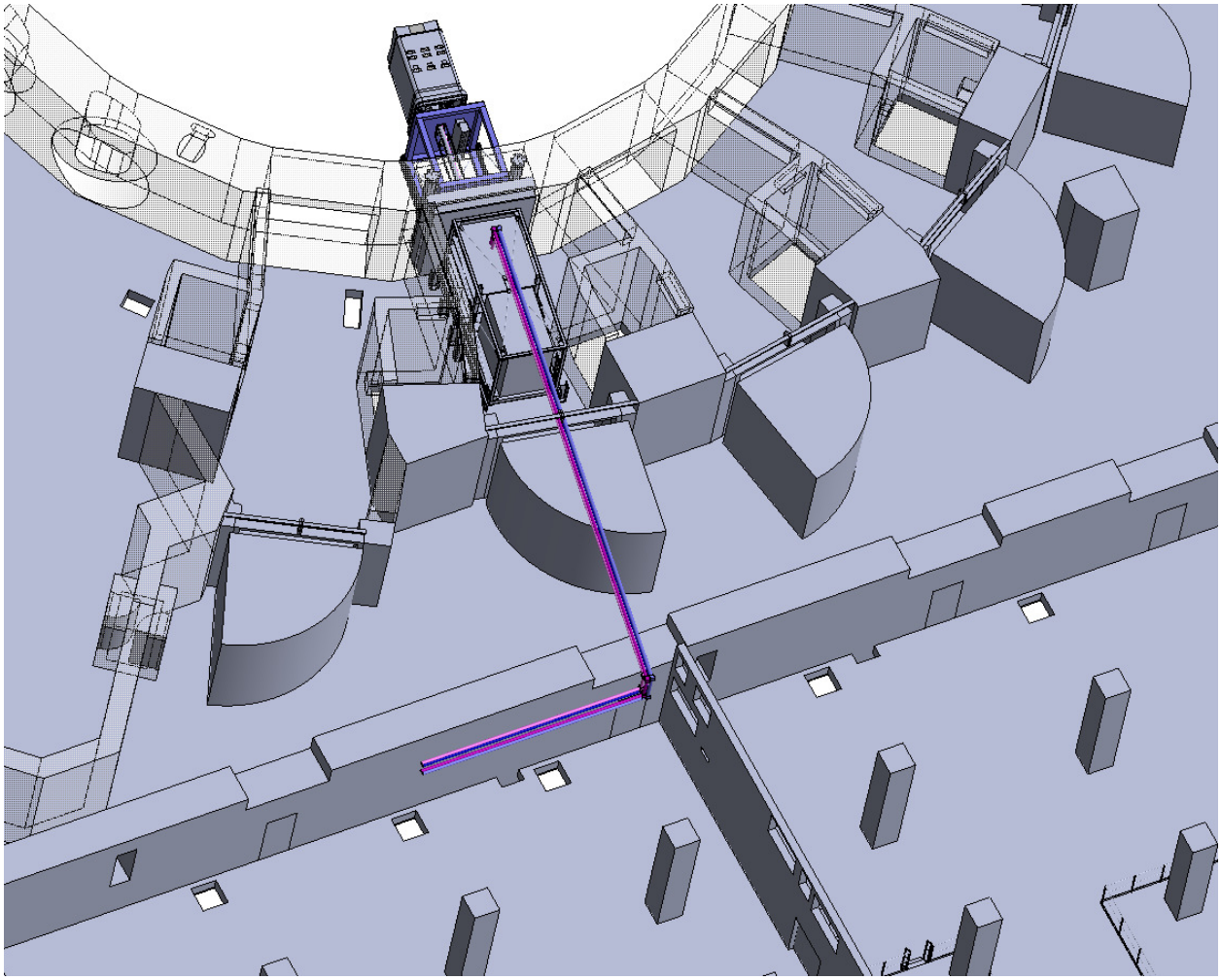

Figure 9.7. ECE transmission line in the Equatorial Port 9 (interspace, port cell, gallery) and in the Diagnostic building (74).

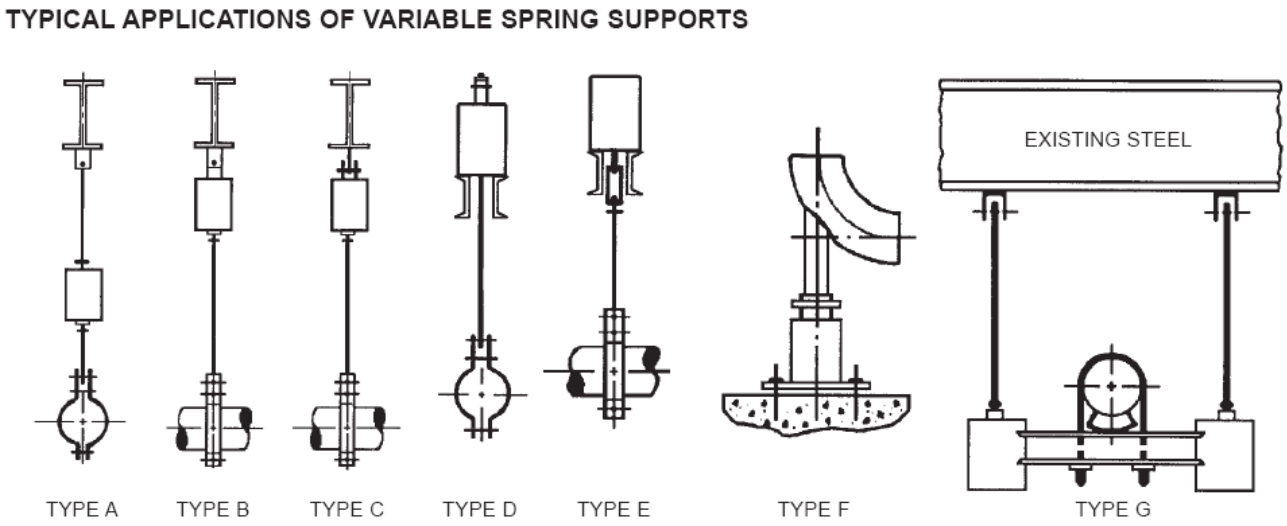

Figure 9.8. Concepts of variable spring supports which can be used for the 55F1 ECE TL; © PHS Industries, Inc.

9.5 Embedments in the Port Interspace

The present CMM model does not show all of the diagnostic requirements for embedded plates; they are, however, included in IS 62-55 which should be used as a reference.

a) Embedments for PBS 23 (RH)

These are also required for PBS-55 (Diagnostics) for the Diagnostic Trolley. PBS55 Requirement Specification should be added to those for PBS 23. This is probably no more demanding in terms of load capacity. There may need to be an accurate location datum defined. The present provision in CATIA is adequate.

b) Embedments for PBS-62-11-BP (BioShieldPlugs)

They will exist in all port cells including those for Diagnostics. The diagnostic Models contain additional shielding and the Technical Specification for the strength etc. of this anchoring must include the requirements for both the standard shielding (PBS62) shielding for man access during maintenance and additional shielding (PBS55) for operation of equipment during plasma operation. The present provision in CATIA is adequate for spatial location, the IS 55-62 gives the loads. Presently, PBS 55 is working on the diagnostic requirements for the Bioshield plug.

c) The Port Interspace Structure Embedded Plates

These will exist in all port cells for Diagnostics. The present provision in CATIA (Fig. 9.9) is adequate for spatial allocation, the IS 55-62 gives the loads. These must be designed in close proximity to the Cryostat embedded plates.

d) The Embedded Plates for PBS-55F1 ECE Waveguides

ECE ex-port plug waveguides, where they are not supported on the Diagnostic Trolley, must be anchored to the port cell ceiling. Embedded plates are required. This type of equipment exists at many port cells, the Enovia DM shows their locations; in Fig. 9.10, 55F1 ECE is illustrated for Eq#9. In all cases of Port Cell transmission line there is a complementary set of lines in the Gallery that are to be supported in the same way. The IS 55-62 identifies them, their location and gives the loads.

Refer to Annex 8.1.3 for further details on embedments.

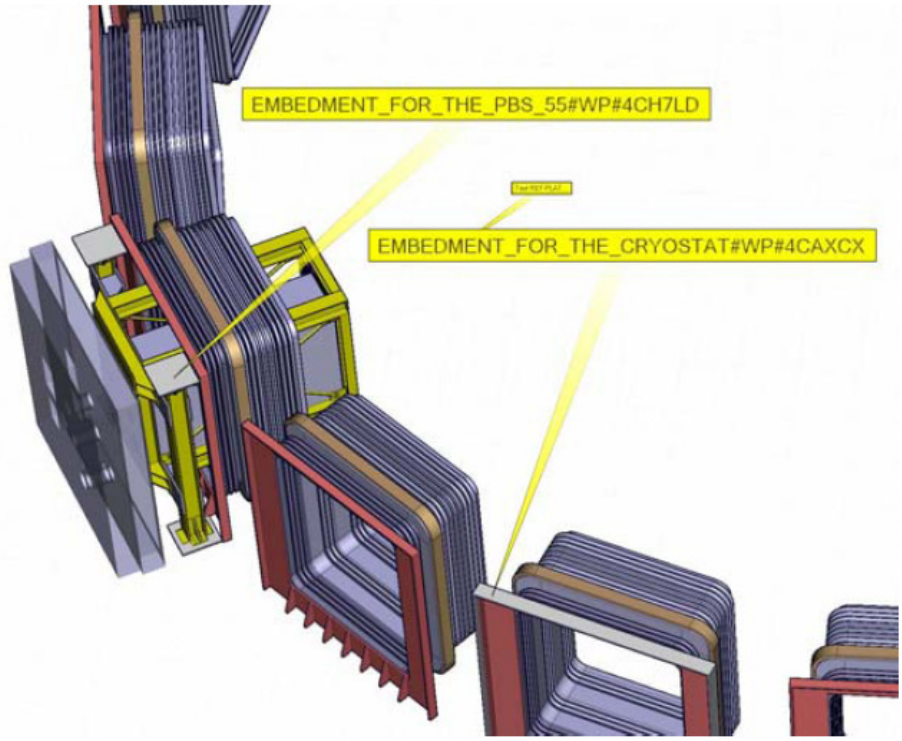

Figure 9.9. Embedments for Interspace Structure of PBS-55-Diagnostics.

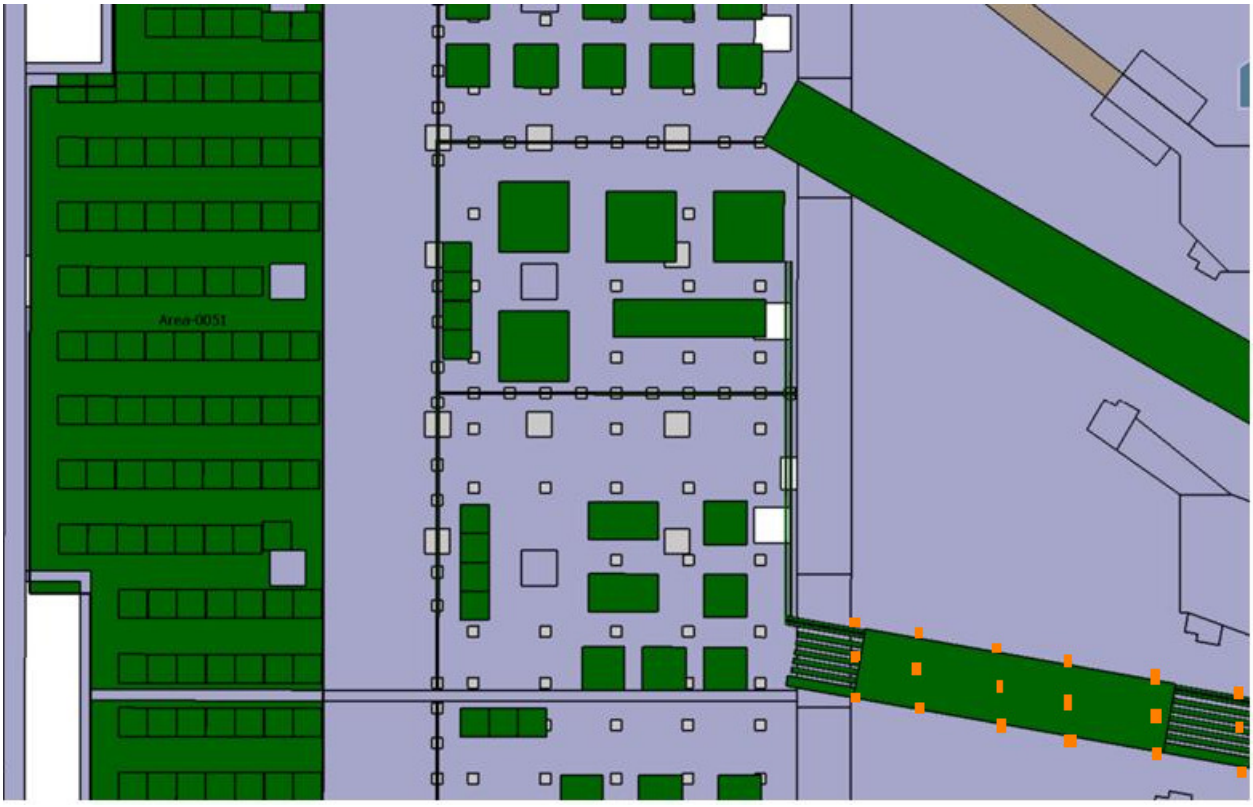

Figure 9.10. Embedments for 55F1 ECE diagnostic waveguides in the gallery (orange rectangles).

9.6 Gate valve and primary confinement barrier

The confinement barrier strategy for the ECE has been discussed in Sections 4 and 8.1.2. Primary Vacuum Window makes up tritium/vacuum containment boundary.

The primary vacuum window is discussed in Section 6.2.4.3 and in the Annex 6.2.2. Natural or synthetic Crystalline Quartz (Z-Cut) are proposed as a window material. These materials have good dielectric properties for use as microwave window (Fig. 9.11). The primary vacuum window is VQC-1A components. The secondary window can be a signle-window assembly made of the same material as the primary windows, or can also be chosen from the material which has low dielectric constant to minimize reflections and loss of microwave signals and, at the same time, satisfy requirements for ITER as indicated in the Vacuum Handbook. One of the candidates is Rexolite Q200.5. The assessment of the secondary window material is planned during the PDR phase. R&D is required to demonstrate window design and performance. The interspace between the primary and the secondary window should be monitored by the SVS.

The gate valve is required to trip the hot source assembly (which is on the back of the Port Plug flange) from the vacuum inside the Port Plug for operational or protection needs. The assembly of the gate valve and the hot source do not protude the no-tresspass line for the RH of the EPP9, so the service is enables in the refurbishment area of the Hot Cell Facility, too. In the non-active operation phase of ITER, the in-situ replacement of the Hot Source assembly is possible.

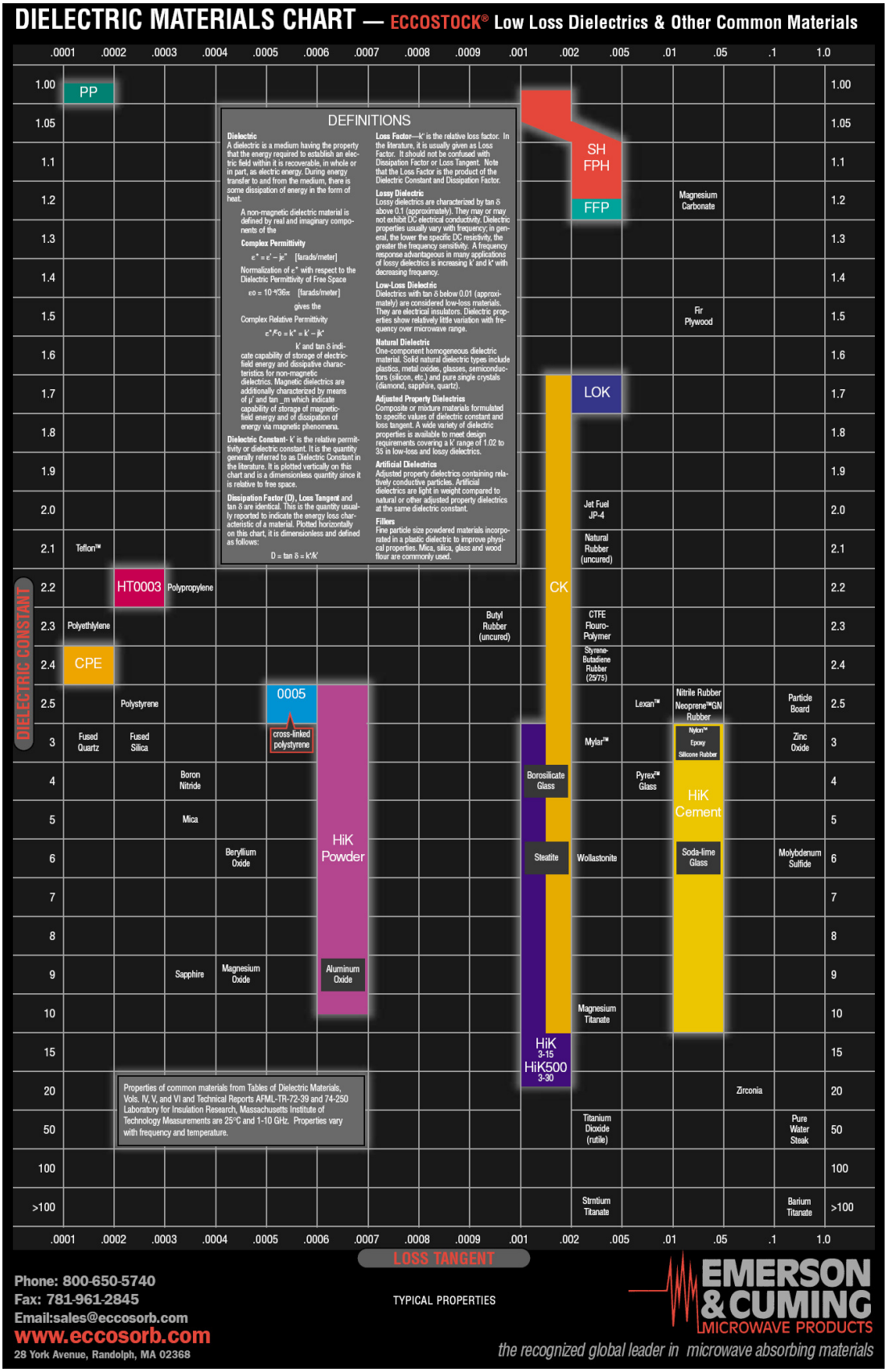

Figure 9.11. Dielectric materials chart as taken from ECCOSORB® website (http://www.eccosorb.com).

9.7 Routing to the Diagnostic Area through the Gallery

The routing of the waveguides through the gallery to the Diagnostic Area in Building 74 is shown in Fig. 9.13. Between the Gallery and Diagnostic building, 3rd window (no vacuum – gallery atmosphere on one side and Diagnostic building atmosphere on the other side) is foreseen to create an additional confinement barrier.

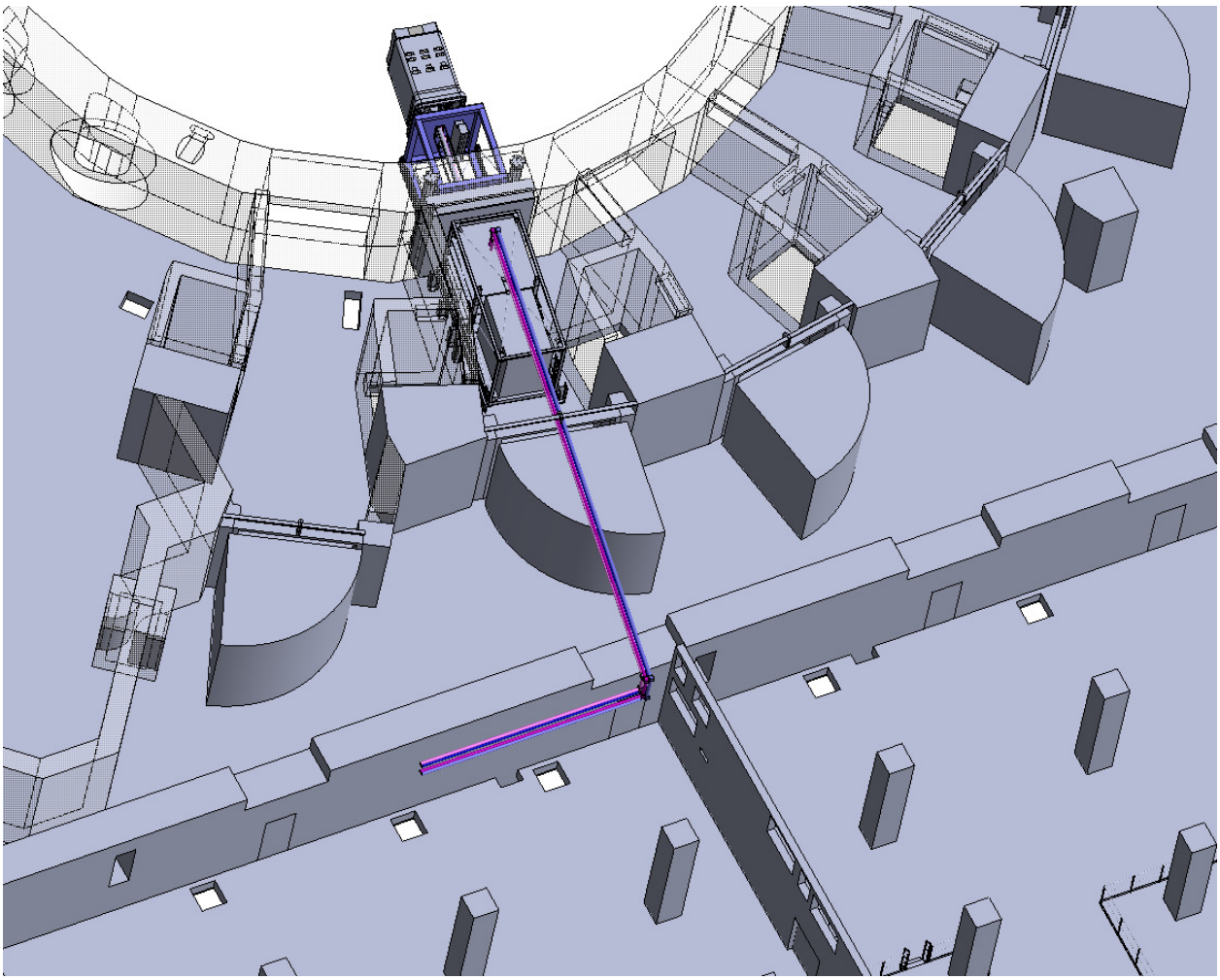

Figure 9.13. Routing of waveguides through the gallery to the Diagnostic Area in Builiding 74.

The ECE room conceptual layput is given in Fig. 9.14.

Table 9.1 gives an overview of requirements for the ECE room in the Diagnostic Building 74.

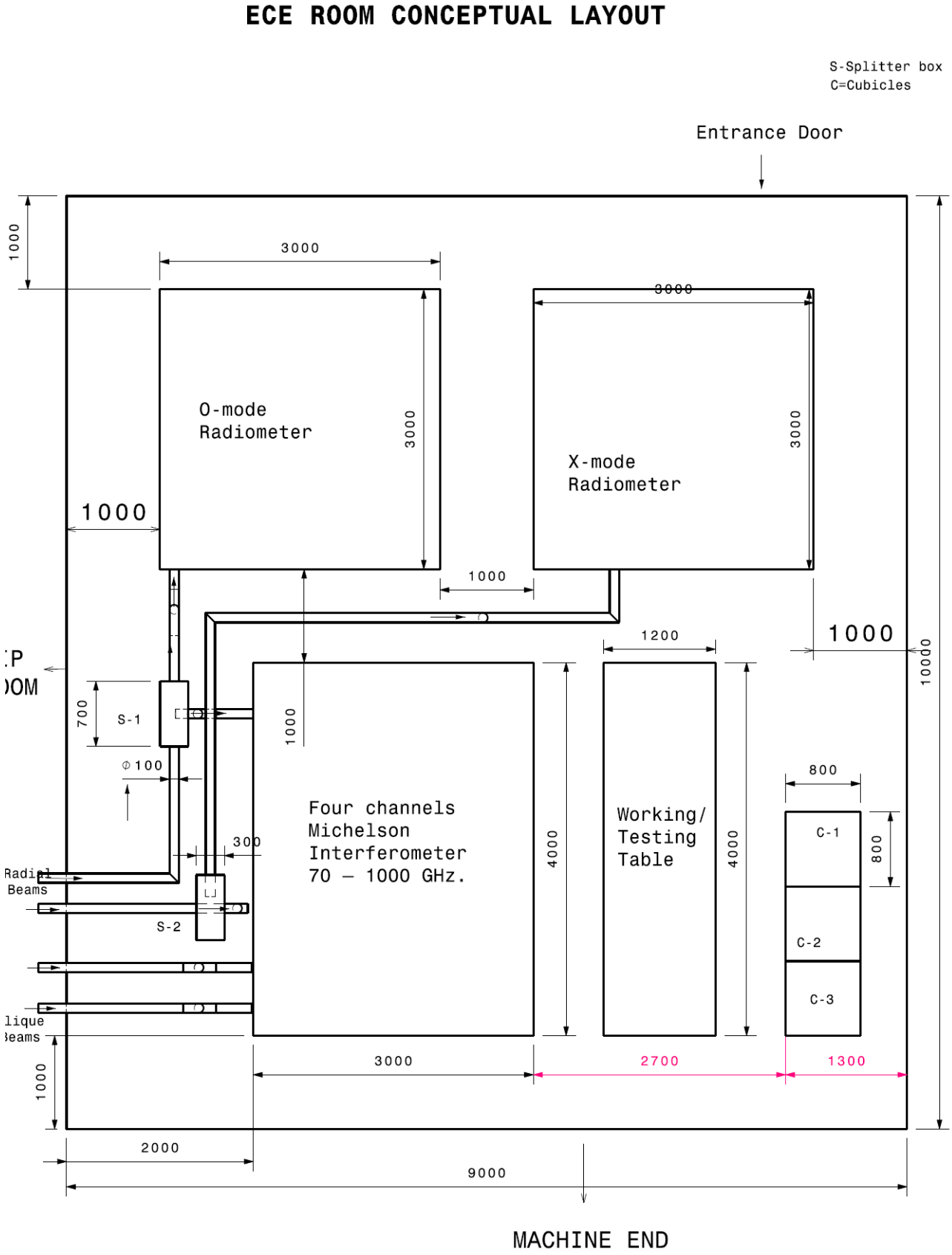

Figure 9.14. Conceptual layout of the ECE room in the Diagnostic Builiding 74.

Table 9.1. Requirements for the ECE room in the Diagnostic Building 74.

Sr.No	Equipment Name	Quantity of equipment's	Size	Weight	Location	Heat Load	Electrical Power load
1	O-Mode radiometer	01	3mx3mx2.5 m	350Kg	Diagnostics Building ECE Room	350W	1kW
2	X-Mode radiometer	01	3mx3mx2.5 m	350Kg	Diagnostics Building ECE Room	350W	1kW
3	Four Channel Michelson Interferometer	01	3mx4mx3m	1200kg	Diagnostics Building ECE Room	500W	2kW
4	Hot Calibration source	01	1mx1mx1.5 m	250kg	Diagnostics building ECE room	2kW	2kW
5	Cubicles	06	(0.8mx0.8m x2.2m)	----	03 cubicles in ECE room and 03 In cubicle section	240W	600W

- Heat load for ECE room is 4Kw and power requirement for room is approximately 7kW
- 03cubicles required (0.8mx0.8mx2.2m) in ECE room
- 03cubicles required (0.8mx0.8mx2.2m)in cubicles section
- No cubicles required in port cell
- Pumps and motors are in port cell
- Voltage (Interruptible AC 230/ 400V)
- Single phase current and voltage

9.8 Connection flanges design

The standard bolted flange similar to this used by ITER ECH transmission lines is proposed as a baseline concept to connect waveguides of the ECE (Fig. 9.15). Two Helicoflex seals on end of corrugated waveguide tube are used to maintain vacuum. Vacuum (SVS) connection for monitoring space between seals is compulsory. This concept is suitable for both corrugated and smooth-wall waveguides.
As has been mentioned earlier, if the hands-on operations are difficult due to high activation level on the back of the port plug flange, a work on the RH-compatible waveguide flange design is currently ongoing as a back-up solution.

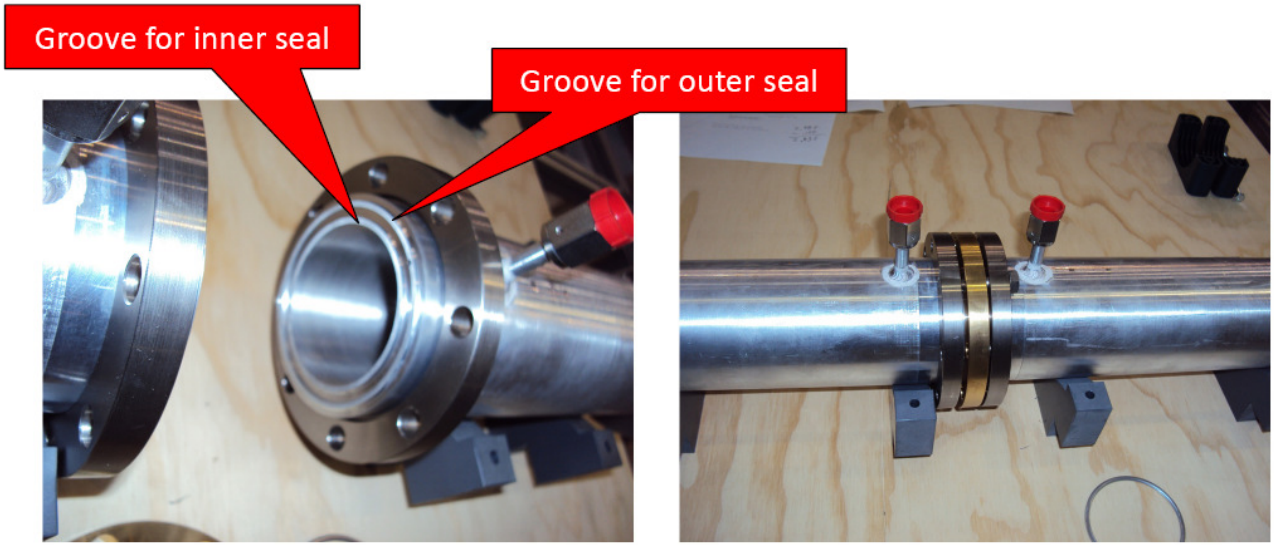

Figure 9.15. Standard hands-on waveguide flange concept.

9.9 Data Acquisition and Control

The concept of data acquisition and software has been described in Section 6.5 of this DDD. Instrumentation and Control are discussed in Section 11.

10 Procurement Package

A summary of the specifications proposed in section 6.1.7 will appear in section 4.3.2 “Specific requirements” of the PA annex B. Note that the Procurement of the ECE diagnostic components will be performed by US DA and IN DA.

11 Instrumentation & Control

The chapters in the instrumentation and control (I&C) section match the design specifications and technical specifications for manufacture in table 6 in the design review procedure (3DBW79). During the various phases of plant I&C design (CDR, PDR, FDR) up to the final design review all of the following design specifications and technical specifications for manufacture must be completed and documented as described in the PCDH report (see http://www.iter.org/org/team/chd/cid/codac/PlantControlHandbook):

Design Specifications:

[I1] Plant system I&C operation and control philosophy.

[I2] Plant system functional analysis.

[I3] Plant system PFDs, mechanical and electrical drawings needed at conceptual design phase.

[I4] A list and short description of main plant system operating states for plant system operation.

[I5] Plant system risk analysis and I&C RAMI requirements.

[I6] System Interface Control Documents (S-ICDs) relevant for the plant system I&C.

[I7] List and specifications of the main protection functions to implement within the plant system or with respect to other plant systems. The specifications include a risk analysis to identify the interlock functions from amongst all of the protection functions

[I8] List and specifications of the main safety functions to implement within the plant system or with respect to other plant systems.

[I9] Technical Specifications for manufacture:

Technical Specifications for manufacture:

[D1] Plant system I&C architecture.
[D2] Plant system I&C boundary definition.
[D3] Plant systems I&C integration plan.
[D4] Plant system P&IDs, mechanical and electrical drawings needed for I&C specifications.
[D5] Plant system controller(s) performance and configuration requirements.
[D6] List of inputs and outputs (I/O) of the I&C controllers.
[D7] List of the process variables handled by the plant system I&C controllers.
[D8] Configuration of I&C cubicles.
[D9] Description of plant system state machines.

The ECE diagnostic includes instrumentation and control for various monitoring, control, interlock and safety functions. The supported main functionalities for the ITER machine are in the areas:

- Machine protection
- Plasma control
- Physics exploitation
- Maintenance

Since the diagnostic systems provide measurements which are the essential input for the above described functions the diagnostics system must be operated in a way which guarantees the required measurement accuracy while ensuring high availability. The operation procedure of diagnostics plants usually includes the following steps:

- Health (check)
- Vacuum monitoring and control
- Configuration (perform or verify)
- Calibration (perform or verify)

- Measurement integrity verification (consistency check with other diagnostic measurement and comparison with previous pulses)
- Troubleshoot (in case of problem)
- Start and stop measurements (including scheduler)

The operating procedures will be automated as far as possible. Functions that cannot be automated will be executed manually by trained operators or plant system experts.

The main I&C functions implemented in the LFS Reflectometry are:

- Receive MM-waves from the plasma
- Routing & distribution of signals
- IF signal analysis
- Real time measurement – electron temperature
- Calibration
- Signal conditioning
- Data acquisition
- Signal processing
- Interface with CODAC

I&C Functional breakdown and allocation to the controllers for 55F1 ECE system are given in Fig. 11.1.

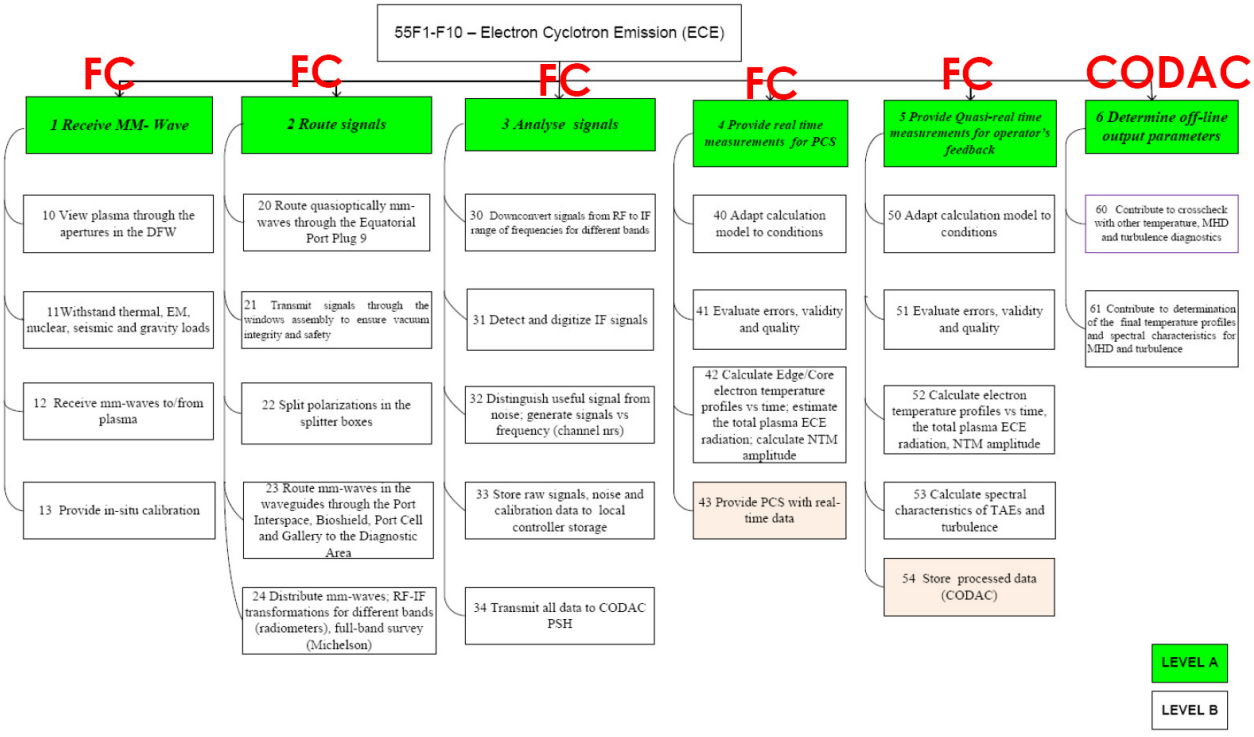

Figure 11.1. ECE diagnostic functional breakdown and allocation to controllers.

(I3) Plant System PFDs, mechanical and electrical drawings

The plant system PFDs are shown in Section 8.

(I4) Plant System Operating States

ITER Plant operation is managed by system operating states, which are composed of three levels of hierarchy.

Global Operating States (GOS)

The GOS represent overall ITER plant system operating states defined by plant-wide operational activities associated with permission or prohibition of the plant operational activities. ITER GOS are defined in Operations Handbook - 2 Operational States (2LGF8N) and given in Table 11.1.

Table 11.1. Definition of Global Operating States.

LTM	Long Term Maintenance
STM	Short Term Maintenance
TCS	Test and Conditioning State
POS	Plasma Operation State

Plant System Operating States (PSOS)

The plant system operating states are specific to individual plant system I&C. The plant system operating state is a mandatory state property that implements detailed and plant-specific state information. Each value of the plant system operating state shall map to one and only one value of the COS.
The plant operating states are given in Table 11.2.

Table 11.2. Plant Operating States (PSOS).

Off	None of the measurements and controls is active
Stand-by	I&C operational
TCS	Test and conditioning (used also for commissioning)
Calibration	Calibration of neutron flux
Ready	Ready for plasma pulse
Pulse	Operational with continuous data acquisition

The mapping of the common operating states (PSOS) to the global operating states (GOS) are shown in Table 11.3.

Table 11.3. Mapping of common operating states (PSOS) to global operating states (GOS).

GOS / PSOS	**LTM**	**STM**	**TCS**	**POS**
Off	**X**	**X**		
Stand-by	**X**	**X**		
TCS	**X**	**X**	**X**	
Calibration	**X**	**X**	**X**	
Ready	**X**	**X**	**X**	
Pulse	**X**	**X**	**X**	**X**

(I5) Plant System Risk Analysis and I&C RAMI Requirements

The plant system risk analysis is described elsewhere (ref) while I&C RAMI requirements are presently developed.

(I6) System Interface Control Documents

The system interface between diagnostics (PBS55) and CODAC (PBS45), CIS (PBS46), PCS (PBS47) and CSS (PBS48) are described in corresponding ICDs. The detailed information is found in the Interface Sheets (ISs). For real-time control, there is an interaction with the Plant Control System (PCS; PBS 47). Relations with Central Interlock System (CIS; PBS 46) are required for the protection from the ECH stray radiation. They will be assessed for PDR.

(I7) Main I&C Protection Functions

Protect torus primary vacuum from a leakage through the vacuum barrier. Monitor pressure and close isolation valve in case of leak.

(I8) Main I&C Safety Functions

There will be no safety functions (nuclear, access and occupational) implemented in the instrumentation and controls section of the 55F1 ECE system.

(D1) Plant I&C Architecture

The plant I&C architecture is shown in Fig. 11.2. A plant system I&C consists of one and only one plant system host, one or many OSI (Open System Interconnection) layer 2 switches and one or more plant system controller(s) interfacing to actuators and sensors via signal interface(s). Plant system I&C components communicate with the CODAC System / Mini-CODAC over the Plant Operation Network (PON). CODAC System / Mini-CODAC implements the human-machine interface. Plant system controllers may be organized in a functional hierarchical manner using one plant system controller supervising the others.

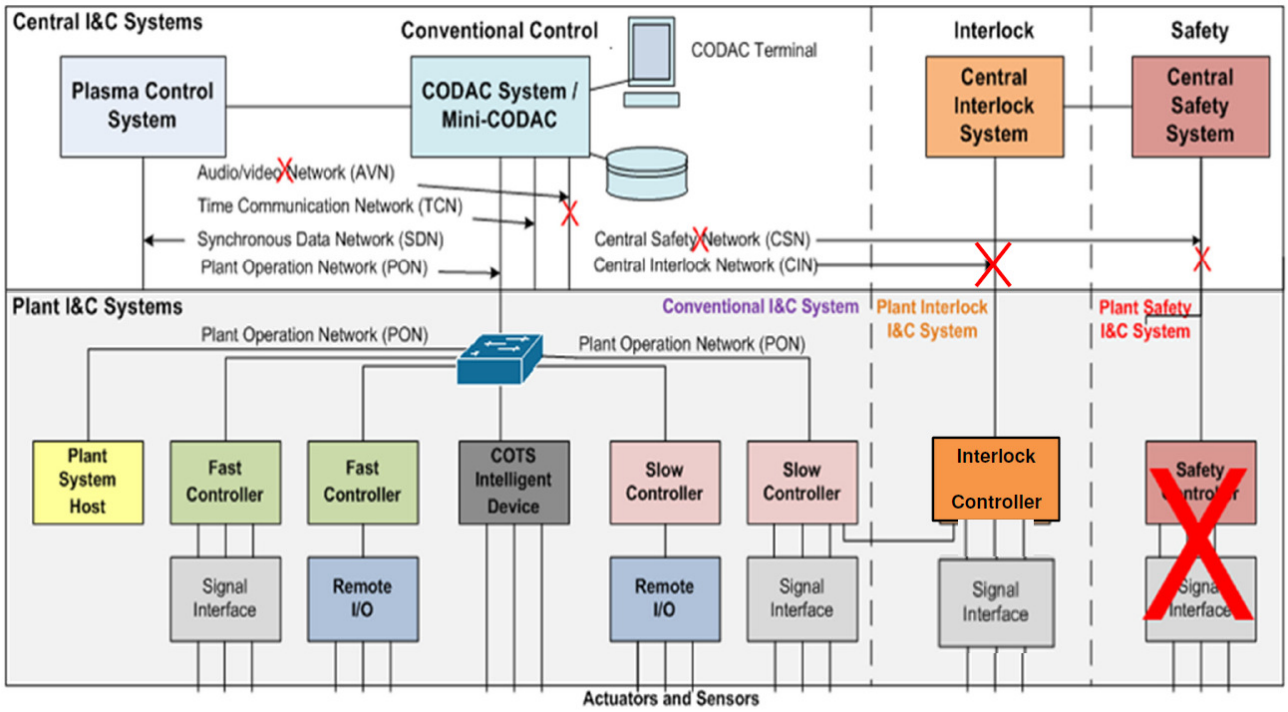

Figure 11.2. Architecture of 55F1 ECE system - Instrumentation and Control.

The PSH is a standardized computer supplied by IO that is a component of the plant system I&C. It is connected to the Plant Operation Network and is designed for implementing the standard functions for plant system I&C, not for plant-specific programming.
The primary functions are:

- Handle commands from the CODAC system / Mini-CODAC and dispatch commands to the plant system controllers.
- Monitor the plant system state and status and update this in the CODAC system / Mini-CODAC.
- Transfer alarms from the plant system I&C to the CODAC system / Mini-CODAC.
- Transfer logging messages from the plant system I&C to the CODAC system / Mini-CODAC
- Distribute software events from the CODAC system / Mini-CODAC to the plant system controllers and vice versa.
- Monitor its own state and update this state in the CODAC system / Mini-CODAC.
- Reconfigure the plant system I&C when in maintenance mode.

Plant system controllers are local units in charge of implementing the functional and physical part of the control and data acquisition of the plant system. All plant system controllers include a processor and I/O interfaces, as required. I/O interfaces are either I/O embedded within the controller hardware system, or remote I/O, interfaced with a field bus.
Plant system controllers are split into two categories: slow controllers and fast controllers. Performance is a discriminating criterion but the main characteristic of the slow controllers is that they are only using COTS industrial components (Programmable Logic Controllers, PLC).

It is planned to have an overlap in the performance ranges of the two categories of controllers. It is assumed however, that only fast controllers implement control loops or data acquisition faster than 100 Hz.

The following rules apply to I&C associated with 55F1 ECE system:

- The plant I&C must be in full compliance with the rules and guidelines proposed by the current version of the PCDH (Plant Control Design Handbook, see http://www.iter.org/org/team/chd/cid/codac/PlantControlHandbook)
- The functional analysis has shown that all 55F1 ECE system functions can be implemented in the proposed standards for fast and slow controllers.
-

The connection of the 55F1 ECE system I&C with CODAC is established via various network links as shown in Fig. 11.3.

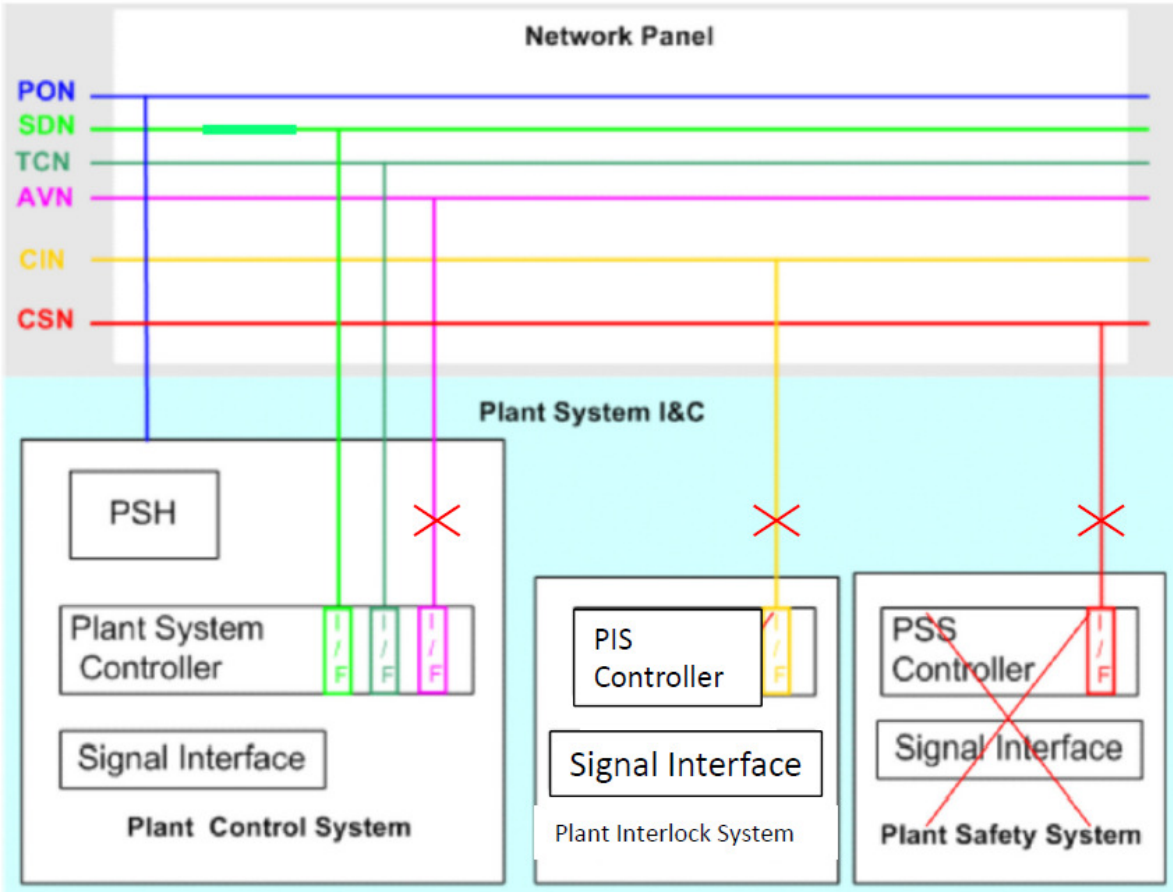

Figure 11.3. Connection of 55F1 ECE system I&C with CODAC.

- PON provides asynchronous interface between plant system
- TCN provides project-wide time synchronization
- SDN provides the synchronous interface and events plasma control
- AVN provides communication for audio and video signals (Not Applicable for 55F1 ECE system)
- PCIe : Peripheral Component Interconnect express (within plant)

- GbE : Gigabit Ethernet (within plant)
- CIN connects plant interlock system and the central interlock system
- CSN connects plant safety system and central safety systems (Not Applicable for 55F1 ECE system)

(D2) Plant System I&C Boundary Definition

The measurement and control functions of the 55F1 ECE system are used by PBS26, PBS34, PBS 45, PBS46, PBS47, and PBS51, PBS52, PBS53, and PBS54. 55F1 ECE system I&C parameters can be set through CODAC. These plant systems can access the measurements available in the 55F1 ECE system through CODAC. The operation of the 55F1 ECE system is accomplished via HMI through CODAC.

(D3) Plant System I&C Integration Plan

Factory acceptance test (FAT) will be performed with Mini-CODAC and site acceptance test (SAT) with connection to CODAC. All required network connections will be available for FAT and SAT.

(D4) Plant System P&ID

The plant system P&ID are shown Section 8.

(D5) Plant System Controller Performance

The plant system controller performance is documented in the Interface Sheets (IS).

(D6) List of Input and Output of the I&C Controllers

The list of inputs and outputs of I&C controllers is documented in the Interface Sheets (IS).

(D7) List of Process Variables handled by I&C Controllers

The list of process variables handled by I&C controllers is documented in the Interface Sheets (IS).

(D8) Configuration of Cubicles

The description will be available for the PDR.

(D9) Description of Plant System State Machine

The description of the plant system state machine will be available for the PDR.

12 Inspection, Testing and Monitoring

These aspects are described in section 8 of the PA Annex B.

13 Interfaces

Diagnostics (PBS 55) have interfaces with a large of number of systems. At a high level these are summarized in the Interface Control Table [2FA7AQ]. The important ones from the point of view of the Electron Cyclotron Emission (ECE) are summarized in the table below. All of these interfaces have Interface Control Documents (ICDs). For some of them, Interface Sheets (ISs) have already been written, describing with more details the interfaces (Table 13.1).

System	PBS	Interface Control Document	Interface Sheet
Machine Assembly & Tooling	22	ICD 22-55 Machine Assembly&Tooling [3V8YX9] v1.0	IS-22-55-035. Not written yet
Remote Handling	23	ICD 23-55 Remote Handling System [33MTMU] v1.6	IS-23-55-009 [64PKDH]: Not written yet
Vacuum	31	ICD 31-55 Vacuum [33SHV8] v1.4	IS-31-55-014 [7A4VDQ] v1.0
SSEN	43	ICD 43-55 SSEN [2KSJ68] v1.1	IS-43-55-001 [3VUL6D] v2.1 IS-43-55-002 [3VV3JT] v2.0 IS-43-55-003 [3XZRQM] v1.2
Cable Trays System	44	ICD 44-55 Cable Trays System [2WH9UJ] v1.2	IS (PBS43, PBS44) - (PBS55) [4ESYDV] v1.0
CODAC	45	ICD 45-55 Codac [33TAMZ] v1.5	IS 45-55.F2-P. Not written yet IS 45-55.F2-L. Not written yet
Plasma Control System	47	ICD 47-55 Plasma Control System [34KGXG] v1.0	IS 47-55-037. Not written yet.
Port Plug Test Facility	58	ICD 55-58 Port Plug Test Facility [34M96J] v1.1	IS 55.EQP10-58, 55.UP1-58. In progress.
Reinforced Concrete Buildings : 11-Tokamak Building 14-Tritium Building 74 Diagnostic Building 21 Hot Cell Facility 13-Assembly Building	62	ICD (PBS 62-11, 62-14, 92-74) - (PBS 55) [2EPQ2V] v1.5 ICD (PBS 62-21) - (PBS 55) [2EPR54] v1.3 ICD (PBS 62-13) - (PBS 55) [3QG3LN] v1.2	IS (PBS 62-11, 62-14, 62-74) – (PBS 55) [34GS5D] v4.1 IS (PBS 62.21) - (PBS 55) [357AB7] v1.2 IS (PBS 62.13) - (PBS 55) [3Y6WHW] v1.2

Radwaste Treatment and Storage Systems	66	Interface Control Document (ICD) between Diagnostics (PBS 55) and Radwaste Treatment and Storage System (PBS 66) (ITER_D_35XUDM v1.0)	IS-55-66-001 (ITER_D_35ZMWC v1.0)

TABLE 13.1. Current status of Interface Control Documents for **ECE (Front End and Receiver)**.

The systems listed below (Table 13.2) have no direct interfaces with the ECE but should be considered respectively for the following reason: ECH has an interface as it is included as a load specification. The signal from ECH protection circuit (as given in Table 2) integrated in the ECE diagnostic may be used by CIS, as well as by any other user which may want it. The applicability of this interface for ECE system will be decided before the PDR of 55F1 (Front End and Receiver) ECE diagnostic. CSS (PBS 48) may have an interface because of occupation safety for maintenance and operation of the diagnostic system. The applicability of this interface for ECE system will be decided before the PDR of 55F1 (Front End and Receiver) ECE diagnostic.

EC H&CD System	52	ICD to be prepared	
Central Interlock System	46	ICD 46-55 Central Interlock System [2LPSQY] v1.2; new version to be prepared	IS-55-46-001. Not written yet IS-55-46-002. Not written yet IS-55-46-003. Not written yet
Central Safety System	48	ICD 48-55 Central Safety System [2LPZ6G] v1.2; to be updated	Not written yet

TABLE 13.2. Indirect interfaces for ECE Diagnostic.

The outstanding features of some of these interfaces with the **ECE** are discussed below.

4.1 Machine assembly and tooling (PBS 22)

The attachment of the ex-vessel transmission line components require interface with Machine assembly and tooling. At the earliest opportunity, the DA will provide an assembly concept, and an alignment and metrology strategy.

4.2 Remote Handling (PBS 23)

The **ECE** requires the maintenance, calibration and refurbishment of the system by Remote Handling (RH).

4.3 Vacuum (PBS 31)

The **ECE)** requires a rough pumping capability to evacuate the interspace between the port flange (windows assembly) and the polarization splitter box.

4.4 SSEN and Cable Trays (PBS 43 and 44)

The supply of the back-end of the system in the diagnostic areas with electrical power is due to the interface with SSEN (PBS 43) and, via 55NE, with Cable Trays System (PBS 44).

4.5 CODAC and Plasma Control System (PBS 45 and 47)

There is an interface with CODAC (PBS 45) and PCS (PBS 47) for instrumentation and control.

4.6 Port Plug Test Facility (PBS 58)

Because parts of the front end of the system are located inside the Equatorial Port Plug 10 and Upper Port Plug 1, there is an interface with PBS 58 for functional and environmental tests in the Port Plug Test Facility.

4.7 Radwaste treatments and storage systems (PBS 66)

Because the in-port plug parts of the diagnostic may produce some amount of the operational radwaste type “B”, there is an interface with PBS 66.

The 3D and 2D CAD Model Approval Inrefacing System Control Sheet for 55F1 ECE diagnostic can be found here: ITER_D_A6UBTX - The 3D and 2D CAD Model Approval Interfacing System Control Sheet (PC-CMAF ECE-CMM-L1-level) v1.0.

Diagnostic First Wall (PBS 55)

The waveguides uses the apertures in the Diagnostic First Wall (DFW) in the Equatorial Port 09 (Fig. 13.1).

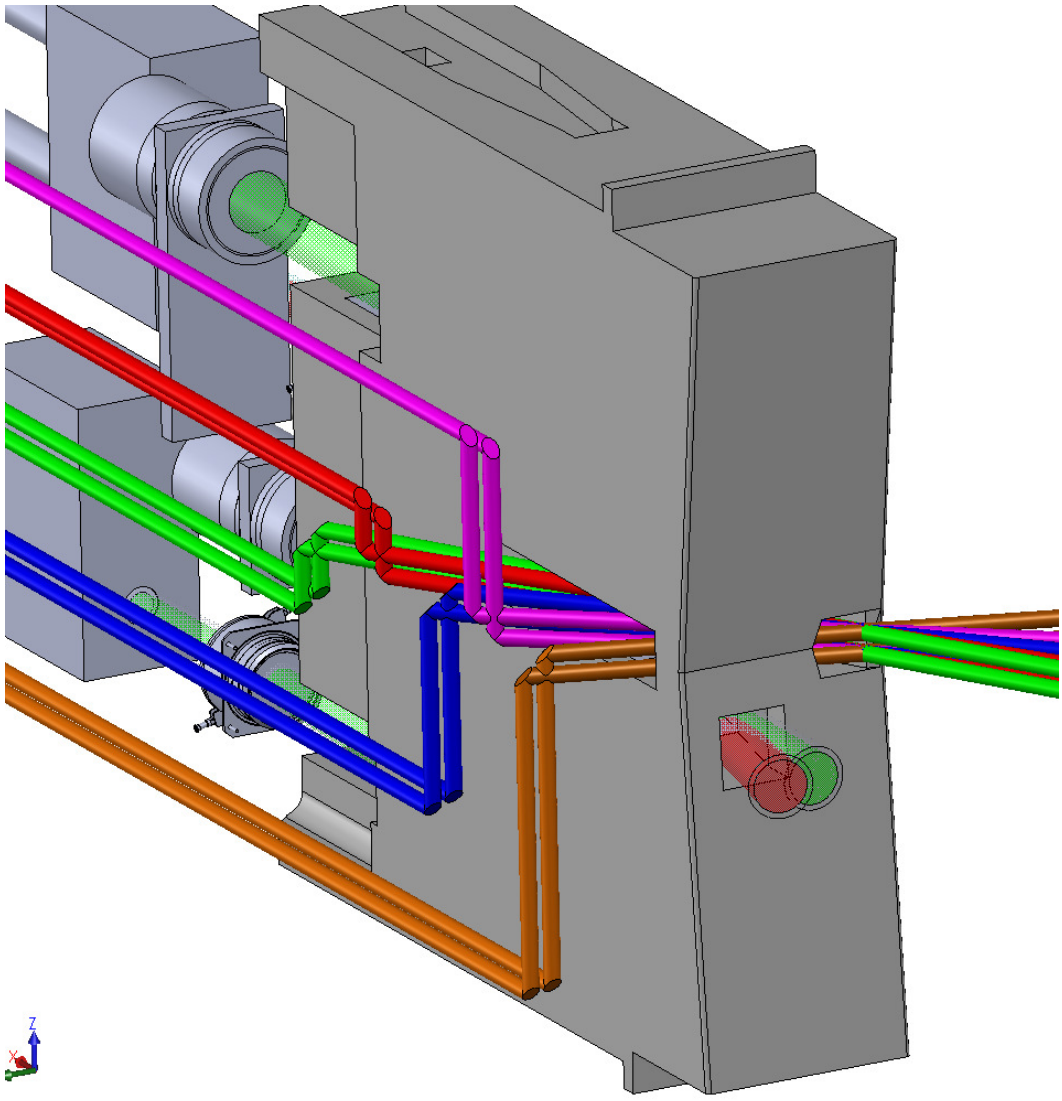

Figure 13.1. Interface between ECE and DFW.

14 Constructability and manufacturability

14.1 Constructability

Reflectometry waveguides and components are manufactured since decades for use in Fusion machines worldwide. At current no showstopper is foreseen, however R&D activity will be carried out on several diagnostic components.

14.2 Design Development Plan

This section aims at describing the project activities, the design progress logic and the work plan for the next design phases.
These activities have been determined according to the sections:

6.2 “Description of design development and optimization”
6.5 “Summary of risk analysis and proposed mitigation plans”

Several tasks have to be performed for the preliminary design (PDR) and its related load and performance analyses. These tasks will aim at mitigating the risks, optimization of the 55F1 ECE system and its implementation in ITER.

Step 1: before Preliminary Design Review

- To be finalized in the Annex B after the CDR.

Step 2: before Final Design Review

- - To be finalized in the Annex B after the CDR.

The main project milestones in IPS for the design after the Conceptual Design Review are:

55F1 Preliminary Design Review,
55F1 Final Design Review,
55F1 Manufacturing Readiness review

One hold point has to be added to the DWS milestones with regards to 55F1 ECE system tests review and approval between PDR and FDR. The design milestones (following PCR-251 schedule) are summarized in the Annex 14.1 and indicated in Table 14.1. The delivery of ECE front-end/ Receiver (EqP9) by US DA to US DA (port integrator) is scheduled for June 2017. The delivery of ECE transmission/ Receivers (EqP9) by IN DA to ITER is scheduled for February 2019.

TABLE 14.1. Design and manufacturing schedule for 55F1 ECE Diagnostic (PCR-251 schedule).

IO.1226.010120	US	Manufacture F1 ECE Front End/Receiver EQ09	06-Jan-2016	01-Sep-2016
IO.1226.010130	US	Manufacture F1 ECE Front End/Receiver EQ09 Completed		01-Sep-2016
IO.1226.010140	US	Factory Acceptance Testing F1 ECE Front End/Receiver EQ09	02-Sep-2016	06-Mar-2017
IO.1226.010150	US	Factory Acceptance Testing F1 ECE Front End/Receiver EQ09 Approved by IO		06-Mar-2017
IO.1226.010160	US	Pack & Ship F1 ECE Front End/Receiver EQ09 to US-DA	07-Mar-2017	02-Jun-2017
IO.1226.010170	US	IPL > - Delivery of F1 ECE Front End/Receiver EQ09 by US-DA to US-DA		02-Jun-2017
IO.1226.011120	IN	Manufacture FC ECE Transmission Receivers EQ09	19-Jan-2017	04-Apr-2018
IO.1226.011130	IN	Manufacture FC ECE Transmission Receivers EQ09 Completed		04-Apr-2018
IO.1226.011140	IN	Factory Acceptance Testing FC ECE Transmission Receivers EQ09	05-Apr-2018	02-Nov-2018
IO.1226.011150	IN	Factory Acceptance Testing FC ECE Transmission Receivers EQ09 Approved by IO		02-Nov-2018
IO.1226.011160	IN	Pack & Ship FC ECE Transmission Receivers EQ09 to US-DA	05-Nov-2018	19-Feb-2019
IO.1226.011170	IN	IPL > - Delivery of FC ECE Transmission Receivers EQ09 by IN-DA to US-DA		19-Feb-2019
IO.1226.011180	IN	Pack & Ship FC ECE Transmission Receivers EQ09 to ITER	05-Nov-2018	19-Feb-2019
IO.1226.011190	IN	IPL > - Delivery of FC ECE Transmission Receivers EQ09 by IN-DA to ITER Site		19-Feb-2019

14.3 Manufacturability and constructability of each component

As a result of the needs for high power microwave transmission lines for ECH, CWG and smooth-wall waveguides development has been ongoing for 30 years. Standard designs and manufacturing techniques are available. The US ITER office has been developing components and manufacturing techniques to complement those available commercially.
The back-end components (electronics) are standard products and can be produced routinely.

15 Status of R&D

R&D activity will be addressed at the Conceptual Design Review and summarized in the present DDD and the Annex B. For the moment, the following R&D activities are identified:

- assessment of the hot source performance and reliability;
- assessment of the TL performance for CWG and smooth-wall waveguides;
- assessment of the secondary window material and construction;
- ECH protection scheme;
- RH-compatible solution (if become necessary) for waveguide flanges.

The responsibility for R&D will be decided before the completion of the Annex B.

ITER ECE system will require four ~40 m long transmission lines (TLs) (two for each O- and X-polarizations per line-of-sight).

The TL has to be chosen to achieve, in conjunction with the detection system, a good overall performance in the frequency range of 70-1000GHz, optimized, on one hand, to ensure the primary measurement roles for electron temperature profile and NTM amplitude measurements, and, on the other hand, to provide as much as possible useful information about the ECE spectra at higher frequencies for the P_{ece} and non-thermal electron population measurements.

The baseline design, after the CDR, includes all four transmission lines which consist of circular, smooth-wall waveguides to fulfil the needs mentioned above. The circular corrugated waveguide, which has been proposed for the perpendicular line-of-sight at the CDR, appears to be an attractive choice for the lower frequencies; however, has degraded performance at frequencies above the Bragg Resonance frequency determined by the size of the corrugations. The performance of this corrugated waveguide at the frequency range of interest is a clear R&D subject to study during the next Design Phase.

There is a need to suppress the ECRH 170 GHz in the TLs . The protection scheme was discussed at the CDR; further R&D is planned in collaboration with US DA to establish the reliable design. The R&D on this subject has many similarities with similar R&Ds for other ITER mm-wave diagnostics and may benefit from them, too.

The size and positioning of optical components to couple efficiently from the QO elements in the port to the TL needs to be verified experimentally.

Towards these goals, IN-DA proposes to undertake the following activities (steps indicated) until the PDR (which is foreseen to be executed together with the ECE front-end):

A. Study of transmission losses in a few types of waveguides

Procure components (straight sections, bends, couplers etc) for setting up a reasonable length of typical TLs of: (a) circular corrugated, (b) circular smooth-wall waveguides; (c) dielectric-coated corrugated waveguides; (d) rectangular smooth-wall waveguides.

Using blackbody sources and a detection system with good (~5 – 10 GHz) resolution, perform experiments, at different frequencies, to obtain useful values of typical loss in straight section, mitre bends and joints in all types of waveguides. It is expected that similar results would become available for other types of waveguides from experiments/experience at other laboratories. In particular, the characterization of TL with rectangular smooth-wall waveguides and a few miter bends, similar to that discussed at the CDR, is planned as a part of this activity. Collaborations with labs possessing broadband interferometers and cryo-cooled detectors for the frequency range of interest will be established.
On the basis of above data, estimates will be made of total loss to be expected in the ITER TLs for different waveguides. The S/N and ease of calibration using available blackbody sources would also be established by these experiments. The main goal is to report the results at the PDR and to make a justified decision about the final choice of the TL type for ITER ECE.

B. Study of the Waveguides performance near and above the Bragg frequency

Set up an experiment with corrugated sections having Bragg frequency in the frequency region which is unlikely to be affected by water absorption bands.
With a tuneable high-resolution (tens of MHz) solid state source and a zero-bias detector, study the transmission above and below the Bragg frequency.
Elucidate any information for the possibility of supressing the transmission of a selected frequency by introducing an appropriate corrugated section. This might be relevant for notching out the 170 GHz frequency in ITER TL.

C. Study of quasi-optical schemes for coupling power to selected waveguides at low frequency (70 to 200 GHz)

Determine the size of the quasi-optical components by using Gaussian beam theory. Then, experimentally study the transmission of the quasi-optical arrangement and the efficiency of coupling between waveguide and the optics.

D. Assess the instrumentation for the broadband frequency measurements and for the radiometers

Assess the performance and designs of the present day FTS for the broadband measurements in the frequency range of interest. Participate in the collaborative experiments to identify the most suitable instruments (in terms of calibration time for the representative losses as expected for ITER ECE TL, physics requirements, integration in the tokamak complex, handling and servicing, etc) for IN-DA deliverables. Follow up the present state-of-the-art for radiometers; refine the design of proposed radiometers for ITER ECE and present it at the PDR.

E. Assess the details of TL integration in ITER tokamak complex and integration of the back-end instrumentation in the diagnostic area

Continue with the integration of the ECE TLs in the Eq. Port 9 (in collaboration with US DA as a port integrator). Assess the mechanical solutions for TL supports, their ability to withstand the required loads and develop the maintenance plan. Assess the further needs for integration of the back-end instrumentation, including the room space allocation, penetrations in the building etc (in collaboration with IO and US DA).

The further R&D activities, if needed, will be identified during the Annex B PA preparation, and between PDR and FDR phases of the project.

16 Initial Assembly, Commissioning and Decommissioning

55F1 ECE diagnostic is located in the Equatorial Port 9. From the DWS, 55F1 ECE front-end (in-port plug components) should be delivered to US DA for integration by no later than June 2nd, 2017.

For the first plasma (late 2018; H/He Operation – phase C1), the full set of ex-vessel waveguides but perhaps a limited set of electronics can be planned to be delivered, subject to negotiations between IO and DAs. The goal for the first phase is to check system components (waveguides, windows etc) and critical Diagnostic Area components. The “strawman” proposal is to use the ECE systems for:

- 122 – 230 GHz (O-mode radiometer for 2nd harmonic X-mode ECE at half-Bt, Michelson).

For the second phase of operation (starts by the end of 2022), full instrumentation will be installed.
The IPS schedule for 55F1 ECE syatem, amongst other diagnostics, is given in Annex 14.1. Upgrades during D-T operation are subject to further definitions and agreements.

Note:

- Commissioning is subject to agreement with US DA and IN DA.

- Decommissioning: there exists an ICD with Radwaste (PBS 66). More details will be defined for PDR.

-The design of 55F1 ECE diagnostic will follow the PR recommendations on General Safety Objectives, Occupational safety (ALARA) and zoning (ITER_D_27ZRW8, ch. 7.2, 7.3 and 7.9).

17 Operation and maintenance concepts – Remote Handling

The 55F1 ECE diagnostic is RH Class 2 for most required RH operations, meaning that its component(s) do not require scheduled remote maintenance but are likely to require unscheduled and very infrequent remote maintenance. This classification is mainly defined by the RH classification of the Equatorial Port Plug 9 in which the diagnostic is integrated. However, for the inspection and cleaning operations and possibly repairs, it should be noted that any maintenance task whether performed every shutdown (scheduled) or regularly (periodic- scheduled) or randomly (but Scheduled), may become RH Class 1.

The only likely RH operations are the refurbishment of the DSM with the 55F1 ECE diagnostic at a RH workstation in the Hot Cell Facility. In particular the shutter mechanism directly behind the front shield has an elevated risk of failure. Replacement of the shutter is required in that case.

The transportation from the tokamak to the Hot Cell Facility is foreseen within the assembly of the EPP9 by means of the RH transfer cask.

The RH Plant Definition Form and Task Definition Forms will be prepared for the CDR. The Remote Handling sequence for the antenna replacement is described in Annex 17.1 (see https://user.iter.org/?uid=4E8SWC for details).

18 Operation modes and Load cases

18.1 Operation modes of 55F1 ECE system

Table 18.1. Definition of Plant System Operating States (PSOS)

Off	None of the measurements and controls is active
Stand-by	I&C operational
TCS	Test and conditioning (used also for commissioning)
Calibration	Calibration/alignment of diagnostic
Ready	Ready for plasma pulse
Pulse	Operational with continuous data acquisition

18.2 Load specifications

This document is written following the "Guidelines for ITER System Load Specifications" (ITER_D_33TTPJ v1.3).

All relevant structural, electromagnetic and thermal loads acting on the ITER 55F1 ECE diagnostic have been defined. These loads should be taken into consideration in the design of the 55F1 ECE diagnostic and its components.

The 55F1 ECE diagnostic will be procured at functional specification level. All other loads and load combinations not specified in the annex will be investigated and reported for the next design review phase.

The purpose of the Load Specification (Annex 18.1) is to:

- define all possible events important for the conceptual design level
- describe the loads affecting the 55F1 ECE diagnostic and their load path through the mechanical connections for the verification of the structural integrity;
- define the interface loads with Equatorial Port 9.

Note:

- The system basic information has been defined in the related SRDs/DDD such as system functions, classification, design basis condition & events, system boundaries and interfaces, etc.
- The components of the 55F1 ECE diagnostic are shown in the related PFDs.
- All modes under which each component undergoes are shown in the related PFDs such as plasma operation, standby, baking operation, idle and maintenance.
- Single loads and load combinations that are obviously no feasibility issue for the structural integrity of the system and its components do not need to be specified.
- States of the system and its components do not need to be described, in case it is obvious that no design driving loads occur in these states.
- The number of occurrence does not need to be given for loads that are not design driving.

The loads acting on the 55F1 ECE diagnostic can be divided into three independent categories:

- Inertial loads: these are caused by accelerations due to gravity and seismic events.

- Electromagnetic (EM) loads: is a strong design driver and act upon nearly all conductive structures during transient events (e.g. plasma disruptions, VDEs, and magnet current fast discharge).
- Thermal loads: caused by temperature gradients inside the Vacuum Vessel due to the heat radiated from the blanket modules and nuclear heating power; caused by temperature transients between plasma pulse and dwell time.
- Loads under incident and accident conditions.
- Interface loads - Stray loads from ECRH system (Annex 18.2).

19 RAMI

RAMI stands for Reliability, Availability, Maintainability and Inspectability. RAMI analysis for the LFS Reflectometry has been launched in collaboration with the ITER RAMI team, following the ITER RAMI Approach Programme (28WBXD), and is summarized in RAMI analysis summary report for ECE Diagnostic (55F1) (Annex 19.1).

The RAMI requirement of diagnostics system shall be in compliance with the requirements specified in Section 6.13 of PR document. The expected reliability and availability of each measurement that belongs to global diagnostics system should not be less than the requirement specified in PR document. The 55F1 ECE diagnostic design should be able to fulfil all the RAMI requirements which are stated in the SRD section 4.3, RAMI Requirement in order to be able to achieve above requirement.

19.1 Functional description of the system

A first step in the RAMI analysis is to determine the functional breakdown of the ECE system. This is given in the Fig. 19.1. Lower level functions were identified accordingly and failure modes were determined for each basic function.

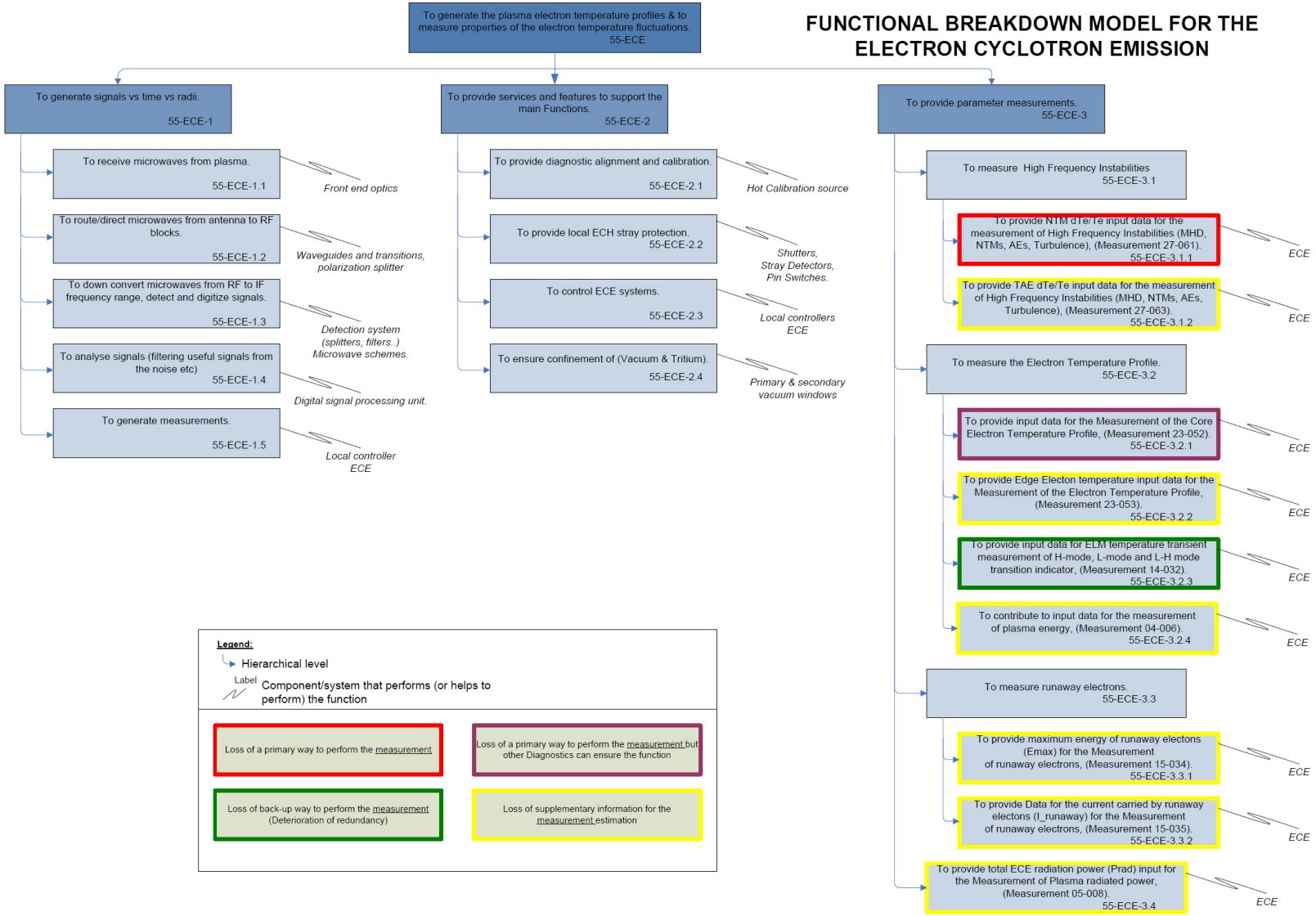

Figure 19.1. Overview of the functional breakdown of ITER ECE Diagnostic from RAMI.

19.2 RAMI compliance

Note: detailed RAMI failure mode analysis and effects analysis will be at PDR level.

The RAMI requirements given previously in terms of availability targets could be achieved only if some risk reducing actions and/or compensating provisions related to the design, test, operation and maintenance are implemented.

For the ECE Diagnostic, the preliminary RAMI analysis highlighted potential risks which may stop the ITER machine operation. Further details of the RAMI analysis for 55F1 ECE Diagnostic can be found in Annex 19.1.

20 Verification and Validation

Integrity Study/Report

The Integrity Report is available in the Annex 20.1.

The document specifies the structural assessments needed to justify the structural integrity of the 55F1 ECE diagnostic in the scope of the CDR. The purpose is to:

- list all failure modes of the system and its components;
- give an overview over the criteria of the structural integrity assessment;
- give an overview over the methods used to verify the structural integrity of the system and its components, e.g. FE analysis or examination test;
- summarize the structural assessments related to each failure mode and make a quantitative conclusion on the results;
- write the structural integrity report following the quality assurance requirements

These loads should be taken into consideration in the design of the 55F1 ECE diagnostic and its components. The report has followed the "Guidelines for ITER Structural Integrity Report" (ITER_D_35QTKD v.1.2)

A list of outstanding actions for PDR is reported.

21 Summary of Compliance with External Criteria

21.1 Design Compliance Matrix

The compliance between SRD requirements and 55F1 ECE diagnostic (at the CDR level) is described in the Design Compliance Matrix, see Annex 21.1.

21.2 System Classifications of the 55F1 ECE diagnostic

The various elements of the 55F1 ECE diagnostic have been classified, consistent with general ITER guidelines. The full table is given in Annex 2.1.

21.3 Safety classification

The components which form the primary vacuum barrier are SIC-1. The building feedthrough (with secondary windows) are SIC-2. All other components are non-SIC. Refer to ITER_D_3G2T8J for details.

21.4. Quality Assurance

ITER Organization shall have overall responsibility to meet the project objectives and safety requirement. All the activities shall be carried out in accordance with ITER Quality Assurance Program (ITER_D_22K4QX v7.3). The ECE system form part of the vacuum boundary, thus the confinement boundary area will be SIC-1 which will be assigned QC1. The 55F1 ECE diagnostic has no measurement for SIC purpose and the loss of the measurements will not cause the stop of machine or plasma operation.

Other area except the confinement boundary of 55F1 ECE diagnostic can be QC2 or QC3 which is in accordance with IO "Quality classification determination" (ITER_D_24VQES v3.0).
The table in the referenced document (ITER_D_24VQES v3.0) describes the actions appropriate to quality class. These include actions indicated in the Table 21.2 of this DDD.

TABLE 21.2. Table of actions.

Quality Classification(1)	**Class 1**	**Class 2**		**Class 3**	
Allowed Nuclear Safety classes	SIC-1 / SIC-2 / SR / NSR	SIC-2	SR / NSR	SR	NSR
Design	Design controls including design reviews and *independent*(2) verifications		Design controls including design reviews and verifications		No design review required, unless otherwise agreed between the parties
Software	Acceptance of Software used for Design and Operation, including life cycle management		Identify and validate software usage		No requirement, unless otherwise agreed
Minimum Documents and Records to be delivered	Quality Plans, Manufacturing & Inspection Plans, Procedures, calculation note (where design is involved), working instructions, Special Process Qualifications (if applicable), Operator Qualifications, 'As Built drawings', Release Note, Certificate of Conformity. Material certification and inspection documents according to EN 10204 Type 3.1 (or equivalent) traceable to the component part and equipment.		Quality Plans, Manufacturing & Inspection Plans, Release Note, 'As Built drawings', material certification and inspection documents acc. to EN 10204 Type 3.1 (or equivalent) traceable to the component part/equipment.		Certificate of Conformity according to to EN 10204 Type 2.1 (or equivalent)
Monitoring of performers	Audit of performers including qualification and surveillance		Limited on-site reviews		No Monitoring, unless otherwise agreed between the parties
Measurements and Test Equipments	Controlled Calibrated measuring and test equipment (M&TE)				Controlled Calibrated M&TE for validation processes
Minimum N.D.E.(3-4) on weldings	100% visual, surface and volumetric inspection	100% visual and surface, 20% volumetric inspection		100% visual, 10% surface and volumetric inspection	
Special processes Personnel Qualifications and Training (i.e. welding, brazing, N.D.E.)	Documented personnel qualifications and training				
QA requirements	QA representative approvals of documents related to special processes and inspections are required		QA representative consultations on special processes and inspections are required		QA consultations on as-needed basis

Notes:

*(1) For systems and component parts of **class 4**: no specific QA requirements.*

(2) 'Independent' means individual, groups, divisions, departments who were not involved in the original design. 'Independent' can also mean a Third Party organization.

21.5 Export Control

IO and United States Export Control regulations have to be taken into account. A document will be produced for the PDR showing the main guidelines/specifications/requests of this topic for the 55F1 ECE diagnostic.

22 Annexes

All annexes are stored in: / **IDM Root** / **Plant Breakdown Structure** / **55. Diagnostics** / **00-Collaborative Working Platform** / **01_Current Configuration** / **55.F* - Microwave Diagnostics** / **55.F1 - Electron Cyclotron Emission** / **02_Technical Documentation** / **02_DDD&Annexes** ;

Web link: https://user.iter.org/?uid=4FJJP6

[A2.1] Diagnostic system classification, ITER_D_ 4D7A7J

[A5.1] System Integration Document for Diagnostic Equatorial Port 9, ITER_D_ 66WK4L

[A6.2.1] Continued development of a prototype Hot Source for the ITER ECE diagnostic, ITER_D_42FZ7U

[A6.2.2] Proposed double-window assembly for the primary confinement barrier for ITER ECE, ITER_D_6TF5CZ

[A6.2.3] Polarizer beam splitter design for ITER ECE, ITER_D_6TQVZE

[A6.4.1] ECH protection for the ECE Diagnostic, ITER_D_ 6WA84E

[A6.6.1] ECE System risk table, ITER_D_6KXF4U

[A7.4.1] US Team ITER ECE Report, May 2011, ITER_D_6WE326

[A8.1.1] ECE Diagnostic Process Flow Diagram (PFD), ITER_D_6KV3XY

[A8.1.2] ECE Diagnostic Single Line Diagram (SLD – Cabling), ITER_D_6KTSNE

[A8.1.3] Cell Embedments for PBS 55.Diagnostics, ITER_D_4C8NN3

[A8.1.4] Interface with SSEPN and Cable trays, ITER_D_4ESYDV

[A17.1] Remote Handling assessment documents for ECE Diagnostic, ITER_D_6XMNTA

[A18.1] Load Specifications for ECE Diagnostic, ITER_D_6XRG6J

[A18.2] Stray RF Power modelling in the Tokamak during EC operation, ITER_D_ 4D377D

[A19.1] RAMI Analysis for 55F1 ECE Diagnostic, ITER_D_ 4DASEP

[A20.1] Structural integrity report for 55F1 ECE Diagnostic, ITER_D_6XWYZ6

[A21.1] Compliance matrix for 55F1 ECE Diagnostic, ITER_D_734AZL